DEVELOPMENT OF TECHNIQUES FOR EXTRACTION OF FETAL BRAIN FROM MAGNETIC RESONANCE IMAGING (MRI) SCANS AND ABNORMALITY DETECTION

A Thesis Submitted
IN FULFILLMENT OF THE REQUIREMENTS
FOR THE DEGREE OF

DOCTOR OF PHILOSOPHY
IN
COMPUTER SCIENCE AND ENGINEERING

P.DURGADEVI
(17SCSE301020)

Supervisor
Dr. S. Vijayalakshmi
Associate Professor
Department of Data Science
CHRIST UNIVERSITY, INDIA

Co Supervisor
Dr. Munish Sabharwal
Professor & Dean
SCHOOL OF COMPUTING SCIENCE & ENGINEERING
Galgotias University, Greater Noida, INDIA

GALGOTIAS UNIVERSITY
UTTAR PRADESH
(September 2021)

CANDIDATE'S DECLARATION

I hereby certify that the work, which is being presented in the thesis, entitled **"DEVELOPMENT OF TECHNIQUES FOR EXTRACTION OF FETAL BRAIN FROM MAGNETIC RESONANCE IMAGING (MRI) SCANS AND ABNORMALITY DETECTION**" in fulfillment of the requirements for the award of the degree of Doctor of Philosophy in COMPUTER SCIENCE AND ENGINEERING and submitted in Galgotias University, Greater Noida is an authentic record of my own work carried out during a period from 2017-2021 under the supervision of

Dr. S. Vijayalakshmi, Department of Data Science, Christ University, India.

The matter embodied in this thesis has not been submitted by me for the award of any other degree of this or any otherUniversity/Institute.

(P.DURGADEVI)

This is to certify that the above statement made by the candidate is correct to the best of our knowledge.

(Dr.S.Vijayalakshmi)
Supervisor
Dept. of Data Science
CHRIST UNIVERSITY

(Dr. Munish Sabharwal)
Co-Supervisor
School of Computing Science & Engineering
GALGOTIAS UNIVERSITY

The Ph.D. Viva-Voice examination of **P.DURGADEVI** Research Scholar has been held on____.

Sign.of Supervisor(s) Sign.of Co-Supervisor(s) Sign. of External Examiner

ABSTARCT

Segmentation of brain from fetal MRI is a relatively new field, with little work published on fully automatic processing. Automatic brain segmentation methods developed for MRI of adult cannot be directly applied to study the developing fetal brain in utero, since the fetal brain is significantly different in terms of geometry as well as tissue morphology. In this thesis, we have proposed three segmentation methods, to extract brain portion from the MRI of human fetus and also estimate the volume of the fetal brain at different gestational week.

In our first fetal brain extraction method, we first enhance the contrast of the boundary of thin layers in fetal brain using brightness preserving bi-histogram equalization (BBHE). Next, the region growing process is done by calculating the distance (D) between the center pixel and 8-neighbour pixels of the contrast enhanced image. An optimal intensity threshold value is calculated using Otsu's method and it is used as the stopping criteria for the region growing process. Using Flood filling algorithm, the holes which are produced in the previous stage are filled that result in fetal brain mask. Finally the fetal brain is extracted using the mask. We carried out experiments by applying our method on five volumes of retrospective fetal T2 - w MR images collected from KGS Scan and Diagnostic Centre, Madurai, India. To evaluate the performance of the method Dice coefficient (D), sensitivity (S) and specificity (Sp) were computed. The results show that our method can successfully segment fetal brain from MRI which are comparable to that of a semi-automatic method.

Our second fetal brain extraction method involves diffusion, morphological filtering, thresholding and connected component analysis. To distinguish the fetal brain from the rest of maternal tissues, we apply anisotropic diffusion technique and gray scale morphological opening process in succession. The filtered image is further processed to generate binary image using improved maximum entropy threshold. The binary image consists of several isolated regions. To extract the fetal brain region from the binary image, we perform a 4 connected component analysis. The largest connected component is taken as brain mask. Finally, the fetal brain is extracted from the original image using the brain mask. The computed values of similarity index (D) and visual inspection of the results of the proposed method-2 show that the proposed method produces results closer to that of the existing fully automatic method, atlas based method and to manually segmented gold standard.

In our third method for fetal brain extraction from MRI, we first detect the fetal head location in 2D MRI slices using mathematical model minima and draw a circle on the input image that encloses the fetal head and is taken as the region of interest (ROI). This is done adaptively. The CSF and amniotic fluid which are surrounding the fetal head appears brighter in the T2-w MR image. We eliminate such high intensity pixels from the ROI using histogram. An optimum intensity threshold value is computed using Otsu's method and is used to obtain a binary image. The morphological opening filter is applied on the binary image to eliminate weakly connected non-brain pixels such as boundary of CSF and fetal skull. Next hole filling and 4 connected component analysis are done to obtain the fetal brain mask. Using this mask, fetal brain is extracted from the original image. We carried out experiments by applying our method-3 on the material pool of 25 volumes collected from Sri Ramachandra Medical University and Hospital, Chennai, India. The result of the proposed method is evaluated against manually segmented gold standard. The computed similarity measures and visual inspection of the results of the proposed method show that this method works well on both normal and abnormal types of T2-weighted fetal MR images.

Finally we estimate fetal brain volume (BV). The BV is computed by the sum of all brain pixels in the segmentation and multiplying by the slice thickness and interslice gap in milliliters. We computed BV, for the brain portion extracted by our method and for results obtained by the manual segmentation for different gestational weeks. The percentage of error is computed between BV for the proposed method and manual segmentation. The linear, exponential and polynomial fit for the BV of our method is computed. These results show that estimated brain volume based on our segmentation method is closer to manual tracing within an average error value of 1.02% and best fits the polynomial model with an r^2 value of 0.986.

All our proposed methods are found to segment brain region accurately and are comparable with the gold standard and other existing methods. Our automatic segmentation methods of fetal MRI will facilitate a wider application to provide assistance in clinical practice. Brain segmentation helps to study the evolution of brain at different gestational periods. Further, analysis of the extracted brain help to identify any deformity in brain and make an informed decision.

ACKNOWLEDGEMENT

The research work presented in this thesis would not been possible without my close association with many peoples. I would like to take this opportunity to extend my sincere thanks and appreciation to all those who made this PhD thesis possible.

First and foremost, praises and thanks to the God, the Almighty, for his showers of blessing throughout my research work to complete the research successfully.

Very special thanks to **Shri Suneel Galgotia, Chancellor and Mr. Dhruv Galgotias, CEO, Galgotias University** for giving me the opportunity to carry out my doctoral research and for their support.

My sincere gratitude is reserved for **Dr. Preeti Bajaj,Vice chancellor, Galgotias University** for all required permission support and for this thesis. I would like to say special thanks to my Co-guide **Dr. Munish Sabharwal. Professor & Dean School of Computing Sci. & Engineering, Galgotias University** for his tremendous support during my PhD and thesis work.

One good teacher in a lifetime may sometimes change a delinquent into a solid citizen. I profusely thank my research supervisor **Dr. S. Vijayalakshmi**, **Associate Professor, Department of Data Science, Christ University** for her valuable guidance, constant encouragement, and support. Her immense knowledge and plentiful experience have encouraged me in all the time of my academic research and daily life. I would like to thank you for introducing me to exciting field and always encouraging, motivating, enthusiasm, and allowing me to do what I think and continuous support throughout my Ph.D., your advice and support have been invaluable. She has always ignited our minds to innovate, and it is because of her constant support I am able to complete this work. She is a great inspiration and a role model. I thank her for all her support during this research.

My special thanks also to **Dr. Naresh Kumar, Professor and Dean (PG& PhD) at** Galgotias University for his continuous support, encouragement, cooperation, and facilitating all the requirements always. My special thanks also to my research coordinator **Dr. K.Sampath Kumar, Professor & PhD Coordinator**, School of Computing Science and Engineering Galgotias University for his continuous support, encouragement, cooperation, and facilitating all the requirements always. His constant support, guidance, motivation always pushing me forward.

I express my deep gratitude to my parents for this life. I thanks to God for this lovely family in which my brother & sister are my best friends. I owe my deepest gratitude towards my husband for his eternal support and understanding of my goals and aspirations. His love and support have always been my strength. As impossible to mention everybody who had an impact to this work even through there are some people those whose spiritual support is even more important. Thanks, God, for being with me always and providing all the strength, happiness, and good health to carry out this study.

Thank You So Much

P.DURGADEVI

TABLE OF CONTENT

Title Page		i
Candidate Declaration		ii
Abstract		iii
Acknowledgment		v
Table of contents		vi
List of Figures		ix
List of Tables		xii
List of Publications		xiii
List of Symbols and Abbreviations		xiv

Chapter 1	**Introduction**	1
	1.1 Gestational Weeks (GW) and Different Prenatal Tests	1
	1.2 Consequence of fMRI in Brain Investigation	8
	1.3 Essential on behalf of Extraction of Fetus Brain	10
	1.4 Goal of the dissertation	10
	1.5 Organization of the dissertation	11
Chapter 2	**LITERATURE REVIEW**	12
	2.1 Introduction	12
	2.2 Survey on medical image processing	15
	2.3 Survey on Medical Image Segmentation	20
	2.4 Survey on Fetal MRI Segmentation	21
Chapter 3	**Fetal MRI**	34
	3.1 Clinical Imaging Modalities	34
	3.1.1 Ultrasonography (US)	36
	3.1.2 Magnetic Resonance Imaging (MRI)	37
	3.2 Basic Principles of MRI	39
	3.3 Fetal MRI	41
	3.4 Clinical Indications for MRI of Fetal Brain	43
	3.5 Normal Fetal Brain Structure	43
	3.5.1 Sulcation	44
	3.5.2 Ventricles	44
	3.5.3 Corpus Callosum	45
	3.5.4 Hippocampus	46
	3.5.5 Deep gray nuclei	47
	3.6 Abnormal Fetal Brain Structures	47
	3.6.1 Ventriculomegaly	48
	3.6.2 Agenesis of Corpus Callosum	48
	3.6.3 Posterior Fossa Abnormalities	49
	3.7 Challenges in the Automated Analysis of Fetal Brain in MRI	50

Chapter 4	**Basic Image Processing Methods and Evaluation Metrics**	51
	4.1 Introduction	51
	4.2 Thresholding	51
	4.2.1 Otsu's Thresholding	51
	4.3 Morphological Operations	56
	4.3.1 Erosion Operation	57
	4.3.2 Dilation Operation	58
	4.3.3 Hole Filling	58
	4.4 Labeling	60
	4.5 Largest Connected Component (LCC)	61
	4.5.1 2-D Region Growing	61
	4.6 Contrast Enhancement using Bi-Histogram Equalization	66
	4.7 Non-Linear Anisotropic Diffusion	68
	4.8 Maximum Entropy Thresholding	69
	4.9 Evaluation Metrices	70
	4.9.1 Dice coefficient (D)	70
	4.9.2 Sensitivity (Sn) and Specificity (Sp)	70
	4.9.3 Hausdorff distance (HD)	72
	4.9.4 Curve fitting	73
	4.10 Materials Used	78
	4.10.1 Dataset 1	79
	4.10.2 Dataset 2	81
Chapter 5	**Fetal Brain Extraction from MR Images using Region Growing Technique**	82
	5.1 Introduction	82
	5.2 Method	83
	5.2.1 Pre-processing	83
	5.2.2 Thresholding	84
	5.2.3 Seeded Region Growing	84
	5.2.4 Holes Filling Inside the Brain Region	85
	5.3 Materials Used	85
	5.4 Results and Discussion	86
	5.5 Conclusion	90
Chapter 6	**Automatic Segmentation of Fetal Brain from MRI of Human Fetus using Improved Maximum Entropy Method**	91
	6.1 Introduction	91
	6.2 Method	92
	6.2.1 Edge Preserving Smoothing	92
	6.2.2 Morphological Opening	93
	6.2.3 Improved Maximum Entropy Threshold	94
	6.2.4 Fetal Brain Segmentation	95
	6.3 Materials Used	95
	6.4 Results and Discussion	96
	6.5 Conclusion	104

Chapter 7	**Fetal Brain Extraction using Mathematically Modelled Local Fetal Minima**	105
	7.1 Introduction	105
	7.2 Method	108
	7.2.1 Data Acquirement	109
	7.2.2 Eliminate high intensity pixels	110
	7.2.3 Thresholding	110
	7.2.4 Morphological Opening	111
	7.2.5 Hole filling	111
	7.2.6 Fetal Brain Extraction	112
	7.3 Materials Used	113
	7.4 Results and Discussion	113
	7.5 Conclusion	120
Chapter 8	**Fetal Brain Volume Estimation from MRI of Human Fetus**	121
	8.1 Introduction	121
	8.2 Method	123
	8.2.1 Computing Area of Fetal Brain in Each Slice	123
	8.2.2 Computing Fetal Brain Volume	124
	8.3 Materials Used	125
	8.4 Results and Discussion	125
	8.5 Measure of Estimation	126
	8.6 Conclusion	131
Chapter 9	**Summary of Conclusions and Scope of Future Work**	132
	Bibliography	137
	List of publications	152

LIST OF FIGURES

Figure No.	Description	Page No.
1.1	Position of fetus (a) Breech presentation (30 GW) (b) Cephalic presentation (30 GW)	2
1.2	Sample of US	4
1.3	Sample of CVS	5
1.4	Example of Amniocentesis	6
1.5	Model of Fetal Echocardiogram	7
1.6	Model of fetal MRI	8
3.1	Fetal Imaging Modalities	35
3.2	Positron emanation tomography	36
3.3	Adjacent slices acquired in different time	40
3.4	fMRI scan (arrow)	41
3.5	MRI orientations in Axial, Coronal & Sagittal plane	42
3.6	fMRI in Axial, Coronal & sagittal plane	42
3.7	fetal brain in (a) T2-w and (b) T1-w MRI	43
3.8	Ventricular zone at 23 GW (bolt)	45
3.8a	Normal appearance of the corpus callosum at 26 GW (arrow)	46
3.9	fbrain show horizontally oriented hippocampus at 27 GW (arrows).	46
3.10	Axial slice show subtle hypo intensity of the deep gray nuclei at 27 GW (arrows) .	47
3.11	Fetal brain abnormalities (a) Ventriculomegaly (b) absence of the corpus callosum (arrow) (c) Dandy-Walker malformation	49
4.1	A Structuring Element (SE) of size 3X3	57
4.2	Structuring element SE with 4-connected neighbours	59
4.3	Hole filling (a) binary image with hole (b) Hole	60

	filled binary image (c) SE	
4.4	Sample image blocks for region growing as (a) 4- neighbor pixels (b) 8-neighbor pixels with (x,y) as the initial seed pixel.	62
4.5	A pixel map of the region growing method	64
4.6	Image obtained from Fig.4.5 by region growing	65
4.7	Venn diagram of Quantitative measures	72
4.8	The Hausdorf distance (HD) calculation	73
4.9	Fitting n data points	74
4.10	Fitting a straight line	76
4.11	Polynomial curve fit	77
4.12	Exponential curve fit	78
5.1	Neighborhood pixels considered for area developing	84
5.2	Row 1 : original MRI images, Row 2 : manually segmentation, Row 3 : Proposed segmentation result	86
6.1	Presence of melted CSF and cortex in Fetal MRI	92
6.2	Three-pixel-radius structural element (SE)	93
6.3	(a) Original MRI slice (b) diffused image (c) filtered image (d) segmented fetal brain	95
6.4	Fetal normal brain MRI (GW 20)	97
6.5	Sample of extracted fetal brain	97
6.6	Fetal abnormal brain MRI (GW 29)	98
6.7	Sample of extracted fetal brain MRI slice	98
6.8	Axial view of a segmented fetal brain obtained via MRI scan. Row 1 presents original images, row 2 presents manual segmentation and row 3 present proposed result.	99
6.9	Coronal view of a segmented fetal brain obtained via MRI scan. Row 1: original MRI images, row 2: manual segmentation, row 3: proposed result.	100

6.10	Sagittal view of a segmented fetal brain obtained via MRI scan. Row 1: original MRI images, row 2: manual Segmentation, row 3: proposed result.	100
7.1	a) Original MRI scan (b) region of interest (c) after removing high intensity pixels in ROI (d) Ib (binary image) (e) morphological opening result (f) hole filled operation result ((g) segmented fetal brain	112
7.2	ROI of MR images achieved in a) Axial plane b) Coronal plane and c) Sagittal plane	114
7.3	Extracted fetal brain MRI from the volume given in Fig.7.2 (a) Axial plane (b) Coronal plane (c) Sagittal plane	115
7.4	Challenging slices producing over and under segmented slices. Column 1 shows the ROI, column 2 shows extracted brain from the ROI and column 3 shows hand segmented brain	116
8.1	Slice thickness and inter-slice thickness	122
8.2	Pixel spacing is the same length as the pixel	124
8.3	BV Data fit in linear, exponential and polynomial fit equations	129
8.4	Quadratic fit for two ranges	130

LIST OF TABLES

Table No.	Title	Page No.
3.1	MR imaging techniques in terms of TR and TE.	40
4.1	Evaluation Parameters.	71
4.2	Details of retrospective T2 –w image.	80
5.1	Computed values of D, Sn , and Sp for the proposed method.	87
5.2	Computed values of D, Sn and Sp by the semi- automatic method.	89
5.3	Features of segmented fetal image	90
6.1	D, Sn and Sp values of the proposed method	102
6.2	D values calculated by popular algorithms	103
7.1	Comparison of universal quality index with FBEMMLFM Algorithm.	117
7.2	Computed values of D, Sn and Sp for this proposed method.	118
7.3	D Values given by presented algorithms	119
8.1	Estimated Fetal brain volume (mL).	126
8.2	The determination (R2) coefficient estimated for linear,quadratic and exponential model by proposed method.	127
8.3	The determination (R2) coefficient calculation for linear, quadratic and exponential fittings by Gholipour et al.[101].	127
9.1	Performance of proposed methods.	133

LIST OF PUBLICATIONS

1. “Review on medical Image Processing”, P.Durgadevi, S.Vijayalakshmi International Conference on Advanced Scientific Innovation in Science, Engineering and Technology (ICASISET -2019), pp.1581-1897.
2. “Deep Survey and Comparative Analysis of Medical Image Processing”, P.Durgadevi, S.Vijayalakshmi, Journal of Computational and Theoretical Nanoscience, 17(5), 2321-2329.
3. “Image Characterization Based Fetal Brain MRI Localization and Extraction”, P.Durgadevi, S.Vijayalakshmi, Journal Annals of the Romanian Society for Cell Biology, 1935-1946.
4. “A Methodological Investigation for fetal brain MRI Segmentation Techniques - Analysis”, P.Durgadevi, S.Vijayalakshmi, International Conference on Advance Computing and Innovative Technologies in Engineering (ICACITEE 2021), pp.684-690.
5. “Fetal Brain Extraction from 20-36 gestational MRI using Enhanced FCM”, P.Durgadevi, S.Vijayalakshmi, Munish Sabbharwal, Design Engineering (Toronto) accepted for publication.
6. “Fetal Brain Extraction using Mathematically Modelled Local Fetal Minima”, P.Durgadevi, S.Vijayalakshmi, International Journal of Biomedical Engineering and Technology (IJBET), accepted for publication.
7. “Fetal Brain Abnormality detection through PSO (Particle Swarm Optimization) and Volume Estimation”, P.Durgadevi, S.Vijayalakshmi, Munish Sabbharwal , Annals of the Romanian Society for Cell Biology, 2700-2714.
8. “Scrutiny in-utero to recognize fetal brain MRI anomalies” ”, P.Durgadevi, S.Vijayalakshmi, Munish Sabbharwal, Advances in Computing, InternationalConference on Advances in Communication Control and Networking - ICACCCN-21,communicated.

LIST OF SYMBOLS AND ABBREVIATIONS

B_0	Magnetic field
E	Exponential
N	total number of slices
$\ominus$	Erosion
$\oplus$	Dilation
$\sum$	Summation
M	Mean
Σ	Sigma
H	Eta
$\emptyset$	Null
$\cup$	Union
$\cap$	Intersection
∂	Partial differential
∇	Nabla
2D	Two Dimensional
3D	Three Dimensional
ACC	Agenesis of Corpus Callosum
BBHE	Brightness Preserving Bi-Histogram Equalization
BV	Brain Volume
CNS	Central Nervous System

CRF	Conditional Random Field
CSF	Cerebrospinal Fluid
CVS	Chorionic Villus Sampling
D	Dice coefficient
DTI	Diffusion-Tensor Imaging
DWI	Diffusion-Weighted Imaging
FGMM	Finite Gaussian Mixture Model
FM	Finite Mixture
fMRI	Functional Magnetic Resonance Imaging
FN	False Negative
FOV	Field Of View
FP	False Positive GA
GA	Gestational Age
GW	Gestational Weeks
HD	Hausdorff Distance
IST	Inter Slice Thickness
LCC	Largest Connected Component
MRF	Markov Random Field
MRI	Magnetic Resonance Imaging
MSER	Maximally Stable Extremal Regions
PD	Proton Density
RF	Radio Frequency
ROI	Region Of Interest

SE	Structuring Element
SIFT	Scale-Invariant Feature Transform
Sn	Sensitivity
SSFSE	Single Shot Fast Spin Echo
ST	Slice Thickness
TE	Echo Time
TN	True Negative
TP	True Positive
TR	Relaxation Time
T1-w	T1 – weighted
T2-w	T2 – Weighted
US	Ultra Sound
PSO	Particle Swarm Optimization
MRI	Magnetic Resonance Imaging

CHAPTER 1

Introduction

The progress from lady to parenthood has been given significance from days of yore. The parenthood is an excellent stage in ladies' life. During pregnancy, care to the mother and baby are fundamental. In this period a few pregnancy related issues are happen to the mother. Mother may endure a few medical conditions, such as morning infection, stoppage, gestational diabetes, sickness and heaving, vision issues and so forth similarly significant is the wellbeing of the baby and its turn of events. Consequently the baby is to be checked persistently till its introduction to the world. The existences of an embryo inside the mother’s belly are isolated in to three periods and are definite in the accompanying segments.

1.1 Gestational Weeks (GW) and Different Prenatal Tests

An ordinary pregnancy period ordinarily goes between 38 to 42 gestational weeks (GW). The pregnancy is separated into three-month time frames called trimeste-rs.

First Trimester (0 to 13 GW) : The initial three-month trimester is by and large determined as beginning the initial day of the last time frame and

goes through the thirteenth seven day stretch of the pregnancy. During this trimester, the embryo inserts into the belly of the lady.

Second Trimester (14 to 27 GW): This period begins in the fourteenth seven day stretch of the pregnancy and goes through the 27th week. During the second trimester, the embryo starts to develop quickly. By about the twentieth seven day stretch of the incubation time frame, most ladies will start to feel development of the hatchling.

Third Trimester (28 to conveyance): This period begins in the 28th seven day stretch of the growth time frame and goes through the introduction of the youngster. During this period, the hatchling increments in size and stretches the uterus and midsection of the lady. In the initial segment of the third trimester, the baby will be at its generally dynamic and development will be self-evident. As the youngster occupies the accessible space, development will turn out to be less yet more grounded and the lady will turn out to be more awkward. The children conceived inside this period is alluded to as full-term babies.

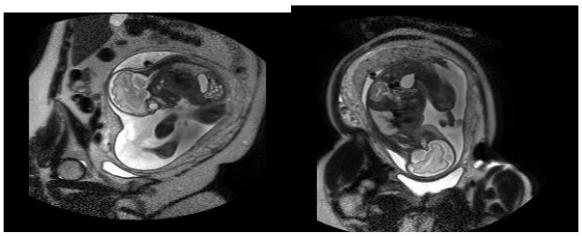

(a) (b)

Fig. 1.1 Position of embryo (a) Breech introduction (30 GW) (b) Cephalic introduction (30 GW)

Be that as it may, during pregnancy, hatchlings precede onward mother's belly and the situation of baby changes from breech to cephalic. The rate of breech introduction, comparing to the feet or sacrum in the pelvic pit (Fig.1.1 (a)), diminishes from about 20% at 28 weeks of incubation to 3-4% at term [1]. Towards the finish of pregnancy, most hatchling transform immediately into the cephalic introduction (Fig.1.1 (b)), with the fetal head slipping into the pelvic depression. The direction of the baby consequently turns out to be more unsurprising as the due date draws near. Pre-birth care improves pregnancy results. Consequently, pre-birth care should be taken for the baby during the pregnancy.

Pre-birth care may incorporate taking extra folic corrosive, normal exercise, blood tests, and ordinary actual assessments. A fundamental pre-birth visit comprises of estimation of pulse, fundal stature, weight and fetal pulse, checking for manifestations of work, and direction for what's in store straightaway. During pregnancy various sorts of tests are performed to notice the fetal development. Not many of such tests are as per the following:

Fetal Ultrasound :

Ultrasound (US) is sound that movements through delicate tissue and liquids, yet it bobs back, or echoes, off denser surfaces. This is the means by which it makes a picture. The expression "ultrasound" alludes

to sound with a recurrence that people can't hear. For indicative uses, the ultrasound is normally somewhere in the range of 2 and 18 megahertz (MHz).

Ultrasound is a term that refers to sound waves with frequencies greater than the upper discernible constraint of human hearing. Ultrasound isn't not the same as "would be expected" sound in its actual properties, then again, actually people can't hear it. This breaking point fluctuates from individual to individual and is roughly 20 kilohertz in sound youthful grown-ups.

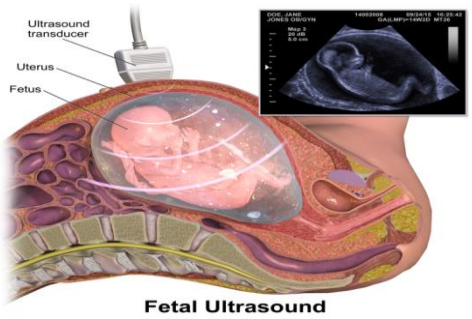

Fig. 1.2 sample of US

Chorionic Villus Sampling :

A pre-birth test like CVS takes chorionic villi from the placenta for examination. The cervix (transcervical) or the stomach divider can be used as an example.

When a woman is pregnant, the placenta provides oxygen and nutraceuticals to the developing infant while also removing waste products from the fetus's blood. The placenta supplies oxygen and

nourishment to the baby, filtering its blood of any toxins. Wispy projections of placental tissue, the chorionic villi share the child's genetic makeup. The test ought to be possible within 10 weeks of pregnancy, which is the expected duration of the pregnancy.

A variety of genetic conditions can be diagnosed via chorionic villus testing, which is used to identify genetic conditions such as Down syndrome and cystic fibrosis. The test, though vital in gauging a child's well-being, poses significant risks and needs to be thoroughly understood in order to properly prepare for the results.

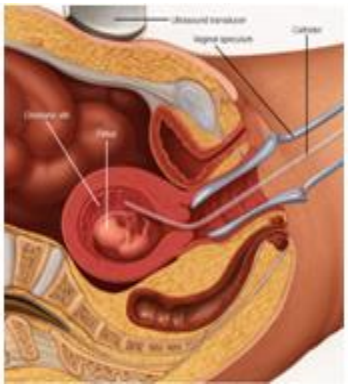

Fig. 1.3 sample of CVS

Amniocentesis:

Amniocentesis is a methodology wherein amniotic liquid is taken out from the uterus for testing or treatment. Amniotic liquid is the liquid that encompasses and secures a child during pregnancy. This liquid contains fetal cells and different proteins. In spite of the fact that amniocentesis can give significant data about the child's wellbeing, it's

essential to comprehend the dangers of amniocentesis — and be ready for the outcomes.

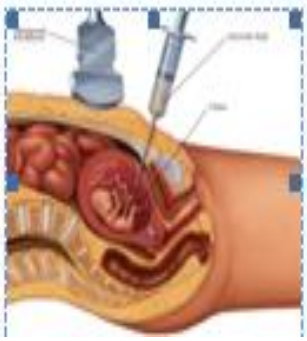

Fig.1.4 Example of Amniocentesis

Fetal Echocardiogram:

Fetal echocardiography is a test like an ultrasound. This test makes it easier for the PCP to observe the unborn child's heart. It's usually done between weeks 17 and 25, which is in the second trimester.

The test uses "reverberation" that reflects off the embryo's heart structures. To take an echocardiogram, first the machine divides the patient's sound waves and forms an image of their heart's interior. This image provides details about the infant's heart's shape and its ability to function normally.

It also additionally allow the primary care physician to see the blood move through the hatchling's heart. To find abnormal blood or heartbeat results, a full scan is given to discover abnormalities at every level of the child's body.

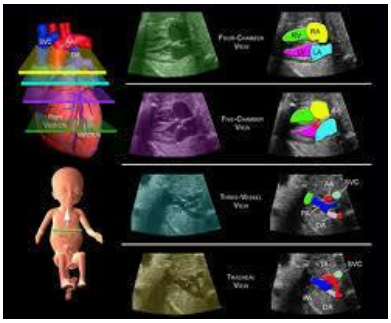

Fig.1.5 Model of Fetal Echocardiogram

Fetal Magnetic Resonance Imaging :

Fetal magnetic resonance imaging (or fetal MRI) utilizes an attractive field and radio waves to make definite photos of an unborn child. This easy test doesn't open the infant to radiation. After ultrasounds and testing, specialists decide the mysterious variations from the norm of the baby. This test gives definite pictures of fetal life structures.

A fetal MRI scan is a non-invasive imaging technique that provides more specific information about a baby's anatomy, such as its anatomical construction, allowing for clearer, more accurate pictures. X-ray, which represents attractive reverberation imaging, utilizes an attractive field, instead of IR radiation, to acquire imgages for assessment. In a ultrafast foetus MRI scan, pictures can be immediately caught by utilizing a "preview" method.

The data given by a foetal MRI is more valuable than that given by standard ultrasound scans, and it can provide even more information on a baby's growth and development. In the second or third trimester of pregnancy, it is performed. In the event of abnormalities in the baby's

central nervous system, spine, or body, this assessment is implemented. A radiologist might use X-rays to confirm or add evidence in difficult cases that involve complex findings on ultrasound.

In the procedure's development, the ultrafast foetal MRI procedure was first completed at Children's Hospital of Philadelphia. The foetal imaging group delivers 600+ foetal MRIs consistently in spite of the 21,000 other MRI scans of youngsters being performed yearly on children in age groups from newborns to eighteen and older.

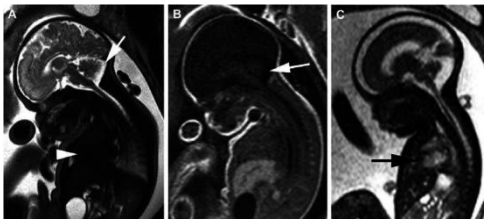

Fig.1.6 Model of fetal MRI

1.2 Consequences of fMRI in Brain Investigation:

The foetal brain is an important part of the body for medical experts; to properly identify the appearance of the foetal brain at various GW, radiologists should familiarise themselves with the typical structure of the foetal brain to be better able to spot and explain foetal brain abnormalities [2-5]. During the most recent twenty years, fetal mental health has become a significant theme in neuroscience because of present day non-obtrusive and computational procedures. The consequences of such procedures permit quantitative portrayal of the fetal brain structure, which incorporates improvement of individual nerve cells and whole

organizations inside explicit brain territories [5]. A few surveys on fetal mental health showed up during the past [6-14].

In-vivo fetal imaging is a significant method in envisioning and assessing the improvement of fetal designs, particularly for fetal brain. While it very well may be obliterating to discover that the baby has an irregularity, pre-birth determination can permit time to settle on educated choices. Examination investigations of fetal MRI of typical brains at various GW permit building up of regularizing measures that can be utilized in early ID of formative brain anomalies [15, 16]. Exploration examinations keep on recognizing an expanding number of explicit quality deformities for brain distortions [17]. The proficient conveyance of hereditary material to the creating fetal brain addresses an advancement in considering mental health and treating of various deadly brain problems [18]. Fetal MRI, particularly with utilizing new groupings, can possibly characterize underlying, physiological, and metabolic parts of brain distortions that can uphold research on quality treatment and lead to the treatment or avoidance of these sicknesses [19-21].

The objective of fMRI information examination is to distinguish connections between's brain actuation and an undertaking the subject performs during the sweep. It additionally intends to find relationships

with the particular intellectual states, for example, memory and acknowledgment, actuated in the subject.

1.3 Essential on behalf of Extraction of Fetus Brain:

In the clinical examination and exploration about fetal brain, there is a need to fragment fetal brain to give quantitative information to fetal biometry. A specialist on brain design can perform manual following on MRI. For examines which include a lot of information, the manual following and division of fetal brain from each cut is tedious, administrator reliant and monotonous. Additionally, such a procedure is probably going to show huge intraobserver and interobserver varieties, hence lessening the legitimacy and meaning of the outcomes. Subsequently, to speed up and exactness of determination, programmed division of fetal brain have been created. In spite of the fact that extraction is a more significant level cycle, it utilizes the words division and extraction entomb variably.

1.4 Goal of Dissertation:

- To perform a literature review on existing methods.
- To use user defined data base and developed a model.
- To compare with manual standard and existing models.
- To use standard database openfMRI, IBSR and develop model for them.
- To develop techniques for Fetal Brain Abnormality Detection.

1.5 Organization of the dissertation:

The thesis remaining sections are organised as follows:

Chapter 2 gives a review of literature on the fetal MRI and fetal brain segmentation algorithms.

Chapter 3 describes the normal and abnormal fetal brain anatomy and the basics of MRI. It also gives the tissue characteristics and orientations of MRI.

Chapter 4 describes image processing approaches applied in the thesis. Methods for measuring their effectiveness are also described. In this chapter, presents the thresholding method, region growing and morphological operations.

Chapter 5 gives the first algorithm for automatic segregation of fetal brain MRI scan using histogram equalization and region growing method.

Chapter 6 gives the second contribution of the thesis. An algorithm for automatic extraction of fetal brain MRI using improved maximum entropy is presented.

Chapter 7 gives the third contribution of the thesis work. In this chapter a method for fetal head identification and brain extraction using Mathematically Modelled Local Fetal Minima.

Chapter 8 gives Fetal Brain Volume Estimation from MRI of Human Fetus.

Chapter 9 gives the conclusions and future scope.

CHAPTER 2

LITERATURE REVIEW

2.1 Introduction

Magnetic Resonance Imaging (MRI) is a fundamental device for the investigation of early human mental health in utero. X-ray shows incredible detail of the creating brain and, as a rule, can give more data about the seriousness of a variation from the norm. This can prompt more educated dynamic by specialists and hopeful guardians.

Precise division of fetal brain from MRI is a critical cycle in pregnancy related issues, however remains very testing because of the profoundly factor size, shape, and life systems of the creating brain, conceivable underlying irregularities, the attributes of the creating tissues, and the nature of the first pictures.

To get a top to bottom information about the fetal brain structure, division of fetal brain divide in a MRI is required. The manual following of fetal brain tissues from MRI takes a lot of time, even an hour for single MRI cut and it is one-sided by the administrator who does the division. k based techniques, self-loader techniques and completely programmed techniques.

Fetal MRI has helped doctors and scientists to understand the growth and size of foetal brain. This knowledge explains why adults have the way they do and why they can't change. Thusly, various division

techniques are there to eliminate fetal brain from MRI. Ultrafast fetal alluring resonation imaging is a non interfering imaging test that offers unequivocal data about anatomic constructions of the infant. Clear, significant standard pictures are quickly discovered using a portrayal strategy. It is necessary to look at foetal brain development because it is essential to finding normal and abnormal emotional wellness and identifying brain growth. In the event of fetal MRI, it is especially trying and gigantic because of the passionate course of the infant, the organs incorporating the highest point of the undeveloped organism, and the irregular hatchling.

The Brain is the basic organ which can oversee and control the impeccable pieces of the human body. The disfiguration in the head/brain can incite different pollutions like, appearance of tumor, contracting of brain, neurological confusion, brain injury, injury, substance lopsidedness, seizures, stroke, dementia [1], Alzheimer Diseases [2], Parkinsons Syndrome, Dementias, Epilepsy, Mental Disorders, Stroke and Transient Ischemic Attack (TIA), and so forth This paper essentially pivots around the fetal brain MRI pictures division. An authoritative point is to thwart or diminish the impact of the illnesses for the kid using the examination on the photos. The fetal brain structure division also strong in seeing the fetal unanticipated turn of events. The fetal brain division

from MRI pictures helps the specialists in getting to the fetal advancement issues.

The goal of this writing survey report is to comprehend the current deals with Fetal MRI Segmentation and their highlights. A definite report has been preceded as a feature of this exploration work in field of clinical medical imaging and related turns of events. The investigation uncovered the focal points and disservices of the current calculations and frameworks accessible and stresses on the requirement for new unique frameworks for the examination, segmenting and preparing of clinical images. The study incorporated various works done by researchers and researchers that have great information in the field and are utilized for the overview of writing. In this part, examines about the different works identified with the proposed works.

The segmentation algorithms are essentially grouped into three kinds. They are: Manual, Semi-automatic and Fully automatic segmentation methods.Previously, the Fetal MRI was segregated physically by the medical specialists. The manual segregation is finished by marking wanted borders straightforwardly onto the crude picture. The master at that point picks power by highlighting a pixel that is by all accounts on the line of a design or the power by hand. Hand-segmentation is time-consuming and prone to high inter-rater and intra-rater variability. To beat these issues, self-loader techniques appeared.

They become famous and utilized generally since the division cycle is quicker than manual division. Yet, the downside of this strategy is that it needs human intercession during the division cycle. To address the downsides of semi-automatic procedures, fully automatic segmentation techniques were created. This method needn't bother with any human mediation. The programmed strategies are not utilized widely as a result of its unpredictability and uncertainness of segmentation brings about various datasets.

2.2 Survey on medical image processing

Haskins, G et al., [3], 2020 the new works that utilization profound figuring out how to perform clinical picture enlistment have been inspected. As every application has its own one of kind difficulties, the creation of the profound learning-based structures should be cautiously planned. Numerous profound learning-based clinical picture enrollment applications share comparative difficulties including the absence of a strong closeness metric for multimodal applications, in which there are huge picture appearance contrasts as well as various fields of view (e.g., MR-TRUS enrollment) [4], the absence of accessibility of enormous datasets, the test related with acquiring divisions and ground truth enrollments, and evaluating the vulnerability of a model's expectation. Application-explicit closeness measurements, patch wise structures, solo methodologies, and variation auto encoder motivated enlistment systems

are models of well-known answers for these difficulties. Moreover, regardless of the complexity of a large number of the techniques examined in this review, resampling and insertion are frequently not among the segments of enlistment that are learned by the neural organization. While scientists began to focus on this perspective [5], the anticipate that more works should fuse these segments into their profound learning-based strategies as the field proceeds to develop. Late victories have exhibited the effect of the use of profound figuring out how to clinical picture enlistment. This pattern can be seen across clinical imaging applications.

Sriramakrishnan, P et al., [6], 2019 built up a technique called as Brain Tumor Segmentation 1 (BTS1) that contains three consecutive stages and these stages upgrade the division and calculation execution of Partial Supervision Fuzzy C Means (PSFCM). The three stages are instatement, change and enhancement. Introduction begins with brain partition extraction utilizing Brain Extraction Method (BEM) calculation for T1 pictures. Alteration in PSFCM is finished by utilizing two marked examples with the help of changed participation lattice and Boolean vector. Execution of BTS1 is improved utilizing three sorts of streamlining and is named as size based advancement (SBO), nearness based enhancement (ABO) and equal based streamlining (PBO) (Kalaiselvi, 2019).

Kalaiselvi et al., [7], 2018 built up a strategy called as BTS2 which is a half and half methodology of predisposition revision joined with the PSFCM grouping to improve the tissue division measure. Time unpredictability of BTS2 is diminished utilizing the parallelization cycle by GPU. There are three stages in BTS2 in particular preprocessing, sequential BTS2 and equal BTS2. In stage 1, the brain extraction and locale of interest (ROI) choice is finished. At that point, the calculation naturally checks the accessibility of designs handling unit (GPU) inside the framework. If not accessible, control moves to stage 3 for equal execution with the accessible GPU arrangement. BTS1 had dice estimation of gray matter, white issue and CSF as 80%, 81% and 31% separately. Computational issue is overwhelmed by the equal BTS2 with the help of GPU CUDA model. String per pixel is utilized to lessen the computational time up to 49X quicker than the consecutive usage (Kalaiselvi and Sriramakrishnan, 2018).

Smith, J. S et al., [11], 2006, A work done by Cha enrolled the strategies for the present status of neuroimaging of brain tumors and talked about three kinds of physiology based MR imaging strategies specifically dissemination weighted imaging(DWI), proton MR spectrosopy and perfusion weighted imaging. They have proposed that the neuroimaging of brain tumors has advanced from a simply life structures based order to one that joins morphologic irregularity with

physiologic changes in extracellular compartment energy, cell digestion, and hemodynamics (Cha, 2006).

Nagpal G et al., [13], 2017, there are different works done utilizing shading measures for clinical pictures. One work is tied in with shading measures utilized for X-beam pictures. Different credits in a X-beam picture may not be unmistakably noticeable in gray scale though a hued X-beam picture can undoubtedly show the credits (Nagpal G 2017). A work done by H Li et al, discusses another methodology for MRI brain picture division utilizing pseudo shading Non evenness and Anti-pressing model with Squares (NAMS). Sub examples are utilized in this technique to lessen repetition. The pseudo hued pictures are then utilized for segmentation of fetal MRI.

Marizzoni, M et al., [12], 2015, A work done by Marizzoni, M et al., researched the two generally significant what's more, generally utilized imaging modalities, for example, MRI and CT checks. They have examined about the huge impails of clinical imaging in patient consideration, specialized improvement of CT and MRI, the utility of difference material in the imaging of brain tumors, which improves the huge discovery and the assessment of brain neoplasms and the part of CT and MRI in the determination of brain tumors.

Pasternak, O et al., [14], 2005, a works done by Assaf and Pasternak, proposed a procedure as dissemination tensor imaging (DTI).

It has gotten quite possibly the most well-known MRI methods in brain research just as in clinical practice. Dissemination tensor imaging empowers representation and portrayal of white issue fascicli in two and three measurements. It has been utilized to consider the white issue design and honesty of the typical and sick brain (various sclerosis, stroke, maturing, dementia, schizophrenia, and so forth) DTI gives an effective device to exhaustive, noninvasive, practical life systems planning of the human brain. This technique sums up the improvement of DTI in the most recent decade as for the explicitness and utility of the procedure in radiology and life structures.

Anand, A. [15] 2017, the author proposed a technique to section tumor with higher exactness. In the preprocessing clamor is eliminated by utilizing Gabor channel. At that point skull stripping is finished by utilizing consolidated techniques for thresholding and morphological activities. After that include extraction is performed with the assistance of Stationary Wavelet Transform (SWT). At last, removed component are given as contribution to the neural organization where highlight are prepared by solo kind of organization i.e. Self-Organizing Maps (SOM). At long last, to fragment the tumor precisely they applied watershed division for high exactness.

2.3 Survey on Medical Image Segmentation

Salem, M. A et al., [8], 2017, Digital pictures and computerized recordings are pictures and movies, separately, which have been changed over into a PC coherent parallel arrangement comprising of legitimate zeros and ones. A picture is an actually picture that doesn't change as expected, though a video develops as expected and for the most part contains moving and additionally evolving objects. A significant element of advanced pictures is that they are multidimensional signs, i.e., they are elements of in excess of a solitary variable. In the traditional investigation of the advanced sign preparing the signs are typically one-dimensional elements of time. Pictures notwithstanding, are elements of two, and maybe three space measurements in the event of hued pictures, though an advanced video as a capacity incorporates a third (or fourth) time measurement too. A result of this is that computerized picture handling, implying that critical computational and capacity assets are required.

Masood, S et al., [9], 2015, it tends to be seen that with progressions during the time spent pursuit and advancement new successful and effective methodologies are still appearing. The strategies order as per the age can be broke down to comprehend this point Development and progress in the field of clinical picture division can be dissected by putting the techniques into various gatherings. This grouping will show us the innovative work did in such manner. Original gathering contains

strategies which require minimal earlier data for handling the picture subsequently includes low level methods. With the progression of time and headway in innovation some new and more successful techniques appeared; second era possesses strategies dependent on improvement, picture and vulnerability models. Third era procedures are exceptionally reliant on earlier data of the picture and require specialists characterized models and rules for order of a picture.

Elnakib, A et al., [10], 2011, precise division of objects of interest is one of the essential necessities of any clinical imaging and CAD framework. As of now, a wide range of shape/ appearance highlights and choice procedures dependent on these highlights are created, tried, and utilized for taking care of use explicit division issues. Because of the quick turn of events and augmentation of clinical picture modalities, new division issues are arising and new techniques are being presented and investigated for their answer highlights and information preparing strategies. The best methodologies consolidate various picture/object. Exact division of 2-D, 3-D, and 4-D clinical pictures to detach anatomical objects of interest for examination is fundamental in practically any PC helped finding framework or other clinical imaging applications.

2.4 Survey on Fetal MRI Segmentation

Kalaiselvi, T et al., [16], 2016, created three strategies for the recognition of brain tumor which are called as BTDM I, BTDM II and

BTDM III techniques individually. In this BTDM I technique, a pre-preparing is finished utilizing altered thresholding technique. In the following stage, tissue division is finished utilizing Fuzzy c Means (FCM). After that irregular Cerebrospinal Fluid (CSF) is distinguished by Fuzzy Symmetric Measure (FSM). It is distinguished among T2 weighted MRI cuts. In BTDM II strategy, picture preprocessing is finished by digit plane cutting. Followed by preprocessing, tissue division is finished utilizing FCM grouping. Anomalous cuts are distinguished utilizing FSM. This is likewise done from T2 weighted cuts. In BTDM III strategy, preprocessing is finished utilizing Top cap, Bottom cap and minima change. Here, tissue division is finished by thresholding strategy. At long last, the unusual cuts are recognized utilizing FSM. Here likewise T2 weighted pictures are utilized. The proposed BTDM techniques were contrasted and FCM and KM bunching and the proposed BTDM strategies produce excellent outcomes for MRI head filters than ordinary FCM and KM techniques. The presentation of BTDM techniques were broke down by the boundaries for example, bogus alert, missed caution and preparing time, and so on.

Karthigai Selvi, et al., [17], 2015, built up a strategy called as Strange Image Detection (AID2) that comprises of three phases to identify the strange pictures from 2D FLAIR image sets. Here an insignificant arrangement of dark level co-occurrence lattice (GLCM) highlights are

separated from typical and anomalous pictures of a volume and afterward the qualities are ordered into two classes by applying least square straight line condition. The pictures which are over the straight line are considered as irregular pictures. AID2 sets aside lesser effort to recognize the pictures in a volume. It can act in all direction of FLAIR pictures since it doesn't think about the spatial subtleties as AID1. Despite the fact that it is sensitive as far as force, it can't actually recognize unusual pictures in antiquity influenced pictures.

Jose, A et al., [18], 2014, A work done by Jose et al., proposed a division calculation, which is done through the k-implies bunching and the fluffy c-implies calculations in which the brain tumor is recognized and its definite area is distinguished. Contrasting with the different calculations the presentation of fluffy c-implies assumes a significant part. At that point K-means calculation is sufficient to extricate it from the synapses. On the off chance that there is any noise present in the MR picture, it is eliminated before the K-implies measure. The noise free picture is given as contribution to the k-means and tumors are extricated from the X-ray picture. At last, inexact thinking strategy was utilized to perceive the tumor shape and position in MRI picture utilizing edge location technique.

Somasundaram, K. et al., [19], 2010, The work done by authors, proposed a programmed strategy to examine the MRI head filters and identify

variation from the norm in brain due to tumors. This technique comprises of four phases: brain extraction calculation, change, fluffy division and fluffy symmetric. This technique is examined utilizing two measures; bogus alert (FA) and missed caution (MA) to measure the presentation of the technique. This technique is absolutely founded on power and is material to MR pictures with single mass impact present with in a MRI brain tumor pictures.

Teo, P. C et al., [20], 1997, a work done by Teo et al., proposed a strategy to portion dim issue from MRI and to make associated cortical portrayals for utilitarian MRI representation (fMRI). The strategy misuses information on the life structures of the cortex and consolidates primary imperatives into the division. To start with, the white issue and CSF areas in the MR volume are portioned utilizing a novel strategy of back and anisotropic dispersion. At that point, the client chooses the cortical white issue segment of interest, and its design is confirmed by checking for pits and handles. After this, an associated portrayal of the dim issue is made by an oblige becoming out from the white issue limit.

Roy, S et al., [20], 2012,A work done by Roy, S et al., proposed a completely programmed calculation to identify brain tumors by utilizing balance investigation. This work distinguishes, fragment the tumor and measure the territory of the tumor. The quantitative investigation of MRI brain tumor permits helpful key pointers of sickness movement. The

complex issue of sectioning tumor in MRI can be effectively tended to by thinking about particular and multi-step moves toward that emulating the human visual investigation measure. The tumor recognition is frequently a fundamental primer stage to tackle the division issue effectively. The analyses appeared great outcomes in complex circumstances. Division of pictures grasps a huge situation in the area of picture preparing. At last in the intelligent division technique, clients can rapidly and productively fragment tumors in MRI pictures.

Kaur et al., [22], 2017, built up a way to deal with recognize the brain tumor in the MRI pictures utilizing Self Adaptive k-implies grouping. While utilizing unique k-implies the client needs to enter the necessary no of groups. It isn't feasible for the client continuously give the right number of groups. To conquer this difficult they proposed a self-versatile k-intends to discover the quantity of groups with the help of tallying the quantity of pinnacles delivered by the histogram. These pinnacle values are taken as the estimation of k. utilizing that pictures are portioned as groups. At long last, the sobal edge discovery procedure is utilized to diminish the thickness of limit lines of districts and improve the exactness of the acquired tumor picture.

Mandwe, A et al., [23], 2016, utilized k-implies grouping to identify the brain tumor from the MRI picture. They utilized middle channel to preprocess the picture what's more, k-implies is received for grouping the

picture. Further, morphological separating and sobel edge identification calculation were utilized to tumor location.

Dawood Dilber, J,[24],2016 , The author proposed a strategy for recognizing the brain tumor utilizing watershed calculation. In this methodology, they utilize dark scale transformation for changing over RGB picture into dark scale picture. At that point a high pass channel utilized to hone the edges just as edge recognition. Finally middle channel is utilized to eliminate superfluous things in the picture. After this, they perform thresholding activities. At long last by applying watershed division procedures to section the tumor structure the MRI picture.

Pandav S, [25], Author proposed a way to deal with distinguish the brain tumor utilizing marker controlled watershed division. At the preprocessing level, they utilize straight separating to smooth the picture. At that point sobel edge location activity is utilized that ascertains the size of slope with the assistance of sobel veil. Subsequent stage is applying watershed division technique; identify the tumor areas without marker expansion. At that point add marker to ROI by utilizing the morphology tasks, opening by reproduction and shutting by recreation. After that computes the territorial maxima to precisely extricate the tumor area. To clean the edges of divided picture they utilize morphological method.

Babu, B. S et al., [26], 2017, author proposed a mechanized framework for brain tumor identification in MRI. They utilized three phases for brain

tumor location as division, include extraction, bunching and characterization. Preprocessing is performed on the preparation informational collection, they utilized editing strategy to eliminate the commotion in the picture and yield the dark foundation. In the division stage, they utilized dynamic form model to section the tumor. Further, Gabor channel, Dim level distinction strategy, dim level histogram and sobel calculation are utilized to remove the highlights. The component feed through SVM classifier and accomplishes 96.5% accuracy.

Gawande, S et al., [27], 2017, proposed a framework to distinguish the brain tumor picture naturally. They utilize 5 stage measures, high pass channel utilized to denoise the picture. Portioning the brain segments by utilizing FCM at that point mark each set of associated part. Further, a few highlights are separated from person locales, they are feed through ANN to decide the tumor is kindhearted or threatening.

Abdalla, H. E et al., [28], 2018, proposed a three phase's strategy to recognize the irregular picture. The cycle pipeline incorporates preprocessing, include extraction and grouping. Smoothening measure upholds denoising, honing supports to improve the picture to advance the difference and surface include. Fourteen Haralicks highlights are given as contribution to the ANN that group the MRI pictures into ordinary and strange.

Shishegar, et al., [29] portrayed cortex interface of a ninety days gestational time of sheep brain. The cut extents were resolved to affirm precision in division results. The cut scopes of internal just as outer cortical surfaces some place in the scope of 0.82 and 0.97 independently, indicating high security in division result got physically. This paper outflanks self-loader strategy. MRtrix programming groups [30] are used for eliminating the streamlines. This paper finishes up with sheep brain through differentiating and the results in self-loader division additionally with customized division.

Vahid Taimouri , et al.,[31] made and investigated a novel design to-slice square organizing approach to manage normally find the brain in fetal X-beam slices through planning a fetal psyche MRI design. It recently used this for brain imprisonment and achieved a high accomplishment rate (94%) and a center limitation precision of 6.45mm in removing a hopping box around the fetal brain. Customized control clears out the prerequisite for manual extraction of fetal psyche zone in volume amusement. The furthermore evaluated the exactness of format to cut planning by handling Target enlistment blunder (TRE) between achievements perceived on the organized fetal brain design and the relating fetal MRI looks at. Creator gained ground speed of 73% and center TRE of 4.2 mm which shows exact enlistment which may be used towards improved development revision, cut level fetal brain X-beam division, and amusement.

B. Caldairou et al., [32] A topologically based grouping method for the cortex division in foetal brain MRI has been proposed, which takes anatomical proficiency preferences into account. The approval conducted on T2 weighted (T2WI) pictures tends to underscore the importance of the proposed strategy, in specific by quantitative and subjective correlation with manual divisions. It has been indicated that the mix of anatomical information, power based highlights and a topological model can recover the cortex. Further work will have little improvement of the division strategy and its approval on extra cases and on 3D remade volumes.

Salehi, et al., [33] developed and tested a two-dimensional U-net and all-voxel completely convolutional association for subsequent segmentation of the foetal brain in foetal MRI. For the voxelwise approach, we used post-processing strategies that maintained the proposed assumption precision in all normal cases ; however, the U-net technique achieved significantly better results on both standard and experimenting test sets with a testing phase at about seconds for every stack without post-processing. This method in dividing the intracranial area of fetal MRI can provoke improved procedures for development area and cure, brain division, moreover, proliferation which are subjects of progressing work.

K.Somasundaram et al., [34] proposed an arrangement of the foetal head and area of foetal psyche as accurately as possible using 2D MRI cuts.

The ROI is normally perceived in this plot using the image's focal point of gravity. The foetal psyche is eliminated through the use of power thresholding and morphological exercises. The strategy's execution is assessed using 25 volumes of foetal data. The figural likeness measures and visual assessment of the delayed effects of the proposed procedure demonstrate that this methodology performs admirably on both conventional and unusual T2-weighted foetal MR images .Michael Ebner et al., [35] In this work, presented a completely robotized pipeline for fetal brain MRI remaking profiting by profound learning based programmed fetal brain confinement furthermore, division and proposed CNN-based coarse division for powerful confinement furthermore, preparing with a multi-scale misfortune work for a fine division of the fetal brain.

Keraudren, K et al.,[36], the limitation technique doesn't require earlier data, for example, gestational age and accomplished prevalent execution in less time. Not at all like [37] which take an entire picture contribution to a CNN, The proposed division technique follows a coarse-to-fine way, and prompts higher division exactness. The author analyses show programmed fetal brain MRI recreations that are practically identical to manual division based reproductions, viably killing the need of any manual interpretation.

Gayathri SP et al., [38] built up a technique to appraise the fetal brain volume from hand sectioned brain divide from the human fetus MRI. The fetal brain volumes at various gestational age were assessed. We discovered that the brain volume increases in a linear way till 32 GW and from that point at a higher rate. At 20GW it is around 67mL, at 26 GW it is 114mL and at 38 GW it is 438mL and the techniques used are Computes the Area and Volume of the Fetal Brain and the cons are segmentations are done by manually.

N. Khalili et al., [39], introduced a modified system for division of the inferior vena cava (ICV) in fetal MRI scan. The procedure uses a multi-scale convolutional neural association in 2dimentional slices to enable taking in spatial information from greater setting similarly as unmistakable neighborhood information. The technique is developed and validated using more than 30 fetal T2-weighted MRI scans (average age 33.2±1.233.2±1.2 weeks postmenstrual age). The set includes ten yields obtained in critical, ten yields obtained in coronal, and ten yields obtained in sagittal imaging planes. All photographs included a reference standard created manually by clarifying the intracranial volume in ten evenly spaced cuts. The modified assessment was conducted by means of planning and evaluating the association by applying channels obtained in the agent imaging plane similarly as solidifying the arrangement data from all image planes. Overall, the modified strategy carried Dice of 0.90

for the essential pictures, 0.90 for the orientation coronal pictures and 0.92 for the sagittal pictures. Joining the arrangement sets achieved ordinary Dice coefficients of 0.91 for the center point pictures, 0.95 for the coronal pictures, and 0.92 for the sagittal pictures. The results display that the surveyed strategy achieved incredible execution in isolating inferior vena cava (ICV) in fetal MR checks paying little brain to the imaging plane and the restrictions are as for picture position.

Jones, S. E et al., [40], Its over-simplification is one advantage of the Laplace procedure. Despite the fact that the Laplace method is applied to the cortical thickness issue here, it very well may be applied to any imaging issue including the thickness between cortical thicknesses. Two surfaces that are discernable and nonintersecting. The volumetric naming is the fundamental portrayal of information Of the three volumes: between the two surfaces and between the two surfaces, Presented another, automated procedure for exploring brain cortical thickness. It is totally three-dimensional, and the thickness is characterized exceptionally for any point that is in the cortex. Building and keeping a library of cortical thickness maps from different brains with ordinary and irregular life systems. The constraints are signal differentiation, picture goal, and registering power. It's not reasonable for irregular brain pictures and for low cortical arch and produce non-consistencies of MRI movements.

Bernhard Kainz, et al., The epic grouping technique that finds the brain was tried by Bernhard Kainz, et al.[41], zeroing in on T2 pictures, and characterized with more than 97 percent exactness. They have likewise presented their own form of the Nvidia CUDA[18] variant. Furthermore, to assess the favored voxel assortment took care of by a descriptor, they utilized Cross-approval lastly acquired the outcomes with a descriptor size between 3to4 millimeters. The creator utilized voxel order technique, for example, Normalization, Non-neighborhood Median Denoising Filter and State-of-the-craftsmanship Classification Forest outfit learning strategy and datasets handles are 50-pre-birth T2 weighted pictures.

In a multi-modular picture situation, Jose Dolz, et al., [42] embraced hyper-thickness connected 3D convolutional unbiased network (CNN) abuses the thick associations. The T1 and T2 pictures are handled independently by HyperDenseNet and afterward interlinked in a thick manner. In cerebro spinal liquid, dim issue, white issue, the dice esteem acquired is 0.956, 0.921 and 0.903 individually and the innovation utilized are quick fourier change that is hyper-thickness associated 3D convolutional neural network and the scope of dataset took care of are 55 cuts from whole brain altas (WBA).

CHAPTER 3

Fetal Brain Magnetic Resonance Imaging

3.1 Clinical imaging modalities:

Clinical imaging modalities, for instance, incorporates attractive reverberation imaging (MRI), ultrasound, clinical radiation, angiography and registered tomography (CT) scanners. What's more, to a few examining strategies to imagine the human body for symptomatic and treatment purposes.

Clinical imaging modalities, for instance, incorporates attractive reverberation imaging (MRI), ultrasound, clinical radiation, angiography and processed tomography (CT) scanners. Likewise, to a few checking procedures to imagine the human body for analytic and treatment purposes. Likewise, these modalities are exceptionally valuable for persistent development, concerning the advancement of the sickness state, which has just been analyzed, and additionally is going through a therapy plan. By far most of imaging depends on the utilization of X-beams and ultrasound (US). These clinical imaging modalities are engaged with all degrees of clinic care. Moreover, they are instrumental in the general wellbeing and preventive medication settings just as in the remedial and further reaching out to palliative consideration. The fundamental target is to build up the right findings.

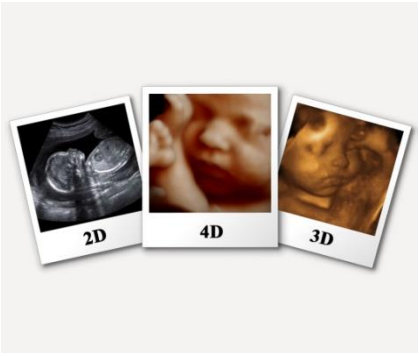

Fig. 3.1 Fetal Imaging Modalities

Medical radiation:

Clinical imaging modalities in a clinical setting are a fundamental commitment to the general determination of the patient and help in the choice of a general treatment plan. New advances in medical science have created new medical imaging procedures. Also present in this wide range of imaging modalities are specialties like atomic medication, PET scans, MRI (an MRI using sound waves), and ultrasound. Generally, imaging for clinical radiation purposes includes a group of radiologists, radiographers and clinical physicists.

Positron emanation tomography (PET):

Positron emanation tomography checking isn't regularly acted in pregnancy yet should be possible whenever required. Fetal dosages of radiation can be limited, and the case embodies the protected use of positron discharge tomography/figured tomography in pregnancy. A 38-year-elderly person in her first continuous pregnancy introduced at 28 weeks' incubation with indicative hypercalcemia. Given a past filled with

parathyroid carcinoma, repeat was suspected. Ultrasound and attractive reverberation imaging neglected to find the sore. In any case, positron emanation tomography/registered tomography recognized a guilty party supraclavicular lymph hub. This was extracted under neighborhood sedation bringing about standardization of parathyroid chemical and calcium levels. A term, sound infant was conveyed. The utilization of positron outflow tomography/figured tomography is adequate when demonstrated, and there are alterations to conventions that can additionally restrict hazard.

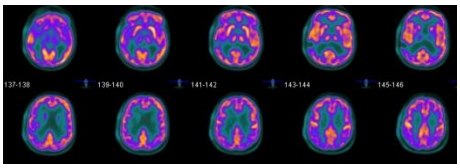

Fig. 3.2 Positron emanation tomography

3.1.1 Ultrasonography (US)

US is utilized to assess the improvement of the baby. It makes a picture of the infant in the mother's belly (uterus). It is alright for both baby and mother, is moderately cheap, permits constant imaging, and is promptly accessible. The underlying output is performed at around 8-14 GW to affirm the pregnancy and decide the due date, and next sweep is at around 18-21 GW to affirm for primary variations from the norm, specifically the head and spine of the embryo [47]. The test might be done either on the mother's midsection (transabdominal) or in the vagina (transvaginal).

There are a few kinds of fetal US:

- Standard US: This strategy utilizes sound waves to make two-dimensional pictures on a PC screen.
- Doppler US: This picture shows the development of blood through the umbilical line, in the hatchling's heart, or between the baby and the placenta.
- 3-D US: This picture shows a reasonable 3D picture of an unborn infant.

3.1.2 Magnetic Resonance Imaging (MRI)

Fetal MRI has been utilized for more than 20 years with the primary report in 1983[48]. It is normally performed after 20 GW when the primary strides of organogenesis are finished. At this stage, the fetal brain comprises of a combination of creating dim matter, creating white matter and other transient constructions like the germinal network. Different utilizations of Magnetic Resonance imaging to the baby are dispersion weighted MRI to contemplate the brain network [48], and utilitarian MRI to examine the brain movement of the hatchling [49].

- **Diffusion MRI**

Imaging techniques such as DWI and diffusion tensor imaging (DTI) are MRI methods [50,51] that give proportions of microstructural tissue honesty [52, 53]. They utilize quick MRI acquisitions to give directionally delicate proportions of water dissemination inside tissue.

Exploration from clinical imaging has shown that DWI is doable in some fetal brain examines [54, 55] where there is restricted movement and that it can give huge extra data in instances of suspected abnormalities[56, 57]. Nonetheless, concentrates regularly have been restricted to few cuts and have restricted anatomical inclusion.

Fetal DTI concentrates regularly include the obtaining of huge number of directional estimation pictures to give a more complete profile of water dissemination at each point in the brain, yet are accordingly considerably more delicate to movement. Despite the fact that it requires a more extended imaging time, it has end up being fruitful [58] in giving experiences into the development of associations inside the brain. Nonetheless, quite a bit of this in utero research has been restricted to investigations of more established embryos or situations where the fetal head is occupied with the maternal pelvis, where fetal movement was compelled, and is consequently not yet doable for general clinical imaging or bigger scope neuroscience considers.

Functional MRI

The fetal brain action is considered utilizing practical attractive reverberation imaging (fMRI) which was presented by Hykin et al. [59]. fMRI is noninvasive and, in light of the fact that it doesn't utilize radiation, represents no danger to the mother or creating baby. It distinguishes blood oxygen level-subordinate (BOLD) changes in the

MRI signal that go with changes in fetal brain movement. Such fMRI pictures can give an early admonition of embryos which are in danger for brain injury.

3.2 Basic Principles of MRI

A MR scanner creates a steady attractive field B0, whose impact is to adjust the attractive snapshots of protons (hydrogen cores) with the course of the B0 field [60]. A radiofrequency (RF) beat is applied to the protons, briefly making a second attractive field B1 symmetrical to B0 that annoys the harmony. When the RF beat is eliminated, the cores realign themselves with the attractive field B0. This re-visitation of harmony includes unwinding measures, portrayed by time constants and the emanation of electromagnetic radiation, from which MR pictures are inferred. The MR signal as distinguished by the scanner is inspected in the spatial recurrence area (k-space), and from that a spatial picture is reproduced utilizing a Fourier change. Force esteems in MRI result from the proton thickness, which is higher in water and fat tissue. The longitudinal unwinding time T1 gives the recuperation pace of longitudinal magnetisation, and the cross over unwinding time T2 gives the rot pace of cross over magnetisation. To get an alternate weighting between these three boundaries, MRI can utilize groupings with various reverberation time TE, which is the time between the utilization of a RF excitation beat and when the focal point of k-space is encoded, and

reiteration time TR, which is the time between two progressive excitations of a similar cut or piece. The TE is typically more limited than the TR. A long TR and short TE compare to a proton thickness weighted (PD) grouping, a short TR and TE to a T1-weighted succession, and a long TR and TE a T2-weighted arrangement. Table 3.1 shows the circumstance utilized for gaining various sorts of pictures. To decrease the output time while evading cut cross-talk ancient rarities, which relate to obstruction between adjoining cuts, touching cuts are not gained consecutively yet in an interleaved way across time (Fig.3.3).

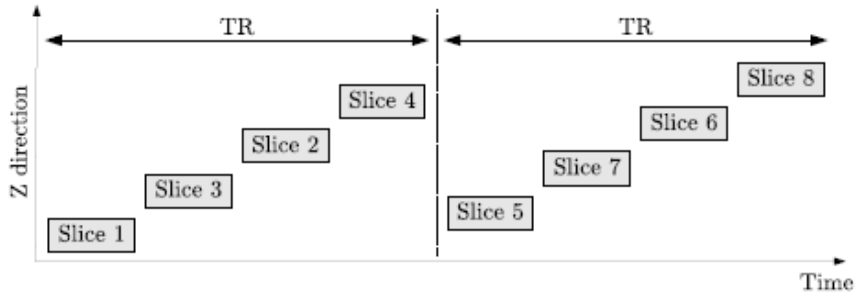

Fig. 3.3 Adjacent slices acquired in different time [61]

Table 3.1 MR imaging techniques in terms of TR and TE

Weighting	TR	TE
T2	long	Long
T1	short	Short
PD	long	Short

3.3 Fetal MRI

Fetal medical imaging is gained on 1.5 T (or higher) MRI scanners utilizing middle or cardiovascular staged exhibit surface curls to permit expanded inclusion of the fetal head and expanded sign to-commotion proportion. The mother lies recumbent (Fig.3.4) throughout the test (ordinarily 45-60 min.)

Fig.3.4 fMRI scan [62]

The pictures can be gotten as T1-w or T2-w groupings in three directions. For ideal sign force in the ensuing arrangements, the fetal brain (district of interest) ought to be inside the focal point of the curl; if this isn't the situation, the loop must be repositioned [63].The most broadly utilized grouping in fetal imaging is T2-w single shot quick turn reverberation (SSFSE). This technique can freeze fetal movement, so every individual cut is by and large ancient rarity free and a solitary cut is obtained in under 1 second, yet piles of cuts needed to give entire inclusion of the fetal life structures might be commonly conflicting. Progressions of T2-w

pictures are acquired in the pivotal, sagittal as well as coronal planes symmetrical to the fetal brain (Fig.3.5 and 3.6). It is useful for phenomenal depiction of brain life structures. Ideal cut thickness is 3 mm with no hole or with cut cover. In certain patients, a 4 to 5mm cut thickness could be required on account of sign to-commotion contemplations [64].

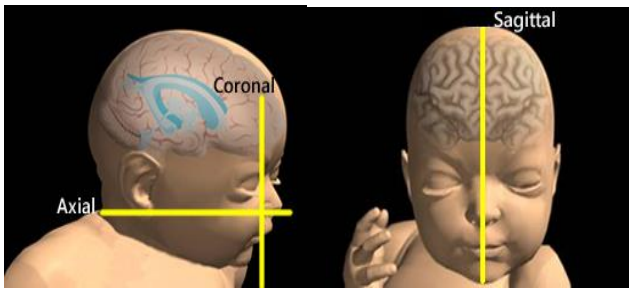

Fig.3.5 MRI orientations in Axial, Coronal & Sagittal plane [65]

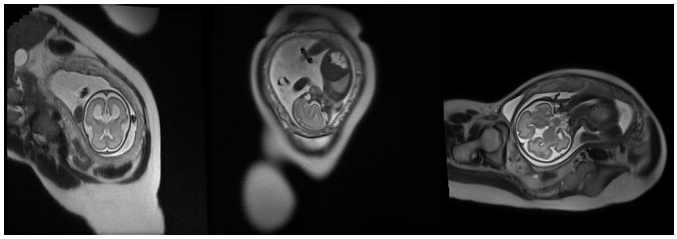

Fig.3.6 fMRI in Axial, Coronal & sagittal plane

T1-w pictures are regularly obtained utilizing ultrafast inclination reverberation groupings or super quick low-point shot. Contrasted with SSFSE securing plans, angle reverberation successions are more inclined to corruption by movement relics and have lower spatial goal. Albeit fetal neuro life structures is less regularly portrayed by T1-w (Fig.3.7) and it is useful in recognizing drain, miniature calcification, fat testimony, and myelination. Fetal pituitary, thyroid, liver, and meconium inside the

entrails are additionally portrayed by T1-w picture hyper force [4], [15], [16].

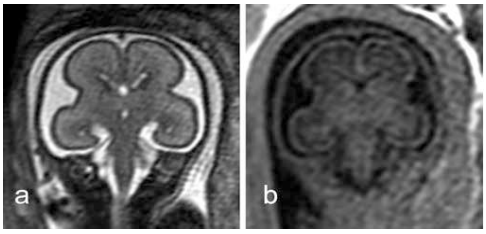

Fig.3.7 fetal brain in (a) T2-w and (b) T1-w MRI

3.4 Clinical Indications for MRI of Fetal Brain

Fetal medical MRI scan straightforwardly picture the creating designs of the fetal brain, like the ventricles, ventricular dividers, germinal grid, creating white matter, and cortex, and offers better tissue balance contrasted and also ultrasound, subsequently permitting improved distinguishing proof of fetal brain variations from the norm. The most widely recognized presumed irregularities are ventriculomegaly, associated agenesis with corpus callosum, complexities of monochorionic twinning, and back fossa variations from the norm which are mysterious in US. The data given by the fetal MRI can help in pre-birth guiding of the current pregnancy just as advising of the repeat danger in future pregnancies.

3.5 Normal Fetal Brain Structure

In utero MRI can assist with understanding the typical mental health beginning at about four months of incubation [16], [66-68]. Fetal brain

has high water content (40%) versus 20% in grown-up, which permits the brilliant tissue balance goal with SSFSE T2 weighted pictures.

3.5.1 Sulcation

During growth, the outside of the fetal brain bit by bit changes from smooth to one with various cortical infoldings or sulci. Sulcal improvement is a marker of cortical development and utilized as a pointer of fetal development. Sulcation tourist spots showed up in the request anticipated by anatomic examinations, however with slack of 0 two months [69]. Essential sulci will in general shape first, trailed by progressively complex auxiliary and tertiary sulci [70]. By and large, a sulcus at first shows up as a simple, superficial, and wide space on the outside of the brain. It at that point dynamically extends and limits with possible development of optional and tertiary sulci.

3.5.2 Ventricles

Ventricle dividers are critical for typical mental health and can be examined using foetal magnetic resonance imaging. The ventricular zone, known as the germinal framework, is considered the deepest surface of the foetal brain hemisphere. The ventricles zone is already thick before the incubation period begins (Fig.3.8). A faint T2-w and good T1-w signal appears, both of which spread out over the ventricles. As with other organs, it tends to decrease in thickness in the third trimester,

especially at younger gestational ages, as ependymal cells emerge to cover the decreasing mass of the lopsided ventricle.

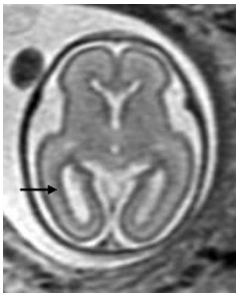

Fig.3.8 Ventricular zone at 23 GW (bolt)

3.5.3 Corpus Callosum

The corpus callosum or callosal commissure creates somewhere lies in the range of 8 to 20GW. It is the biggest commissural association (Fig.3.8a) of the brain halves of the globe and is personally identified with the arrangement of the foremost and hippocampal commissures too. Fetal MRI is the most effective way to survey the corpus callosum, which can be done using slender (3 mm) medial sagittal images. The region in the ventricles appeared to be of higher quality than the fornix with its T2 hypointense curvilinear structure. In contrast to other things, the corpus callosum of a child is uniform in size. A callosum grows as gestation grows.

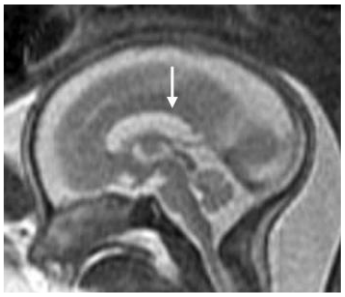

Fig.3.8a Normal corpus callosum appearance at 26 GW (arrow)

3.5.4 Hippocampus

The hippocampus start to create by eighth GW. It is obvious on fetal MRI as a T2- hypointense lesion through the average surface of the transient flap nearby the hippocampal sulcus [71] which is probably the most punctual sulcus distinguished by fetal MRI. The hippocampus (HC) is at first situated vertically, and goes through reformist turn to show up more flat in direction by around 21-24 gestational age (Fig.3.9). Using the fetal MRI technique to detect the fetal hippocampus's rotation is possible through detecting the hippocampus's infolding point, which appears to increase in complexity as the fetus matures.

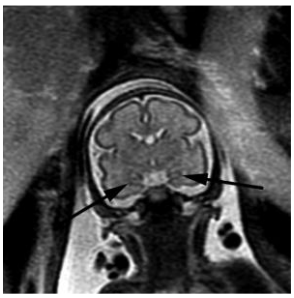

Fig.3.9 fbrain show horizontally oriented hippocampus at 27 GW (arrows).

3.5.5 Deep dim cores

The presence of the profound dim cores (Fig.3.10) on fetal MR scan relies upon the gestational week of the hatchling. The hypointense to isointense profound dim cores were already visible as they are developing alongside the white matter in T2-w pictures. Hyperintense on T1-w images, they appear more powerful at near 27 GW [72].

Different designs of the creating brain can likewise be pictured by fetal MRI in many babies as ahead of schedule as 19 GW and on the whole embryos at > 26 GW.

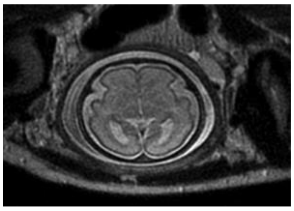

Fig.3.10 Axial slice show subtle hypo intensity of the deep gray nuclei at 27 GW (arrows).

3.6 Abnormal structure of Fetal Brain

Fetal MRI can straightforwardly picture the creating designs of the fetal brain (like the ventricles, ventricular dividers, germinal lattice, generating white matter, and also cortex) and always offers good tissue contrast contrasted with US, it permits enhanced recognizable proof of brain irregularities for example, ventriculomegaly, agenesis of corpus callosum, Posterior Fossa anomalies.

3.6.1 Ventriculomegaly

Ventriculomegaly (Fig.3.11(a)) is the most widely recognized CNS irregularity distinguished on pre-birth US [73] and is perhaps the most well-known signs for fetal MRI. It is characterized as the widening of ventricles to more prominent than 10 millimeters on US. Estimations of the atrial width on pivotal pictures have been accounted for utilizing fetal MRI [74-76]. Despite this, it is worth noting that MRI estimates of ventricular size may be up to 2 mm greater than estimates from US imaging in the plane of maximal lumen diameter. When estimated in the coronal plane, both MRI and US estimates of the ventricular chamber are quite accurate [77].

3.6.2 Agenesis of Corpus Callosum

The corpus callosum creates between gestational weeks 8 and 20 GW and it is very best surveyed by fetal MR scan utilizing slim (3 millimeters) midplane sagittal pictures. Agenesis of corpus callosum (ACC) (Fig.3.11 (b)) is an uncommon problem and it is described by a fractional or complete nonappearance (agenesis) of a region of the brain that associates the two brain halves of the globe. The analysis of ACC is preposterous before 22 GW [78] and along these lines they are all the more effortlessly identified in fetal MRI as contrasted and pre-birth US.

3.6.3 Posterior Fossa Abnormalities

Fetal MRI permits direct perception of the cerebellar halves of the globe, vermis, and brainstem in three symmetrical planes and serves to appraisal the morphology. It is useful in assessing variations from the norm of the back fossa like Dandy-Walker mutation (Fig.3.11 (c)), Dandy-Walker variation, uber cisterna magna, arachnoid pimple, Blake pocket sore, cerebellar dysplasia, cerebellar hypoplasia, cerebellar discharge and so forth Agenesis or hypoplasia of the cerebellar vermis in relationship with a broadened back fossa, expanded retrocerebellar liquid space (uber cisterna magna), raised tentorium, and the fourth ventricle cystic enlargement which is alluded as Dandy–Walker abnormality are straightforwardly pictured by fetal MRI. Milder types of vermian hypoplasia with a more ordinary seeming back fossa have been alluded to as the classic Dandy–Walker variation (DWv).

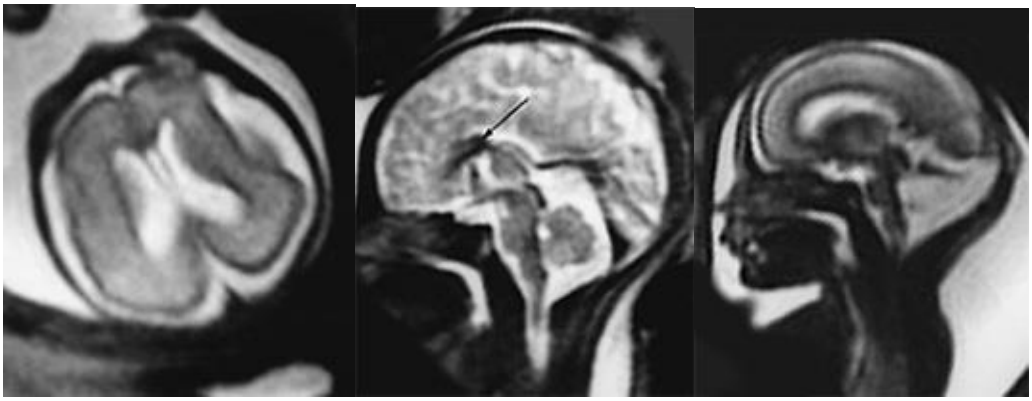

(a) (b) (c)

Fig.3.11 Fetal brain abnormalities (a) Ventriculomegaly (b) corpus callosum absence (arrow) (c) Dandy-Walker malformation

3.7 Challenges in the Automated Analysis of Fetal Brain in MRI

- The self-assertive position and direction of the hatchling.
- The hatchling is washed in amniotic liquid and encompassed by maternal tissues.
- Large inconstancy fit as a fiddle and size of fetal mental health.
- The presence of movement antiques brought about by both the embryo and the mother.

CHAPTER 4

Basic Image Processing Methods and Evaluation Metrics

4.1 Introduction

In this part, presents the fundamental picture preparing strategy and different techniques that utilizes for growing new strategies to remove fetal brain parcel from fetal MRI. Measurements utilized for assessing the presentation of the proposed techniques are additionally given in this part.

4.2 Thresholding

Thresholding is a non-straight interaction of registering or choosing an incentive for the force of a pixel that will isolate the power estimation of the pixels in a picture into two districts [79]. There are numerous productive techniques to locate the ideal limit esteem. The edge esteem is generally chosen by inspecting the picture histogram. Image histograms track pixel counts for each dim level to show picture levels. In the perfect thresholding method, a limit esteem is utilized to isolate the picture into light and dull areas. It can likewise be gotten by iterative technique and utilized the Otsu's thresholding for changing over the dark level picture into a parallel picture.

4.2.1 Otsu's Thresholding Method

Otsu's technique [80, 81] is utilized to discover the limit esteem which limits the intra-class fluctuation (inside class difference) or augments the

between class change (between – class difference) to isolate the information picture into two classes to create the twofold picture. This thresholding strategy depends on calculations performed on histogram of a picture.

Let the set {0, 1, 2,3,4,….., L-1} presents the intensity level in an M X N size image. And n_i represents the no. of pixels which have an intensity value i, in that image. So the total no. of pixels is

$$MN = n_0 + n_1 + n_2 + \ldots + n_{L-1}.$$

The normalized histogram is given by

$$P_i = \frac{n_i}{MXN} \qquad (4.1)$$

where P_i is the probability of occurrence of that particular intensity level.

Hence $\sum_{i=0}^{L-1} P_i = 1, \quad P_i > 0$ (4.2)

Suppose, if the selected a threshold T(k)= k, 0 < k < L-1, and use it to divide the image into two regions (or) classes C_1 and C_2, where class C1 consists of all intensity values from 0 to k, and C_2 consist of the pixels with values in the range k+1 to L-1.

The probability $P_1(k)$ that a pixel is assigned to c1 is given by

$$P_1(k) = \sum_{i=0}^{k} P_i \qquad (4.3)$$

Similarly for class C_2

$$P_2 = \sum_{i=k+1}^{L-1} P_i = 1 - P_1(k) ,$$

Since $P_1(k) + P_2(k) = 1$

$$P_2(k) = 1 - P_1(k) \tag{4.4}$$

Mean intensity value of the pixels assigned to class C_1 is

$$m_1(k) = \sum_{i=0}^{k} iP\left(i/C_1\right) \tag{4.5}$$

where, $P\left(i/C_1\right)$ denote probability of i occurring in C_1 and multiply by i value. By Baye's theorem,

$$P\left(A/B\right) = P\left(B/A\right).P(A)/P(B) \tag{4.6}$$

Using the Eqn.(4.6), get Eqn.(4.5) as:

$$m_1(k) = \sum_{i=0}^{k} iP\left(\frac{C_1}{i}\right)\frac{P(i)}{P(C_1)} \tag{4.7}$$

But probability of C_1 is $P(C_1) = P_1(k)$ .Inside class C_1, the probability of C_1 is $P\left(\frac{C_1}{i}\right) = 1$. Therefore, the probability within the same class is 1. Hence Eqn.(4.7) becomes

$$m_1(k) = \frac{1}{P_1(k)}\sum_{i=0}^{k} iP_i \tag{4.8}$$

Similarly, the mean intensity value of the pixels assigned to class C_2 is

$$m_2(k) = \frac{1}{P_2(k)} \sum_{i=k+1}^{L-1} iP_i \quad (4.9)$$

The cumulative mean upto level k is given by

$$m(k) = \sum_{i=0}^{k} iP_i \quad (4.10)$$

and the average intensity of the entire image is given by

$$m_G = \sum_{i=0}^{L-1} iP_i \quad (4.11)$$

But,

$$P_1 m_1 + P_2 m = m_G \quad (4.12)$$

and also $P_1 + P_2 = 1$ (4.13)

To determine the threshold's goodness at level k and, use the normalised, dimensionless metric ( ) as follows:

$$\eta = \frac{\sigma_B^2}{\sigma_G^2} \quad (4.14)$$

whereσ_G^2 is the global variance , given by

$$\sigma_G^2 = \sum_{i=0}^{L-1} (i - m_G)^2 P_i \quad (4.15)$$

andσ_B^2 is the between class variance , given by

$$\sigma_B^2 = P_1 (m_1 - m_G)^2 + P_2 (m_2 - m_G)^2 \quad (4.16)$$

Eqn.(4.16) can also be written as :

$$\sigma_B^2 = P_1 P_2 (m_1 - m_2)^2 \tag{4.17}$$

$$= \frac{(m_G P_1 - m)^2}{P_1(1-P_1)}$$

where, m_G is constant and P_1 is variable.

From the above Eqn.(4.17), that the larger the difference in (m_1 - m_2) larger will be σ_B^2. It illustrates that the between variance classes is a measurement of how separable the classes are. As it is a constant, so it's a separability measure, and maximising means maximising as well. The between class variance σ_B^2 for the threshold k is computed using Eqn. (4.17) as:

$$\sigma_B^2(k) = \frac{[m_G P_1(k) - m(k)]^2}{P_1(k)[1-P_1(k)]} \tag{4.18}$$

Therefore to get a optimum threshold value, k^*, maximize between class variance $\sigma_B^2(k)$:

$$\sigma_B^2(k^*) = \max_{0 \le k \le L-1} \sigma_B^2(k) \tag{4.19}$$

Once k^* is achieved , f(x,y) an input is extracted as :

$$g(x,y) = \begin{cases} 1 & iff(x,y) > k^* \\ 0 & if(\, f(x,y) \le k^* \end{cases} \tag{4.20}$$

For x=0,1,2,3,4,5,6…,M-1 and y=0,1,2,3,4,5,6…,N-1.

Otsu's algorithm :

1. First calculate the input image normalized histogram. The histogram component is denoted by the P_i , i=0,1,2,3,4…,L-1.
2. Calculate the cumulative sums, $P_1(k)$, for k =0,1,2,3,4,5,…,L-1, by using Eqn.(4.3)
3. Calculate the cumulative means, M(k), for k=0,1,2,3,4,5,6…,L-1, using Eqn.(4.10)
4. Find global intensity mean, M_G, by using Eqn.(4.11)
5. Calculate the between-class variance, $\sigma_B^2(k)$, for k=0, 1, 2,3,4,5,6…,L-1, using Eqn.(4.18)
6. Achieve Otsu threshold (k^*), as a K value for which $\sigma_B^2(k)$ is maximum.
7. Take k^* as the optimum threshold T_{opt}.

4.3 Morphological Operations

Morphological operations [82-84] are known as a shape based methods for image processing. These operations are performed either to separate or join regions by using structuring elements (SE), as shown in Fig.4.1. The two basic mophological operations are dilation and erosion.

Some other operations are opening, closing, and top-hat (white-top-hat) and bottom hat (black-top-hat) which can be derived from dilation and erosion.

0	1	0
1	1	1
0	1	0

Fig. 4.1 A Structuring Element (SE) of size 3X3

4.3.1 Erosion Operation

It can be done either on a gray scale image or in binary image. In this thesis all the proposed erosion operations are done on binary images and use this process to disconnect weakly connected regions. Erosion achieved by using structuring element SE. The SE is applied on each and every pixel positions in X (input image) and also compared with pixel corresponding neighbourhood in an image, and fits the X (input image). So Y(i,j) = 1 if structuring element fits to X otherwise i twill be 0, the same will be repeated for every pixel coordinates (i,j).

Erosion operation is represented by :

$$Y = X \ominus SE \tag{4.21}$$

where, $\ominus$is the erosion operator.

4.3.2 Dilation Operation

Dilation is a process of adding some pixels to the image boundaries and it is obtained by applying structuring element. For this, SE is to placed on every pixel positions in X (input image) and compared with the pixel corresponding neighbourhood, Here Y (i, j) = 1 if structuring element hits X otherwise i twill be 0, the same process is repeated for every pixel coordinates (i, j).

Dilation operation is represented by :

$$Y = X \oplus SE \qquad (4.22)$$

where, $\oplus$ is the dilation operator.

4.3.3 Hole Filling

A hole is an area in a grey or black-and-white image that has dark pixels surrounded by white pixels or black pixels surrounded by white pixels. More details about hole can be found in Sonka et al. [84]. Let's consider the following. Consider that each region (denoted as Ri, , and I = 1…n) is an area with a set of n disjoint (and non-touching) points that have a relationship to be contiguous, and these regions cant touch the image limits . Region R combines all regions $R_{i.}$ R^c is the region complement with respect to the image. The subset of R^c is known as a background region and rest of the part is known as a holes.

Dilatation, complement and intersection are used by the hole filling algorithm. Let A be a set of connected 8-points, where each point lies within a background (hole). You will be given a point in each hole, and your assignment is to fill all holes. Begin by creating a vector, X_0, made up of zero values of the same length as A. Locations in X_0 which correspond to the pixel are assigned the value 1. SE with 4-connected neighbours is given in Fig.4.2.

0	1	0
1	1	1
0	1	0

Fig.4.2 Structuring element SE with 4-connected neighbours

The below operation is applied to fill the holes with all 1s in X_k :

$$X_k = (X_{k-1} \oplus SE) \cap A^c \qquad (4.23)$$

In above equation, k = 1,2,3,4,5,6…

The algorithm will be stop at step k where $X_k = X_{k-1}$ .At the end, all the holes are filled in X_k. Fig. 4.3 shows the hole filling process in a binary image.

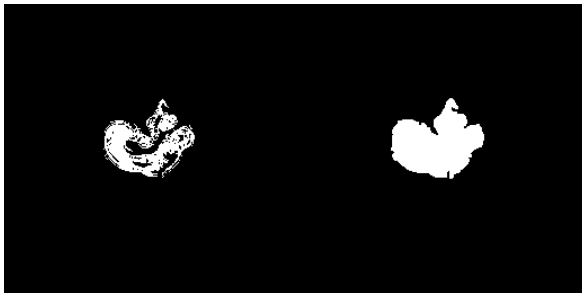

0	1	0
1	1	1
0	1	0

(a) (b) (c)

Fig.4.3 Hole filling (a) binary image with hole (b) Hole filled binary image (c) SE

4.4 Labeling

An image has different objects in it. When such an image is binarized, different regions are obtained. It is then necessary to identify each of the region (representing different objects) in the binary image. For that each region is assigned a unique label and processed further. This is known as region labeling. Labeling regions with run length encoding is a quick and easy method. The algorithm [84] consists of two stages. The first pass analyses the runs for neighbourhood and labels them row-by-row. The first pass's label collision problem is resolved in the second pass.

1. First Pass: Create a new label for each continuous run that is not part of the image's background in the first row.
2. Compare the positions of runs in the second and subsequent rows.
    a. Assign a new label to any run in a row that does not have a neighbour (in the 4 or 8 sense) in the previous row.

b. Assign the previous row's label to the new run if a run is exactly adjacent to one of the previous row's runs.

c. A label collision has occurred if the new run is adjacent to more than one run from the previous row.

Collision data is stored in an equivalence table, and the new run is labelled with the label of any of its neighbouring runs.

3. Second Pass: Scan the image carefully and re-label it using the equivalence table.

4.5 Largest Connected Component (LCC)

When regions are labeled, it is then possible to find the area of each distinct region. Using the area, LCC out of several regions, in given image can be found out. Let the given image R consists of several regions R(i), i=1,2,3.4…...n. such that:

$R = \bigcup_{R(i)}$, i=1,2,3,4,5,6,……,n.

Assume $R_A(i)$be the area of the i^{th} region. largest connected component R_{LCC} in the obtained as :

$$R_{LCC} = R(arg \max R_A(i)) \quad (4.24)$$

In above equation, $R_A(i)$ is the area of i^{th} region R(i) and is the total number of pixels in that region.

4.5.1 2-D Region Growing

Region growing [85, 86] is a technique used to divide an image into non overlapping regions. In terms of intensity, each pixel in each region is similar. Generally, region growing segmentation technique depends on

seed selection and a threshold selection which is used as stopping criteria. Selection of seed point depends on the user criteria that define a region. Then the region is grown from this initial seed and it is compared with its neighbor pixels either 8-neighbour or 4-neighbour. Sample image blocks considered for region growing are given in Fig.4.4.

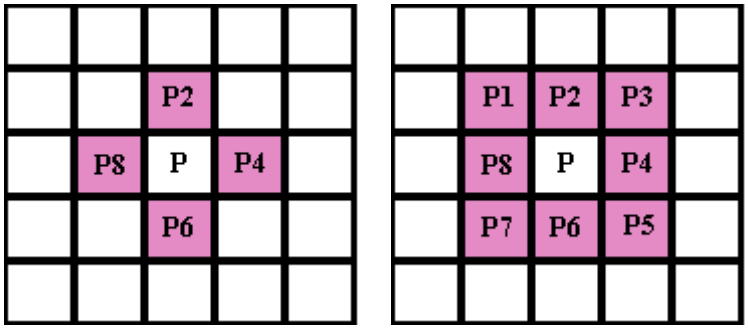

(a) (b)

Fig.4.4 Sample image blocks for region growing as(a) 4- neighbor pixels (b) 8-neighbor pixels with (x,y)as the initial seed pixel.

If the neighboring pixel intensity is within the range of defined threshold value, then the pixels are appended with the region in which the seed pixel belongs to, otherwise the pixel is left out. This process is repeated for all intensity upto the threshold value. Region growing process is presented in Fig.4.4. Consider that a pixel in the middle of the region grows outward from a seed point. There are 8 pixels in the 3x3 square immediately surrounding the centre pixel that fulfil the condition for a successful matching after the first run. The square has gotten 3x3 and its pixels are all located together in a region.

In the second iteration, the pixels in the 5x5 neighborhood are examined for similarity condition. There are 16 new pixels in the 5x5 neighborhood, out of which 9 pixels satisfy the similarity criterion. These pixels are now included in the region. This growing process is continued until the stopping criterion is met. Thus the region is grown to a level as shown in Fig.4.6.

After looking at the first iteration's results, the algorithm examines pixels in a 5x5 section. Among the new pixels in the 5x5 area, 9 meet the similarity criteria. The region now includes these pixels. The process is repeated until it stops. As shown in Fig. 4.5, the region is at that level.

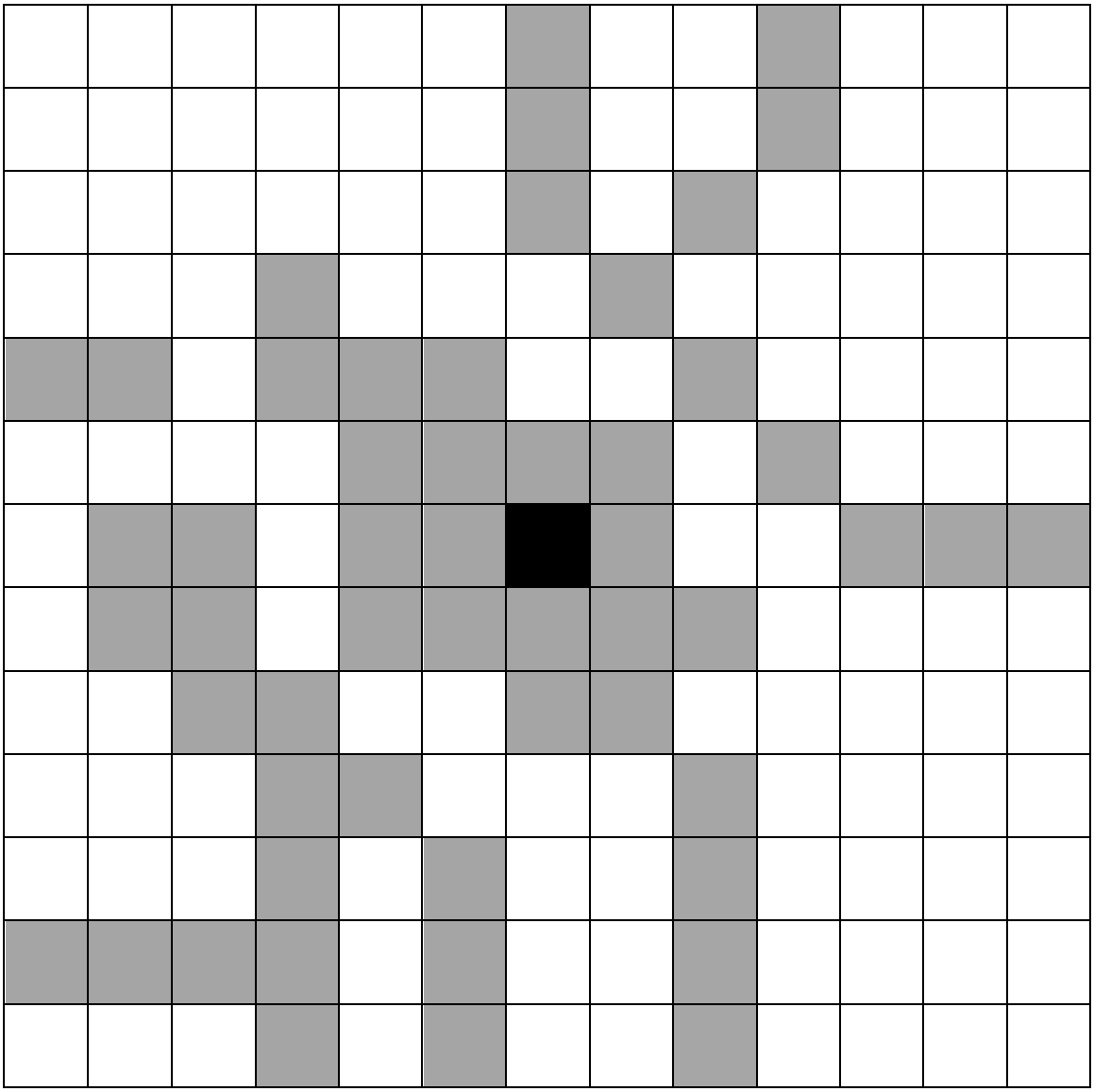

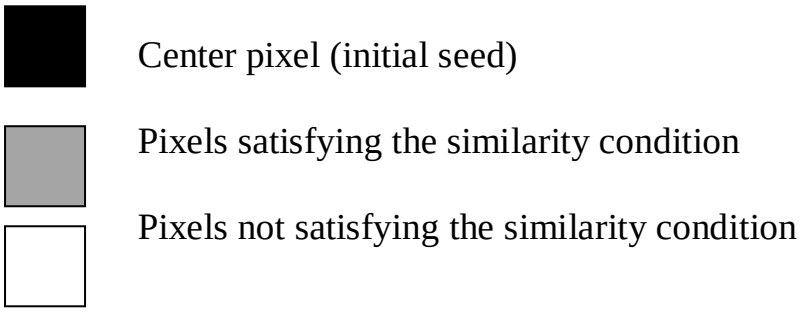

Fig.4.5 A pixel map of the region growing method.

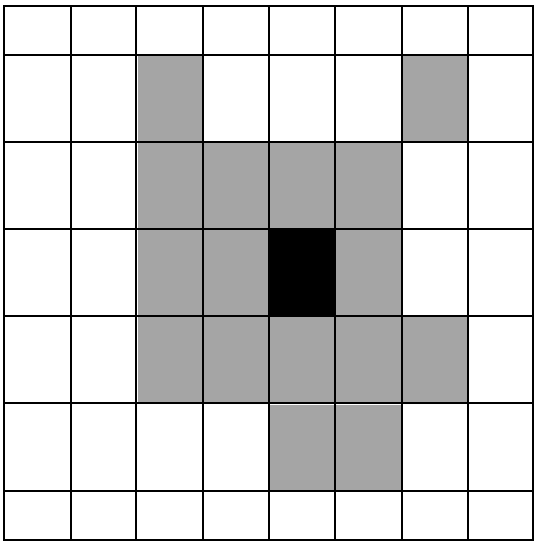

Fig.4.6 Image obtained from Fig.4.5 by region growing

The region growing method makes use of following properties:

a. The region must be fully segmented and contain every pixel.

   $R = \cup_{i=1}^{n} R_i$ where, R_i is an i[th] fully connected region.

b. The region must be disjoint i.e. $R_i \cap R_j = \emptyset$ for all i = 1,2,…,n. So that a clear segmentation from each other can be found.

c. When a pixel's grey level falls within the range of that region, it is said to belong to that region.

The make use of 2D region growing method. In proposed method and use center pixel in the MRI as initial seed for region growing. A growing criterion will be defined so that at each step, the neighboring intensity that fall in this growing criteria will be added to the region. The growing

process will continue until there is no other neighboring intensity of the region of interest (ROI) that satisfies growing criteria.

4.6 Contrast Enhancement using Bi-Histogram Equalization

Brightness-preserving bi-histogram equalisation (BBHE) [87] keeps the image's mean brightness while increasing contrast. The BBHE first divides an image into two subimages based on its mean. It contains two subimages, one for samples less than or equal to the mean and the other for samples greater than the mean. That's when the BBHE takes over and equalises the subimages based on their histograms, with the constraint that samples in one set must be mapped into the range of minimum grey level to input mean, and samples in another range of mean to maximum grey level. Based on the respective histograms, one of the subimages is equalised up to the mean, while the other is equalised away from the mean. Thus, the equalised subimages are bounded around the input mean, preserving mean brightness.

Assume X_m *is* the mean of the X and Xm $\in\{ X_0,X_1,\ldots,X_{L-1}\}$. The input image is divided into two subimages by the mean $X_L$andX_U as

$$X = X_L \cup X_U \tag{4.25}$$

where

$$X_L = \{X(i,j) | X(i,j) \leq X_m, \forall X(i,j) \in X\} \tag{4.26}$$

and

$$X_U = \{X(i,j) | X(i,j) > X_m, \forall X(i,j) \in X\} \tag{4.27}$$

where $X_L=\{X_0,X_1,\ldots,X_m\}$ and $X_U=\{X_{m+1},X_{m+2},\ldots,X_{L-1}\}$ (4.28)

The probability density function of the sub image X_L and X_U as

$$p_L(X_k) = \frac{n_L^k}{n_L}, \quad \text{where k=0,1,..m} \tag{4.29}$$

and

$$p_U(X_k) = \frac{n_U^k}{n_U}, \text{ where k=m+1,m+2,…,L-1,} \tag{4.30}$$

In above equation n_L^k and n_U^k are the respective numbers of $\{X\}_L$ and $\{X\}_U$, and n_L and n_U are numbers of samples in $\{X\}_L$ and $\{X\}_U$, individually.

The CDF for $\{X\}_L$ and $\{X\}_U$ are calculated as

$$c_L(x) = \sum_{j=0}^{k} PL(X_j) \tag{4.31}$$

and

$$c_U(x) = \sum_{j=m+1}^{k} PU(X_j) \tag{4.32}$$

where $X_k = x$ and $C_L(X_m) = 1$,$C_U(X_{L-1}) = 1$

As a transform function, the cumulative density function is used and it is defined as

$$f_L(x) = X_0 + (X_m - X_0)c_L(x) \tag{4.33}$$

and

$$f_U(x) = X_{m+1} + (X_{L-1} - X_{m+1})c_U(x) \tag{4.34}$$

The decomposed subimages are equalised independently using these transform functions, and the composition of the resulting equalised subimages constitutes the BBHE. The output (Y) is defined as

$$Y = \{Y(i,j)\} \tag{4.35}$$

$$= f_L(X_L) \cup f_U(X_U) \tag{4.36}$$

where

$$f_L(X_L) = \{f_L(X(i,j)) | \forall X(i,j) \in X_L\} \tag{4.37}$$

$$f_U(X_U) = \{f_L(X(i,j)) | \forall X(i,j) \in X_U\} \tag{4.38}$$

4.7 Non-Linear Anisotropic Diffusion

The anisotropic diffusion filter, which was proposed for the first time by Perona and Malik [88], is a non - linear filter that promotes intra-region smoothing while inhibiting inter-region smoothing [89]. The non-linear diffusion equation for an image *I* is given by :

$$\frac{\partial I}{\partial t} = div(C(\nabla I).\nabla I)) \ , \tag{4.39}$$

The authors in [88] specified the diffusion function as follows:

$$C(\nabla I) = \exp\left(-\left(\frac{|\nabla I|}{k}\right)^2\right) \tag{4.40}$$

Eqn. (4.39) can be discretized by using4 closest pixels as:

$$I_{i,j}^{n+1} = I_{i,j}^{n} + \Delta t(C_N \cdot \nabla_N I + C_S \cdot \nabla_S I + C_E \cdot \nabla_E I + C_w \cdot \nabla_w I)_{i,j}^{n} \ , \tag{4.41}$$

We use North (N), South (S), East (E), West (W) to describe local gradient (∇I) and set our iteration constant as Δt. In this iterative

approach the diffusion is managed by the iterations. More iterations will result in more blurring, but the outcome will be subtle when compared to changes in the diffusion constant k. The nearest neighbour differences are used to calculate the local gradient, which is as follows:

$$\left.\begin{aligned} \nabla_N I_{i,j} &= I_{i-1,j} - I_{i,j}, \\ \nabla_S I_{i,j} &= I_{i+1,j} - I_{i,j}, \\ \nabla_E I_{i,j} &= I_{i,j+1} - I_{i,j}, \\ \nabla_W I_{i,j} &= I_{i,j-1} - I_{i,j} \end{aligned}\right\} \quad (4.42)$$

4.8 Max Entropy Thresholding

Maximum entropy [90, 91] is calculated by taking the probability of the intensity into account that correctly segment the given input image I and the entropy H is computed as:

$$H = -\sum_{i=1}^{L} p_i \log(p_i) \text{ and } p_i = \frac{n_i}{N} \quad (4.43)$$

where, L is taken as no. of gray levels in the image, the probability (p_i) of gray level *i* being found in image, the number of pixels (n_i) with intensity *i*, and the total number of pixels (N) in the image. The maximum entropy is achieved by choosing an intensity I that maximises H.

4.9. Evaluation Metrices

The performance measurement of the segmentation method is to be computed to find the suitability of using that method for any application. Performance is evaluated by comparing the output of the method against a standard result. Here the segmented image by a method is compared with the result obtained manually. The manually segmented result by an expert is taken as gold standard.

4.9.1 Dice coefficient (D)

For the purpose of comparing two images, several well-known measures of structural similarity are available. Dice (D) coefficient is a measurement of asymmetry information for two A & B binary regions.

The Dice value [92] is calculted by:

$$D(A,B) = \frac{2|A \cap B|}{|A|+|B|} \qquad (4.44)$$

In above equation, A and B represent 2 datasets. In A and B region the D will be 0 & 1 for disagreement and agreement.

4.9.2 Sensitivity (Sn) and Specificity (Sp)

The gold standard segmentation results are taken as Truth vale and the results computed by the proposed technique as the Test values. In segmentation correctly segmented values are taken as Positive, and the remaining as Negative. Test values, Positive and Negative obtained by

the proposed are then compared and defined as TP, FP, FN & TN as presented in Table 4.1 and in the Venn diagram shown in Fig.4.7.

Table 4.1 Evaluation Parameters

Truth / Test	Positive (1)	Negative (0)
Positive (1)	TP (True Positive)	FP (False Positive)
Negative (0)	FP (False Negative)	TN (True Negative)

The sensitivity (Sn) and specificity (Sp) of the hand segmented result by medical experts & the corresponding section generated by the proposed automatic technique are estimated by using these factors (parameters). The sensitivity (Sn) and specificity (Sp) parameters are defined as the proportion of ROI voxels and non-ROI voxels that an algorithm recognises, respectively.

Sensitivity and Specificity are calculated as :

$$Sn = \frac{TP}{TP+FN} \tag{4.45}$$

$$Sp = \frac{TN}{TN+FP} \tag{4.46}$$

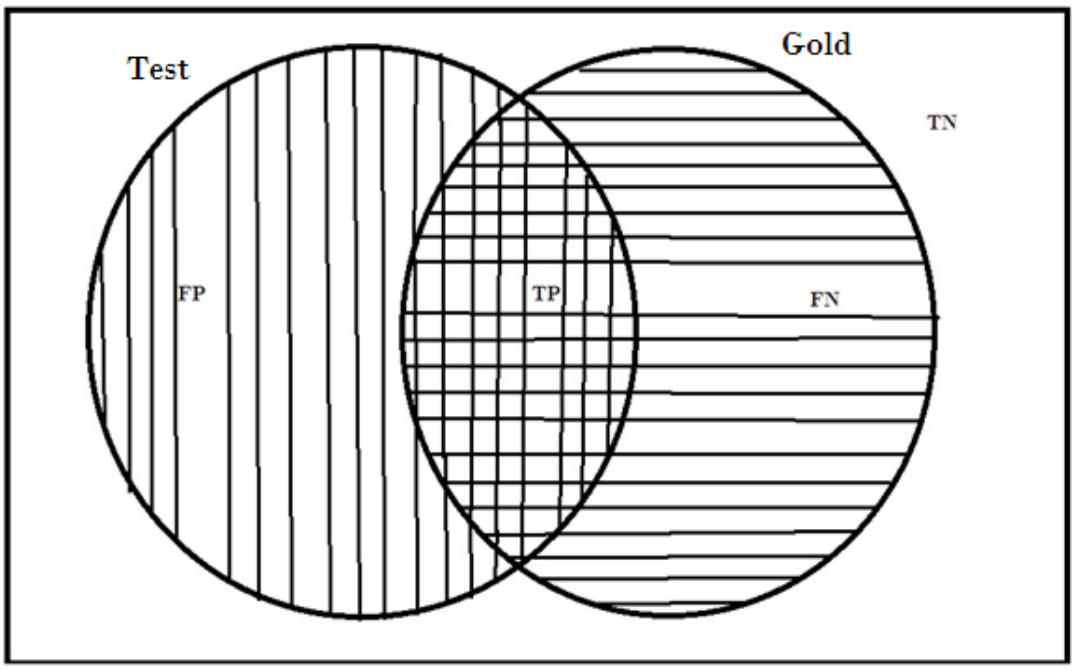

Fig.4.7 Venn diagram of Quantitative measures

4.9.3 Hausdorff distance (HD)

Hausdorff distance [94-96] calculate the distance between two segmented regions named as manually (A) and automatically (B). HD is calculated in a twostep process. First, the minimum distance between every point in A and every point in B is computed. Let dH_{ab} presents the highest of this set of loweset distances.

In this case, the minimum distance between the ithsurface pixel in A and the set of surface pixels in Bis, and thus dHabis is the maximum value that can be assigned to all surface pixels in A's surface distance, as defined by:

$$dH_{ab} = \max\{d_i^{ab}\}, i = \{1 \ldots \quad (4.47)$$

Similarly let dH be distance into B and A. The hausdorf distance between A and B is calculated in the second stage as follows:

$$\mathrm{HD} = \max\{dH_{ab}, dH \qquad (4.48)$$

In above equation a is point of A and b is points of B sets, respectively.

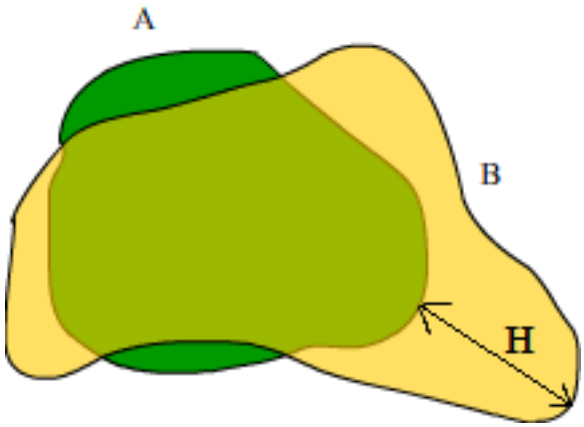

Fig.4.8 The Hausdorf distance (HD) calculation

4.9.4 Curve fitting

Curve fitting [97] plays an important part in research and analysis, either in the interpretation of the data or in its empirical representation. Curve fitting is nown as a process of determining the best fit curve equation that is most helpful in estimating the unknown values. Thus, curve fitting is a mathematical term that refers to an exact association between two variables based on algebraic equations. Curve fitting determines the coefficient values necessary to make a function fit the data as accurately as possible.

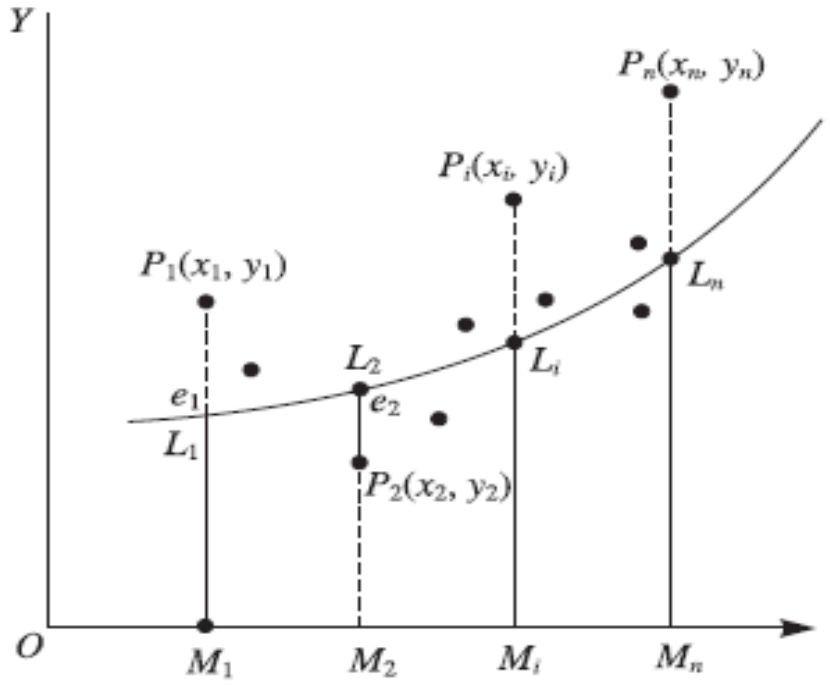

Fig.4.9 Fitting n data points

Let the curve $y = a + bx + cx^2 + ...kx^{m-1}$ (4.49)

fitted to n data points (x_1, y_1) , (x_2, y_2) , (x_3, y_3) ,… (x_n, y_n).

At $(x = x_i)$ the ordinate's experimental value is $y_i = P_iM_i$ and on the fitting curve, the corresponding value (i) is $a+bx_i+cx_i^2+... \ kx_i^m = L_iM_i$ which is the expected value. The difference between what was observed and what was expected is $P_iM_i - L_iM_i = e_i$. This difference is referred as error at $(x = x_i)$. A few of the errors, e1, e2, e3,…, ei,…, will have a positive value, and the rest will have a negative value. Each error must be squared to make all errors positive by two,. *i.e.* $S = e_1^2 + e_2^2 + e_3^2 + ... + e_i^2 ... e_n^2$ the principle of least square states that the curve of best fit is for which the errors are as small as possible; the error is smaller when the standard

deviation is low (S). The theoretical values for x_1, x_2, ..., $x_n$may be $y_{\lambda 1}$, $y_{\lambda 2}$, ... $y_{\lambda n}$.

Straight line Fitting

Let $y = a + bx$ *as a straight line* (4.50)

that is fitted to the (x_1, y_1) , (x_2, y_2) , (x_3, y_3) , (x_4, y_4) …, (x_n, y_n) data points.

Let $y_{\lambda 1}$ be the theoretical value for x_1 then $e_1 = y_1 - y_{\lambda 1}$

$$e_1 = y_1 - (a + bx_1)$$

$$e_1^2 = (y_1 - a - bx_1)^2$$

Now , $S = e_1^2 + e_2^2 + e_3^2 + \ldots + e_n^2$

$S = \sum_{i=1}^{n} e_i^2$ and $S = \sum_{i=1}^{n} (y_i - a - bx_i)^2$

According to the theory of least squares, S is the smallest possible number, so

$\frac{\partial S}{\partial a} = 0$ and $\frac{\partial S}{\partial b} = 0$ (4.51)

On solving Eqn.(4.51) and dropping the suffix,

$$\sum y = na + b \sum x \quad (4.52)$$

$$\sum xy = a \sum x + b \sum x^2 \quad (4.53)$$

The Eqn.(4.52) and (4.53) are called as normal equations. By finding solution of Eqn. (4.52) and (4.53), the a and b can be computed as :

$$a = \frac{n \sum xy - \sum x \sum y}{n \sum x^2 - (\sum x)^2} \, , \; b = \bar{y} - a\bar{x}$$

Putting the value of a and b Eqn. (4.50), the equation (Fig.4.11) of the line best fit.

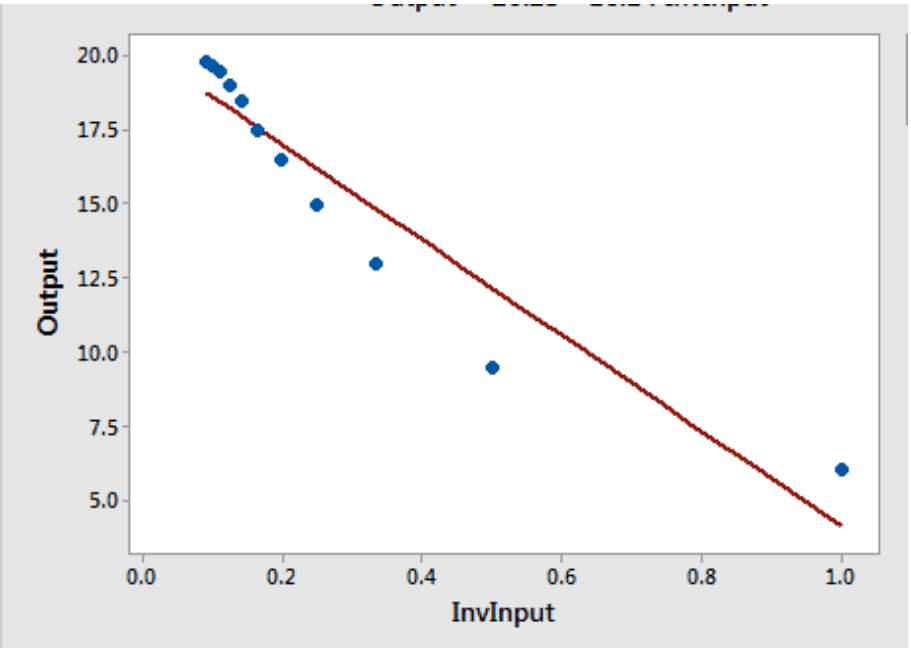

Fig.4.10 Fitting a straight line

Polynomial curve fit

Let $y = a + bx + cx^2$ (4.54)

which is fitted to a given data

$(x_1, y_1), (x_2, y_2), (x_3, y_3), (x_4, y_4)\ (x_5, y_5)\ (x_6, y_6)\ldots\ldots, (x_n, y_n)$.

If y_λ is the theoretical value for x_1 then

$$e_1 = y_1 - y_\lambda$$

$$e_1 = y_1 - (a + bx_1 + cx_1^2)$$

$$e_1^2 = (y_1 - a - bx_1 - cx_1^2)^2$$

Now,

$$S = \sum_{i=1}^{n} e_i^2 \text{ and } S = \sum_{i=1}^{n} (y_i - a - bx_i - cx_i^2)^2$$

$$\frac{\partial S}{\partial a} = 0, \frac{\partial S}{\partial b} = 0 \text{ and } \frac{\partial S}{\partial c} = 0 \quad (4.55)$$

Solving Eqn. (4.55) and dropping suffix,

$$\sum y = na + a\sum x + b\sum x^2 \quad (4.56)$$

$$\sum xy = a\sum x + b\sum x^2 + c\sum x^3 \qquad (4.57)$$

$$\sum x^2 y = a\sum x^2 + b\sum x^3 + c\sum x^4 \qquad (4.58)$$

The Eqn.(4.55), (4.56) and (4.57), are normal statements. To get a,b,c value the Eqn.(4.55), (4.56) and (4.57) is solved. Put a, b and c value in Eqn.(4.54), the equation of polynomial of best fit. Fig.4.11 shows polynomial curve fit.

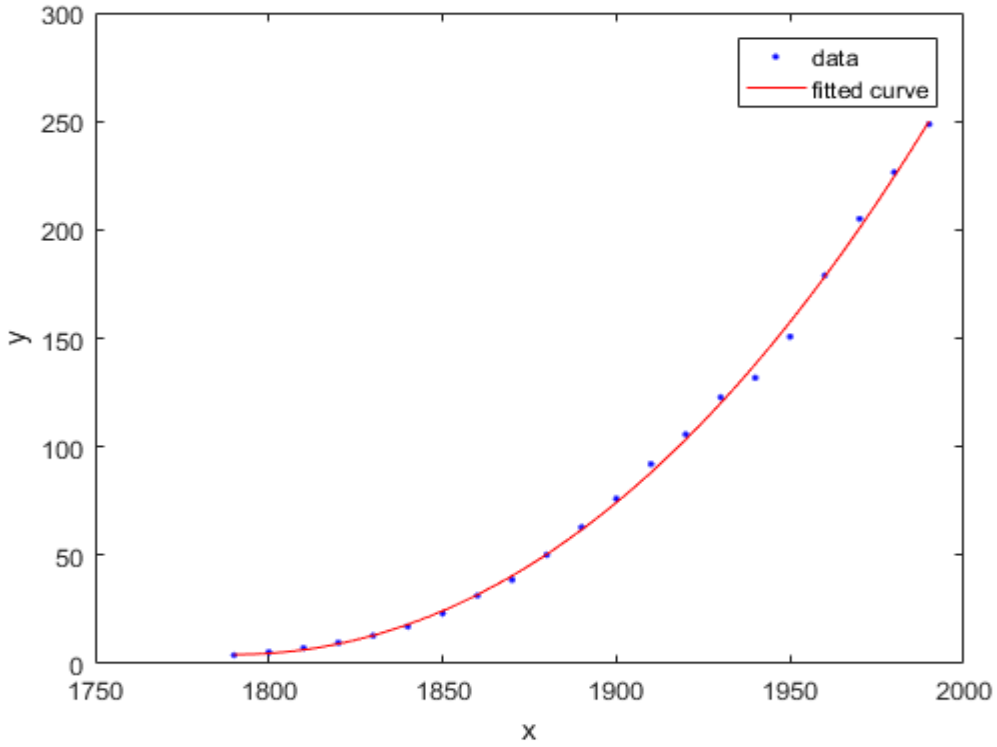

Fig.4.11 Polynomial curve fit

Exponential curve fit

Let $y = ae^{bx}$ (4.59)

Taking logarithm on both the sides,

$\log_{10} y = \log_{10} a + bx \log_{10} e$

i.e., $Y = A + Bx$ (4.60)

in above equation $Y = \log_{10} y$, $A = \log_{10} a$ and $B = b \log_{10} e$.

The mathematical equations for equation (4.59) are,

$$\Sigma Y = nA + B\Sigma x$$

$$\Sigma xY = A\Sigma x + B\Sigma x^2$$

Value of A and B can be computed by using above two equations as :

$$A = \frac{n\Sigma xY - \Sigma x \Sigma Y}{n\Sigma x^2 - (\Sigma x)^2}, B = \bar{Y} - A\bar{x}$$

Here a= antilog A, b=B/$\log_{10}$e. Fig.4.13 shows exponential curve fit.

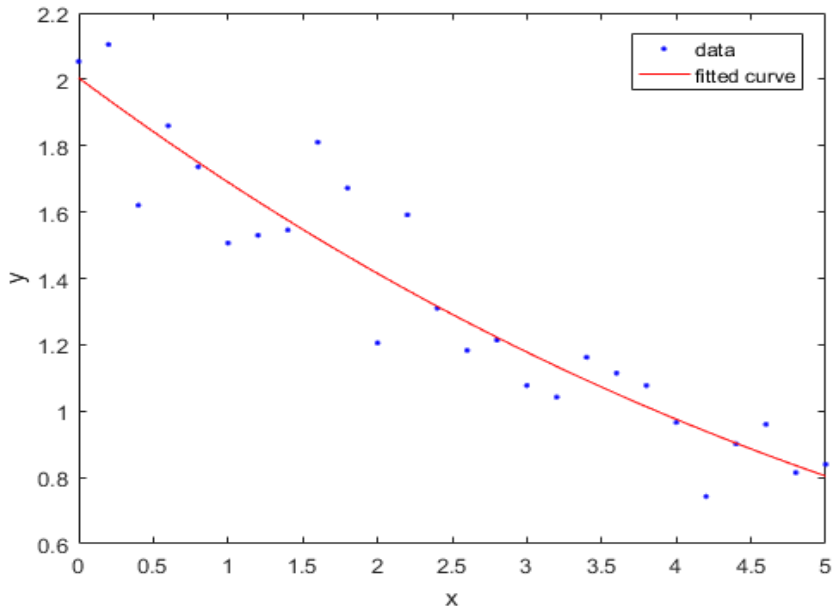

Fig.4.12 Exponential curve fit

4.10 Materials Used

The data sets used for proposedexperiments in this work were taken from SRM (Sri Ramachandra Medical) University and Hospital, Chennai, India [98] and KGS Scan and Diagnostic Centre, Madurai, India [99].

4.10.1 Dataset 1:

Review T2W single-shot (SS) quick turn reverberation MR imaging were gathered from SRM (Sri Ramachandra Medical) University and Hospital, Chennai,India [98]. Moral endorsement was allowed by the committee (morals no. IEC-NI/14/OCT/43/65) of a similar university. T2-weighted SSFSE is especially helpful in examining brain structure and primary irregularities as it gives high in-plane goal and proper difference for the creating brain in-utero. The informational index comprise of twenty volumes. Table 4.2 shows the primary boundaries of the informational indexes utilized. These boundaries incorporate the gestational age (GA) of the hatchling, no. of cuts and cut thickness in mm. Different boundaries are: reiteration time (TR) changing somewhere in the range of 800 and 1,350 ms; reverberation time (TE) fluctuating somewhere in the range of 86 and 91 ms; variable framework size somewhere in the range of 160 and 512; and cut thickness of 3.5 – 6 mm. The gestational age scope of these hatchlings are somewhere in the range of 20 and 36 weeks. Pictures were gained in fetal pivotal, coronal and sagittal planes of 20-24 cuts for every volume.

Table 4.2 Details of retrospective T2 –w image obtained from Sri Ramachandra Medical University Chennai. [98]

No.	GA	Flip angle	Thickness of Slice (millimeters)	gap in slice (milli meters)	Repetition time (TR)	Echo time (TE)	FoV
					(millise conds)	(millisec onds)	(millimet ers)
1	20-21	170	4	4	850	86	188x280
2	20-21	170	3.5	3.5	1350	89	280
3	20	170	3.5	3.5	800	89	270
4	29	90	4.5	5	718	92	350
5	36	170	3.5	3.5	1790	89	270
6	31	90	4.5	4.8	473	91	380
7	29	170	4	4.2	1350	91	300
8	27	90	5	5.2	642	93	350
9	26	170	4.5	4.5	700	89	280
10	23	170	4	4.2	1350	91	320
11	29	170	4	4.2	1350	91	300
12	33	90	4	4	1062	88	320
13	20-21	170	5	5.5	1350	91	320
14	35-36	170	4	4	1350	91	300
15	38	90	4	4.5	676	88	400
16	28-29	170	4	4.2	1350	91	280
17	31	90	3.5	3.7	709	90	420
18	32-33	160	3	3	900	89	279x350
19	22-23	160	3.5	3.9	1000	85	350x279
20	35-36	90	4	4.5	695	92	420

4.10.2 Dataset 2:

Five volumes of review fetal T2 - w MR pictures acquired for three patients were gathered from KGS Scan and Diagnostic Center, Madurai, India [99]. These outputs were gotten on the solicitation of the patients for their necessity. The pictures were procured by 1.5Tesla MRI scanning machine(Magnetom Avanto, Siemens) utilizing SS (single shot) quick turn reverberation arrangements during the time frame, June-September 2013. The volume size is 256 x 256 x (6-19) pixels with the accompanying boundaries: redundancy time (TR=1000-1300ms), reverberation time (TE=83-91ms), flip point 150o - 180o , cut thickness = 4-6 mm. Volumes were physically divided by a clinical master worked in the fetal brain life structures and are utilized as best quality level.

CHAPTER 5

Fetal Brain Extraction from MR Images using Region Growing Technique

5.1 Introduction

In this section, it presents the proposed method is the first fetal brain extraction technique. Attractive Resonance (MR) pictures of hatchling assists with contemplating fetal mental health in uteri. Such investigations require fetal brain division. Programmed division of fetal brain from MRI is trying, because of the profoundly factor size and state of the creating brain, conceivable brain structure irregularities, development of embryo and a helpless goal of fetal MRI examines. This is rather than grown-up brain division, where the brain structure is steady and a few set up strategies exist.

The current programmed techniques have constraints with power non-consistency, helpless division in brain areas, for example, frontal projection and so forth and furthermore take a lot handling time in division. Consequently no single calculation seems to have created exact fetal brain division without instatement and computational intricacy. To conquer not many such issues, this examination proposes a basic, solo and information based programmed fetal brain extraction strategy.

5.2 Method

The proposed technique starts from a pre-handling process that incorporates contrast upgrade to enhance the differentiation of the flimsy layers limits in fetal brain. The fetal brain division measure further continues with thresholding, cultivated district developing and opening filling.

5.2.1 Image Pre-Processing

The fetal brain has seven main layers that can be identified by vitro MR imaging [100]. Out of the seven layers, because of differentiation constraints, Only 3 or 4 layers are imaginable, and the flimsy cortical dim matter and white matter layers are also contiguous. Thus, the data used in this study require pre-processing in order to improve the differentiation of the limit of fetal brain dainty layers. Brilliance saving bi-histogram balance (BBHE) [87] technique is utilized for contrast upgrade. This technique safeguards the splendor of the information picture I(m,n) . The difference of the information picture I(m,n) is upgraded by a change to get another picture g as:

$$g(m,n)=T(I(m,n)) \qquad (5.1)$$

In equation (5.1), m,n are image width and stature and T presents the bi-histogram balance change work which levels the I histogram.

5.2.2 Image Threshold

An ideal power edge esteem T0 is gotten for the differentiation improved picture g(m,n) by applying Otsu's technique [80]. T0 is the ideal limit esteem, that augments the between class change , which is characterized as, $T_0 = \arg max_{0 \le t \le L-1} \sigma_B^2(t^*)$ (5.2)

Here, L presents quantity of dark levels. T_0 is utilized as the halting rules for area developing technique.

5.2.3 Seeded Region Growing

A locale developing technique [85,86] needs an underlying point, called seed to begin the development. This is chosen from the reality, that the MRI of embryo contains the brain partition at the middle taking all things together the cuts. Henceforth the middle pixel (C) in the MRI is taken as starting seed. The middle pixel power is acquired as $C = I(\frac{m}{2}, \frac{n}{2})$ Following that, the region is grown by computing the difference (Dt) between the centre pixel C and its eight neighbours pixels at $(x + i, y + j)$ as follows :

$$Dt(i,j) = \sqrt{(I(x+i, y+j) - C)^2} \quad (5.3)$$

where, i = -1 to 1, and j = -1 to 1. The growing process is given in Fig 5.1.

(X-1,Y-1)	(X-1,Y)	(X-1,Y+1)
(X,Y-1)	(X,Y)	(X,Y+1)
(X+1,Y-1)	(X+1,Y)	(X+1,Y+1)

Figure.5.1 Neighborhood pixels considered for area developing

In the event that the distance (Dt) is not exactly the limit T0, the middle pixel and the neighbor pixel are named as having a place with same area. The yield of locale developing gives an unpleasant paired picture IB of the fetal brain.

$$I_B = \begin{cases} 1 & if\ (Dt(x,y) < T_0 \\ 0 & otherwise \end{cases} \quad (5.4)$$

5.2.4 Holes Filling Inside Brain Regions

During the region growing process, the CSF with a lower intensity value than the surrounding brain regions is removed, resulting in holes within the rough brain area I_B. The holes in I_B are filled by applying the filling [84] method, and the completed brain mask I_M is obtained as

$$I_M = \begin{cases} 1 & if\ I_B(x,y) = 0\ (holes) \\ 0 & otherwise \end{cases} \quad (5.5)$$

Using I_M (brain mask), the fetal brain is segmented.

5.3 Materials Used

The input used are five volumes of retrospective fetal T2 - w MR images corresponding to three patients collected from KGS Scan and Diagnostic Centre, Madurai, India [99]. These scans are obtained on the request of the patients for their requirement. The images are acquired by 1.5Tesla MRI scanner (Magnetom Avanto, Siemens) by using single shot fast spin echo sequences during the period, June-September 2013. The volume size is 256 x 256 x (6-19) pixels.

5.4 Results and Discussion

The proposed technique was tested on a material pool imaged at various gestational weeks. These 5 volumes were manually segmented by a medical experts and are used to compare and evaluate the proposed automatic method. Medical experts say that when compared to manually segmented results, the proposed automatic method's results are comparable. The proposed method's segmented brain portion is shown in Fig.5.2.

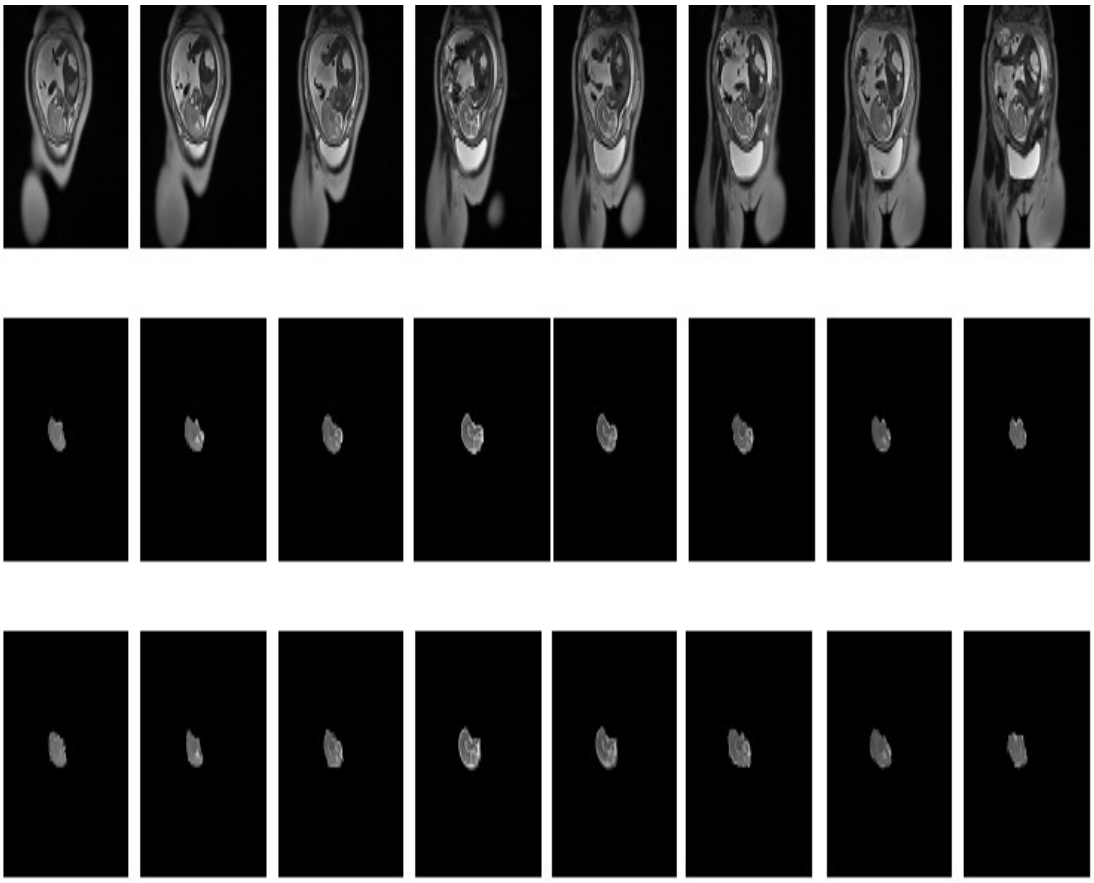

Fig.5.2 Row 1 : original MRI images, Row 2 : manually segmentation, Row 3 : Proposed segmentation result

For quantitative evaluation, the values for Dice coefficient D, sensitivity S_n and specificity S_p are computed for the proposed method by using the gold standard (manual segmentation) and are presented in Table 5.1.

Table 5.1 Calculated values of Dice (D), Sensitivity (S_n) , and Specificity (S_p) for this proposed technique：

Test Images		Dice (D)	S_n	S_p
Orientations	**Volume. No.**			
Axial	1	0.8837	0.9298	**0.9972**
	2	0.9390	0.9660	0.9944
	3	0.9116	0.9217	0.9962
Sagittal	1	0.8842	0.9504	0.9967
	2	0.9449	0.9672	0.9960

From Table 5.1, it is noticed that for axial images, the calculated values of D, Sn, Sp are 0.9390, 0.9660 and 0.9972 respectively and for sagittal images they are 0.9449, 0.9672 and 0.9967. Table 5.2 shows the quantitative measures obtained by A.Gholipour et al. [101]by their supervised method for a different data set. Features of segmented fetal image is shown in table 5.3.

The mean value T of the fetal images is calculated as:

$$T = \frac{\sum_{I=1}^{m} \sum_{j=1}^{n} A(i,j)}{mxn} \qquad (5.6)$$

Where,

An (i, j) is defined as the intensity's pixels at i^{th}&j^{th} location

The standard deviation D of the fetal images is computed as:

$$SD = \sqrt{\frac{1}{N}\sum_{i=1}^{N}(x_i - y)} \qquad (5.7)$$

Wherever,

N is the number of samples of fetal images

$$y = \sum_{i=1}^{N} x_i \qquad (5.8)$$

Where,

y is the mean and S is the standard deviation

x_i *is the ith pixel,*

$N = mxn, s\ the\ total\ number\ of\ pixels\ and\ i = 1, 2, 3, 4, \ldots . N.$

The skewness of fetal images S as follows:

$$S = \frac{n\sum_{i=1}^{n}(x_i - y)^3}{(n-1)(n-2)s^3} \qquad (5.9)$$

The kurtosis of a fetal images *R* as follows:

$$R = \frac{1}{n}\sum_{i=1}^{n}\left(\frac{x_i - \mu}{\sigma}\right)^4 \qquad (5.10)$$

Where μ is the mean of the fetal images and σ is the standard deviation of fetal images.

The variance of fetal images Var (A) as calculated:

$$\text{Var (A)} = \Sigma\ (Ai - B)^2 / N = \Sigma\ ai^2 / N \qquad (5.11)$$

Wherever,

N: the no. of fetal images in a given set of fetal images

B: mean of N fetal images.

Ai: ith fresh fetal images in the given amount of fetal images

ai: ith deviance fetal images in the given amount of fetal images

Var(X): variance of fetal images of the given sample dataset.

Table 5.2 computed values of Dice, Sn and S_p by the semi automated method by Gholipour et al.[101] for randomly selected 5 fetuses from dataset

Measure	Fetal MRI Volume Detail				
	C3	C6	C11	C13	C16
D	0.9329	0.9208	0.9481	0.9576	0.9701
S_n	0.9499	0.9446	0.9206	0.9595	0.9944
S_p	0.9978	0.9949	0.9985	0.9954	0.9979

The covariance of fetal images Cov (X) as calculated:

$Cov(X) = \Sigma (Xi - x) (Yi - y) / N = \Sigma xiyi / N$ (5.12)

Where,

N is the no. of fetal images in every group of facts

x is the mean of the N scores in the head dataset

Xi: ith fresh score in the first set of fetal images

xi is the ith deviation fetal images in the first set of fetal images

y is the mean of the N fetal images in the second data set

Yi is the ith raw score in the second set of fetal images

Yi is the ith deviation score in the second set of fetal images

$$E = sum(pXlog2(p)) \qquad (5.13)$$

The contrast C of the insignificant fetal pictures is followed as:

$$C = \sum_{i,j} |i - j|^2 A(i,j) \qquad (5.14)$$

Wherever , An (i,j) is the strength's pixel at (i, j)th position

Table 5.3. Features of segmented fetal image

Features	Value of the image element
E	1.0828
S	0.0476
T	0.4882
Cov(X)	min(0.049) max(0.059)
R	1.0037
Σ	11.2

This study's data sets are not identical to Gholipour et al[101]data sets. It is presented to understand the range of values obtained by their introduced methods. The experimental values achieved for D, Sn, and specificity by Gholipour et al [101] method are all greater than our proposed method. But their introduced method is semi-automatic, and requires several pre-set threshold values. Our proposed approach produces fetal brain surface data that shows better agreement with manual segmentation, both qualitatively and quantitatively.

5.5 Conclusion

The proposed method developed a low complex, fully automated technique to segregate fetal brain from brain MRI. This method employs contrast enhancement method to increase the contrast between thin layers of the fetal brain's boundary.The thresholding and region growing techniques are further used to obtain fetal brain. Experiments show that this proposed technique works well and also produces results that are consistent with the gold standard. Additionally, the results obtained using the semi-automated method are compared.

CHAPTER 6

Automatic method for extraction Fetal Brain from Human Feus MRI using Improved Maximum Entropy Method

6.1 Introduction

Because of the low resolution, low-signal contrast, and tissue changes in developing brain, segmenting the fetal brain from MR images is extremely difficult. In T2-weighted fetal MRI, images of bone structures like skull are hypointense, while those of CSF are hyperintense. If the interface between CSF and skull portion is effectively identified by an algorithm, then the automatic segmentation of fetal brain is made simple. The analysis of ground truth, the hand segmented image, presents that the CSF and cortex intensity distributions in few of the slices are melted (Fig.6.1) because of low contrast into fetal brain tissue. As a result, a single conventional segmentation technique is not able to segregate fetal brain from all MRI voume slices. As a result, segmentation using a single algorithm results in anatomically incorrect segmentation of the fetal brain. Therefore in this chapter, It presents the proposed second segmentation method involving many techniques such as edge smoothing, fetal brain filtering and enhanced maximum entropy threshold.

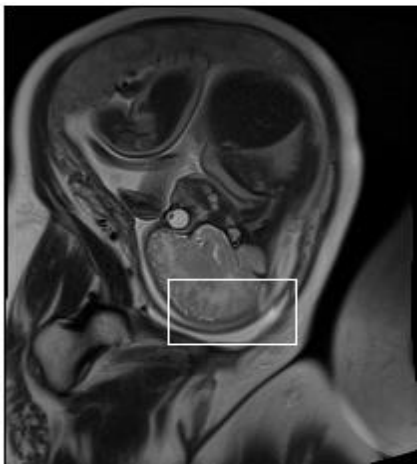

Fig.6.1 Presence of melted CSF and cortex in fetal MRI

6.2 Method

Diffusion imaging, morphological operations, image thresholding, and connected component analysis (CCA) are all used in this proposed method.

6.2.1 Edge Preserving Smoothing

In this we used 2D fetal MRI slices are used as input (I). Smoothing and filtering processes are used in sequence to seprate the fetal brain from the other parts of the maternal tissues. First, the diffuse the input image to make their edges smoother. The image gradient is monotonically degraded by the diffusion function. The non-brain part of the image is attenuated using 2D anisotropic diffusion, which involves each pixel updation of the image by an amount equal to the flow contributed by the 4 nearest neighbours of the pixels. The I_d (diffused image) is acquired using anisotropic filter formulated by authors in [90]. The filter behaviour relies upon the k. In proposed method, set k to ten which is nominal for

both the maternal and foetal head edge gradients. Fig. 6.4(b) presents I_d (diffused image).

6.2.2 Morphological Opening

To obtain more accurate segmentation result, additional smoothing is required because of intensity overlap in between white matter and cortex of fetal scan. Due to the thin nature of layer of the foetal cortex, a morph opening filter is used to smooth the edge at the CSF-brain interface and performs morphological opening operations on I_d , to get an image I_o as :

$$I_o = (I_d \ominus SE) \oplus SE \qquad (6.1)$$

In equation, $\oplus$ is dilation & $\ominus$ is erosion operators with radius 3 (SE) (Fig. 6.2).

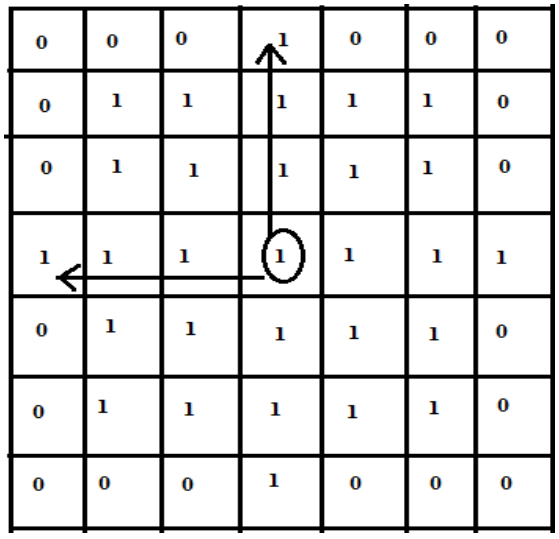

Fig.6.2 Three-pixel-radius structural element (SE)

Additionally, this morphological opening filter contributes to the suppression of numerous smaller areas of high intensity pixels in, which

are affected by maternal tissues in fetal MRI (Fig.6.4 (c)).

6.2.3 Enhancement of the Maximum Entropy Threshold

The filtered image is made into a binary image through additional processing. This process involves finding the highest possible entropy threshold. The highest entropy [88,89] is acquired by considering the intensity probability of the correctly segmenting the given image. For estimating the entropy H (as described in section 4.8), the filtered image I_O is taken. The highest entropy (E) is calculated by taking an intensity i which makes H maximum and then determine an optimal threshold for intensity T_{opt}, using the max entropy (H), S.D (σ_{I_O}) and mean (μ_{I_O}) of the filtered image as:

$$T_{opt} = H + \mu_{I_O} + \sigma_{I_O} \tag{6.2}$$

The optimum threshold T_{opt} is applied to segregate objects from the uniform background. By applying the optimum threshold T_{opt} and obtain a binary image I_B as :

$$I_B(i,j) = \begin{cases} 1 & if\, I_o(i,j) \geq T_{opt} \\ 0 & otherwise \end{cases} \tag{6.3}$$

I_B (sample binary image) is given in Figure.6.4 (d).

6.2.4 Fetal Brain segregation

I_{br} a fetal brain is segregated from the original MRI I by applying the mask (I_M) as:

$$I_{br}(i,j) = \begin{cases} I(i,j) & If\ I_M(i,j) = 1 \\ 0 & otherwise \end{cases} \quad (6.4)$$

some segmented sample fetal brain is given in Fig.6.3 (f).

(a) (b)

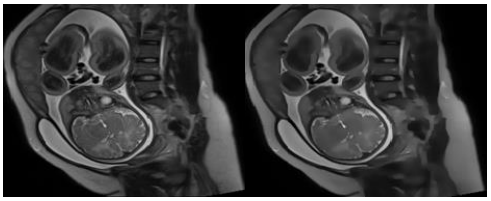

(c) (d)

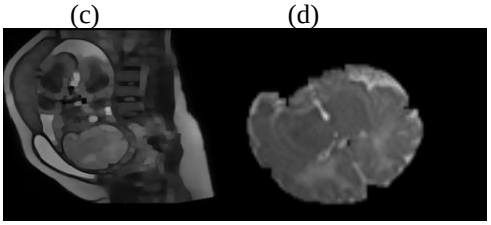

Fig.6.3 (a) Original MRI slice (b) diffused image (c) filtered image (d) segmented fetal brain

6.3 Materials

Review T2W single-shot quick turn reverberation MRI colloected from SRM (sri Ramachandra medical) University and Hospital, Chennai, India [98]. Moral endorsement was conceded by the council (morals no. IEC-NI/14/OCT/43/65) of a similar University. T2-weighted SSFSE is especially valuable in contemplating brain structure and underlying anomalies as it gives high in-plane goal and fitting difference for the creating brain in-utero [38,39]. The informational collection comprise of 16 volumes in this ten are typical volumes and six are irregular volumes.

The unusual contain Agenesis of Corpus Callosum, Blake's pocket blister, Archanoid growth, Meningocele, Dandy walker variation and Sacrum. The subtleties of the boundaries relating to the informational indexes are given in segment 4.10. These boundaries incorporate the gestational week (GW) of the baby, number of cuts and cut thickness in millimeter. The gestational week scope of these hatchlings was somewhere in the range of 20 and 36 weeks. Pictures were obtained in fetal hub, coronal and sagittal planes of 20-24 cuts for each volume. All volumes were physically fragmented by a clinical master worked in the fetal brain life structures and are utilized as best quality level.

6.4 Results and Discussion

The procedure was tested on the image material acquired from the gestational age. The specialists, by contrasting the proposed outcomes and the highest quality level, thought that the proposed outcomes are in acceptable concurrence with manual division. For representation, a dataset of baby with ordinary brain imaged at 20GW (Fig.6.4), and the brain sectioned by the propsed technique are appeared in Fig. 6.5. An anomalous brain imaged at GW29 (Fig.6.6) and fetal brain separated are appeared in Fig.6.7. It very well may be seen in Fig.6.5 and Fig.6.7 that proposed technique can fragment the fetal brain in many cuts.

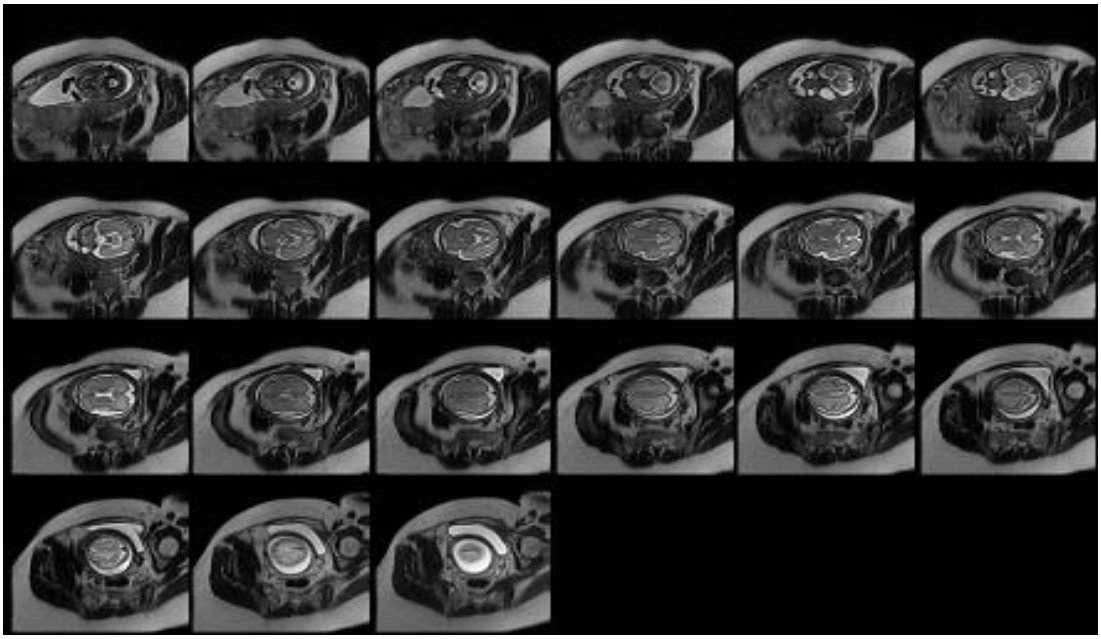

Fig.6.4 Fetal normal brain MRI (GW 20)

For cuts 1-3 in Fig.6.6 and cuts 1-9 in Fig.6.7, hardly any non-brain pixels were distinguished as brain since the lower cuts don't contain the brain area. This is because of the way that accepted that in each cut that the brain parcel lies at the midpoint of each cut.

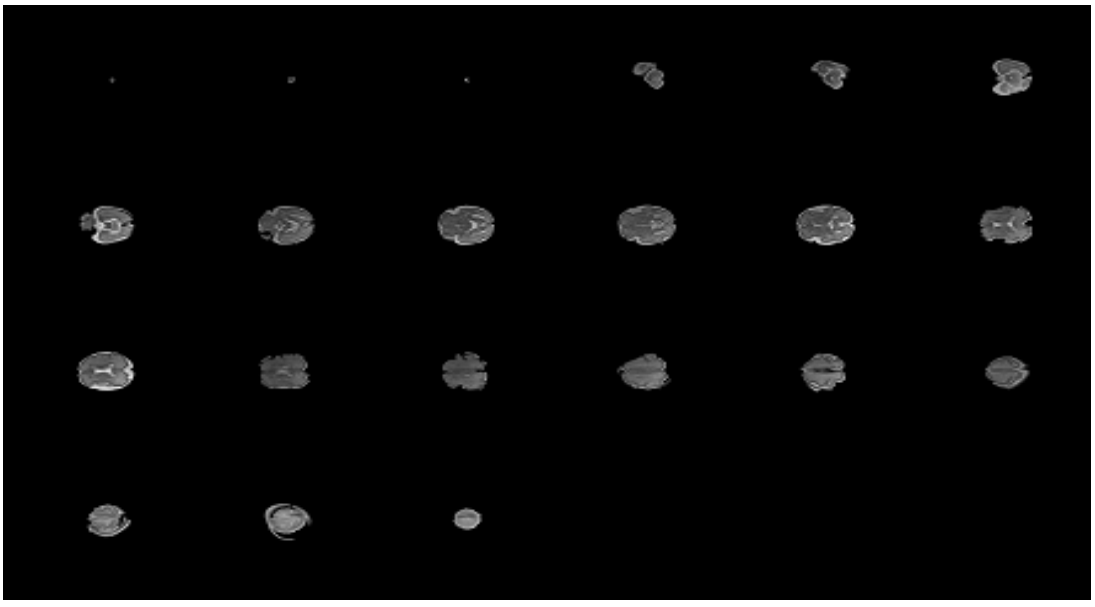

Fig.6.5 Sample of extracted fetal brain

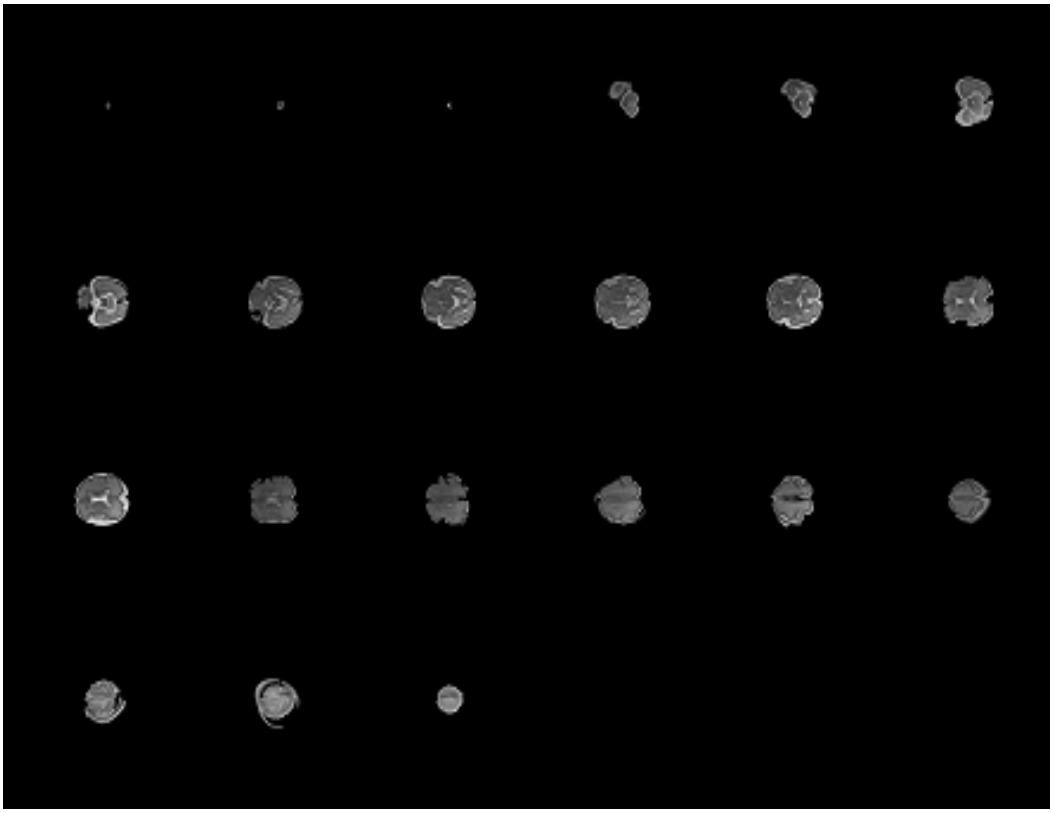

Fig.6.6 Fetal abnormal brain MRI (GW 29)

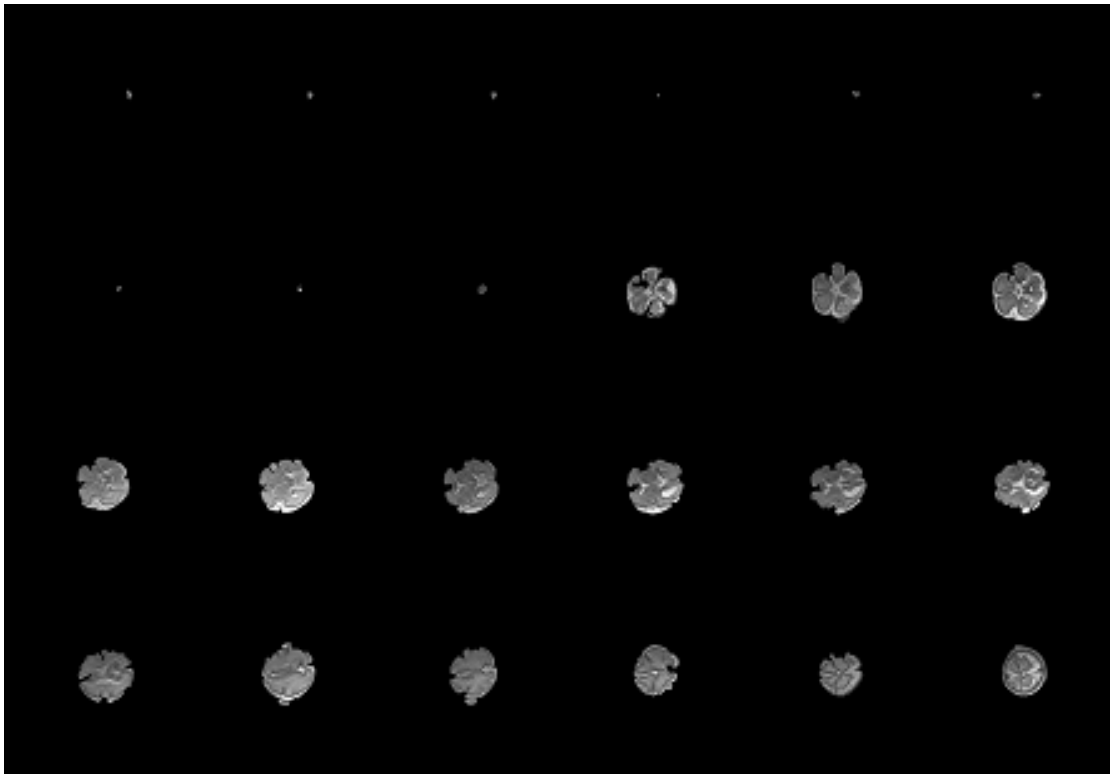

Fig.6.7 Sample of extracted fetal brain MRI slice

For subjective assessment, fetal brain separated by the proposed technique and physically sectioned brain are appeared in Fig.6.8, 6.9 and 6.10. Column 1 of Fig.6.8, 6.9 and 6.10 shows the first cuts chose from pivotal, coronal and sagittal planes individually. The outcomes got by manual division and by the proposed strategy are appeared in column 2 and line 3 individually and noted from Fig.6.8, 6.9 and 6.10 that the proposed technique created worthy outcomes.

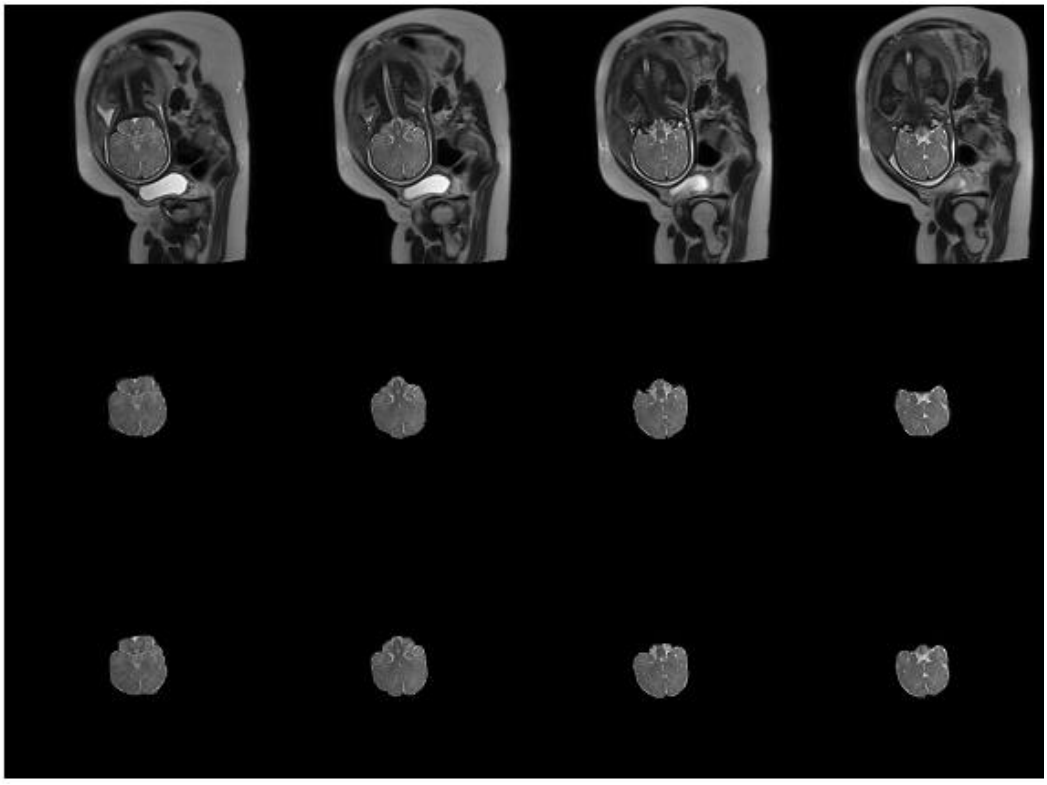

Fig.6.8 Axial view of a segmented fetal brain obtained via MRI scan. Row 1 presents original images, row 2 presents manual segmentation and row 3 present proposed result.

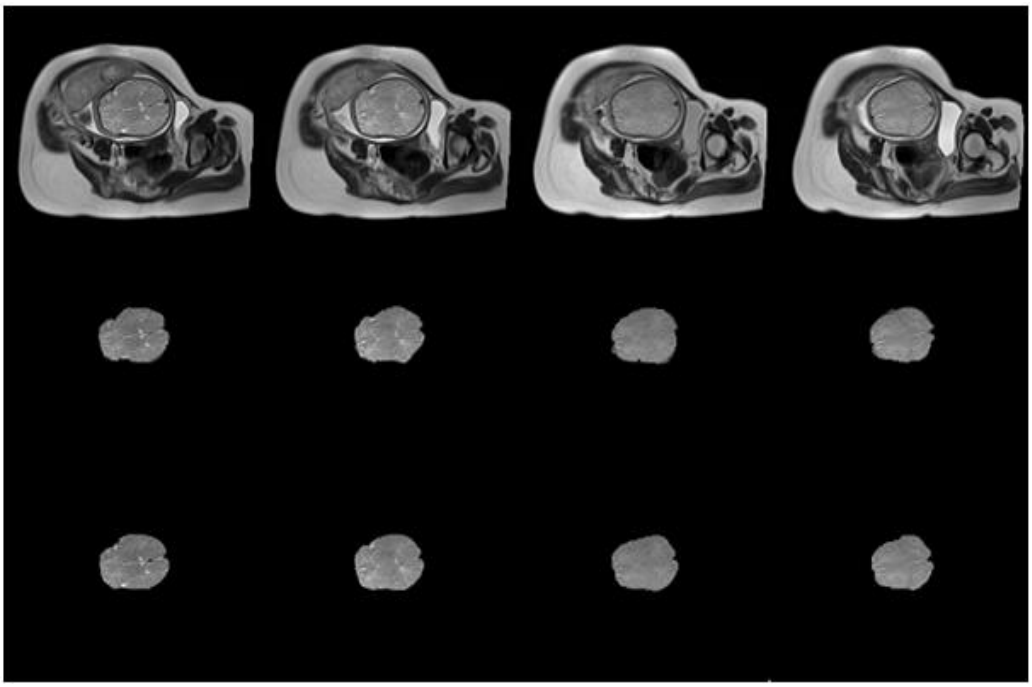

Fig.6.9 Coronal view of a segmented fetal brain obtained via MRI scan. Row 1: original MRI images, row 2: manual segmentation, row 3: proposed result.

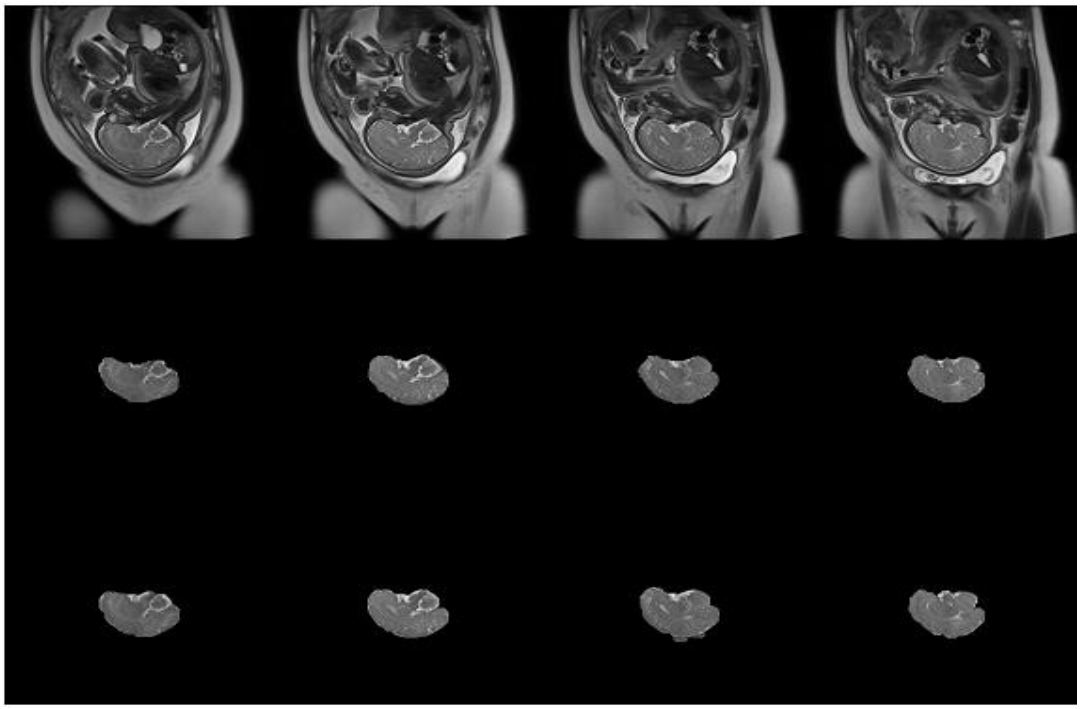

Fig.6.10 Sagittal view of a segmented fetal brain obtained via MRI scan. Row 1: original MRI images, row 2: manual Segmentation, row 3: proposed result.

For quantitative evaluation of the presentation of proposed strategy, the registered the qualities for D, Sn and Sp between the highest quality level and the outcomes created by the proposed technique and are given in Table 6.1. According to Table 6.1, out of 16 volumes the incentive for Dice for 5 volumes ranges from 0.91 to 0.928, while the value for excess volumes ranges from 0.80 to 0.88. S and Sp have normal estimates of 0.95509 and 0.99612, respectively. This implies that proposed technique will in general better incorporate brain pixels (S_n) and avoid non-brain pixels (Sp). The value of low Hausdorff distance esteem 3.3 millimeters for volume no. 8, created by proposed strategy presents that there is a decent understanding among manual and proposed programmed technique.

FBEEFCM Algorithm:

- Read the fetal brain MRI Image
- Preprocess the input slice
  - Non-ROI Removal
    - Morphological opening filter-Application
- Image Enhancement
  - Smoothing- Anisotropic diffusion
  - Hole-filling-Flood fill method
- Segmentation
  - Application of EFCM

Table 6.1 D, Sn and Sp values of the proposed method

Existing System				Proposed System		
Volume Label	**Dice (D)**	**Sensitivity (Sn)**	**Specificity (Sp)**	**Dice (D)**	**Sensitivity (Sn)**	**Specificity (Sp)**
1	0.8543	0.952	0.9782	0.8456	0.9982	0.9942
2	0.8631	0.9781	0.9867	0.8652	0.9865	0.9967
3	0.8707	0.9347	0.9823	0.8806	0.9656	0.9878
4	0.8945	0.9627	0.9798	0.8532	0.9852	0.9978
5	0.8933	0.9529	0.9892	0.9941	0.9641	0.9952
6	0.9209	0.8724	0.9935	0.9856	0.8951	0.9985
7	0.8768	0.8294	0.9965	0.8956	0.8562	0.9987
8	0.9053	0.9658	0.993	0.9862	0.9764	0.9956
9	0.9369	0.9209	0.9903	0.9954	0.9451	0.9978
10	0.875	0.9673	0.9921	0.8951	0.9785	0.9989
Average	0.88908	0.93362	0.98816	0.91966	0.95509	0.99612

To contrast the exhibition of the strategy and different strategies, the quantitative measures got by latest examinations for the cortex division regarding Dice are presented in Table 6.2 for our introduced technique,and existing techniques presented by author in [43] and by [30]. Kainz et al. have gotten a Dice score of near 0.90 with no. of 50 childers. The constraint of authors work is that it will quit fragmenting the area where there is an enormous anatomical variation from the norm and for line cuts where a couple voxels were identified as brain. The technique for Tourbier et al.[30] delivered better D incentive by utilizing the technique MAF than the single-chart book procedure. MRI dataset used by authors Kainz et al.[43] and authors Tourbier et al.[30] are unique in relation to that of proposed algorithm and accurate correlation

of the presentation of the two strategies can't be made. Notwithstanding, the estimations of Dice in Table 6.2 presensts a general thought regarding the presentation of the proposed strategy and noted that D qualities got by the proposed strategy lies extremely near that of Kainz et al.[43].

Table 6.2 D values calculated by popular algorithms

Author Name	No.of Datasets	Best D value
Kainz et al. (2014)	50	0.9
Tourbier et al. (2015)	46	0.93
FBEEFCM method. (proposed)	24	0.78

The dice values is presnted in Table 6.2 for both the proposed method and existing method presented by authors Anquez et al.[28]. Comparing the results of the two algorithms is not possible because they each used different datasets. Noted from Table 6.1 D, Sn and Sp values of the proposed method are higer than of existing Anquez et al.[28] method.

6.5 Conclusion

In this part, the proposed algorithm is a programmed technique for division of fetal brain structure from fetal MRI. It is a power based strategy. The technique utilizes successive uses of dissemination, morphological sifting and most extreme entropy thresholding. This technique functions admirably for T2-w pictures taking all things together the three directions hub, sagittal and coronal. The processed estimations of closeness records and visual review of the aftereffects of the proposed technique show that the proposed strategy produces serious outcomes to that of existing completely programmed strategies. The proposed strategy gives a normal estimation of 0.89 for D.

Chapter 7

Fetal Brain Extraction using Mathematically Modelled Local Fetal Minima

7.1 Introduction

Picture Segmentation is the course toward disengaging a robotized picture into various area or sets of pixel [1–3] and is fundamentally used to find objects and their cutoff focuses. The idea driving division is to upgrade the portrayal of a picture into something more critical and more direct to examine. The division calculations can be secluded into two general classes subject to the two basic properties, explicitly, (1) Discontinuity and (2) Similarity. These two colossal properties are constrained by dull level. All through the long stretch, the division is applied for different PC vision applications specifically component extraction, obvious proof, picture selection, and so on.

In this chapter, have presented a picture division strategy utilizing the smoothing polynomial bend fitting method thinking about the higher request polynomial dispersion. By utilizing the bend fitting interaction, it can develop a careful fitting bend where the information point can be built utilizing numerical capacity which is otherwise called smooth capacity. Concerning information fitting, these bends are utilized for the

depiction of information. Here the information is simply thinking about the pixels. There are various orders of polynomial condition. Considering the higher requesting polynomial condition applied on a picture gives more suitable and promising outcomes. The smoothing framework is essentially more noticeable for denoising the result isolated pictures. In, two or three picture quality assessment records are applied for the presentation appraisal of the result constrained by applying the proposed check. There are two specific ways of thinking for picture quality appraisal.

The progress from lady to parenthood has been given significance from days of yore. The parenthood is an excellent stage in ladies' life. During pregnancy, care for the mother and baby are fundamental. In this period a few pregnancy-related issues happen to the mother. The mother may endure a few medical issues, such as morning affliction, stoppage, gestational diabetes, queasiness and heaving, vision issues, and so forth similarly significant is the soundness of the hatchling and its turn of events. Accordingly, the embryo is to be observed persistently till its introduction to the world.

The fetal brain is one of very powerful construction, that is significant for madical radiologists to acquaint them with the typical presence of the fetal brain at various GW to be better ready to recognize and portray fetal

brain anomalies [4-7]. During the most recent twenty years, fetal mental health has become a significant subject in neuroscience because of current non-obtrusive and computational strategies. The aftereffects of such strategies permit quantitative depiction of the fetal brain structure, which incorporates the improvement of individual nerve cells and whole organizations inside explicit brain territories [7]. A few audits on fetal mental health showed up during the past [8-16].

In-vivo fetal imaging is a significant method in picturing and assessing the improvement of fetal design, particularly for the fetal brain. While it very well may be extremely wrecking to discover that the baby has a variation from the norm, a pre-birth determination can permit time to settle on educated choices. Exploration investigations of fetal MRI of typical brains at various GW permit building up of regularizing measures that can be utilized in early distinguishing proof of formative brain irregularities [17, 18]. Examination examinations keep on recognizing an expanding number of explicit quality imperfections for brain mutations [19]. The productive conveyance of hereditary material to the creating fetal brain addresses an advancement in examining mental health and treating various deadly brain problems [20]. Fetal MRI, particularly with utilizing new successions, can characterize primary, physiological, and metabolic parts of brain mutations that can uphold research on quality

treatment and lead to the treatment or counteraction of these infections [21-23]

7.2 Method

The proposed division is an improved way to deal with fragment the fetal brain MRI. The proposed calculation is clarified in the FBEMMLFM Algorithm. It includes nine phases. At the principal stage, read the input fetal image.

In the second stage, localization of fetal head by using historical analysis, next mathematical modelling of fetal brain minima and extracting the fetal brain by fitting curve next smoothing the curve image by using edge preserve smoothing technique and assigning the index and determines the closed index value and the filtered image are processed by using maximum entropy thresholding and at last obtain the segmented the fetal brain MRI. If Ai is the physically portioned fetal brain MRI images of the ith cut, the priori shape model A for the,

$$A = \bigcap_{(i=1)}^{n} A_i \quad (7.1)$$

FBEMMLFM Algorithm:

- Read the fetal brain MRI Image
- Fetal Brain Localisation
  - Historical Analysis
- Mathematical modelling of fetal Minima
- Curve
  - Fetal Brain Minima
- Smoothing the curve
- Index Assignment
- Closed index value determination
- Thresholding

- Segmentation

7.2.1. Data Acquirement

The datasets used here is freely open online [32]. This is accumulated by a clinical gathering at Harvard clinical school. Pregnant patients denoted an informed consent regarding MRI receptiveness at the association where the clinical sign, for example, evaluations of an adnexal mass, inspects were performed. Furthermore, institutional review board approval was obtained, as well as informed consent from the patients. Thusly, the assessment didn't search for the ethics board/IRB to underwrite the examination.

The dataset contains 227 MRI channels for undeveloped organisms, with the GA ranging 15–39 weeks. More depiction can be opened in Reference [33]. Stacks of T2w fetal yields in coronal plane, huge, and also sagittal view were safe &secure with a particular shot, RARE social event procedure. As a result of the fetal advancement through the test, each getting fills in as the scout for the ensuing acquisition. A typical blueprint use a resounding confining of 4.2 millisecond, a resonation time time echo of near 60 millisecond, a long reverberation train of indistinguishable from 71, 1 securing of 4 mm divide thickness, a 25 × 25 cm FOV, and 193 × 256 acquisition grids. In order to reduce the amount of RF control clarification needed, the 130-degree arrangement heartbeat was used. 430 milliseconds of time was spent securing each cut. In these pictures, limiting brain partition in MRI can be accomplished by collecting the historical data from the various medical

universities, diagnostic centre across the world as well as from ISBR [34] (Internet Brain Segmentation Repository) and https://openfmri.org/dataset/.

7.2.2 Eliminate High Intensity Pixels

The T2-w MR image of the fetal head's Brain spinal fluid and amniotic fluid looks brighter, which eliminates the high intensity pixels and makes the ROI's histogram get the highest intensity (h_{max}) as :

$$h_{max} = \max(H(ROI)) \tag{7.2}$$

where, H means ROI histogram. Pixels intensity which is greater than or equal to h_{max} , are set to zero (0) and others are keep as such. The elimination results in another image I_h as :

$$I_h(i,j) = \begin{cases} 0 & if ROI(i,j) \geq h_{max} \\ ROI(i,j) & otherwise \end{cases} \tag{7.3}$$

Fig.7.2(c) presents the image I_h ,after removing the high intensity pixels.

7.2.3 Thresholding

The Maximum entropy [35, 36] is gotten by considering the probability of the power that viably segment the given data pictures I, and the entropy H is prepared as:

$$H = -\sum_{i=1}^{L} p_i \log(p_i) \text{ and } p_i = \frac{n_i}{N} \quad T_{opt} = \arg\max_{0 \leq t \leq L-1} \sigma_B^2(t^*) \qquad 7.4$$

7.2.4 Morphological Opening operation

The hyperintensity boundary and hypointensity is frequently incorrectly classified as brain parenchyma tissue and here morphological opening filter is applied to filter thin layer and present morphological opening on image I_b , to get an I_o as :

$$I_o = (I_b \ominus SE) \oplus SE \tag{7.6}$$

where, $\oplus$ and $\ominus$ are morphological operators respectively, Here SE of radius 3 is used. These morph opening operations can be applied to eliminate week connected maternal tissues from fetal brain MRI. A sample I_o is presented in Fig.7.2 (e).

7.2.5 Hole Filling

By extracting high-intensity cerebrospinal fluid from the ventricular system, holes are created within the binary image I_o . Flood filling [84] applied here to fill the holes. The I_f hole filled (Fig.7.2(f)) image is achieved by:

$$I_f = \begin{cases} 1 & if\ I_0(x,y) = 0\ (holes) \\ 0 & otherwise \end{cases} \tag{7.7}$$

As explained earlier (Section 7.2.1), the binary image $\mathbf{I_f}$ hold at least a potion of the fetal brain always. So, it looks for a connected region throughout the mid point of $\mathbf{I_f}$. For this, perform a 4 neighbour CCA [84] throughout the midpoint of $\mathbf{I_f}$

7.2.6 Fetal Brain Fragmentation

The fetal brain (I_{br}) is extracted from the MRI scan (I) by applying the mask I_M as:

$$I_{br}(i,j) = \begin{cases} I(i,j)I_M(i,j) = 1 \\ 0 \qquad otherwise \end{cases} \tag{7.8}$$

Some extracted fetal brain is presented in Fig.7.1(g).

(a) (b) (c) (d)

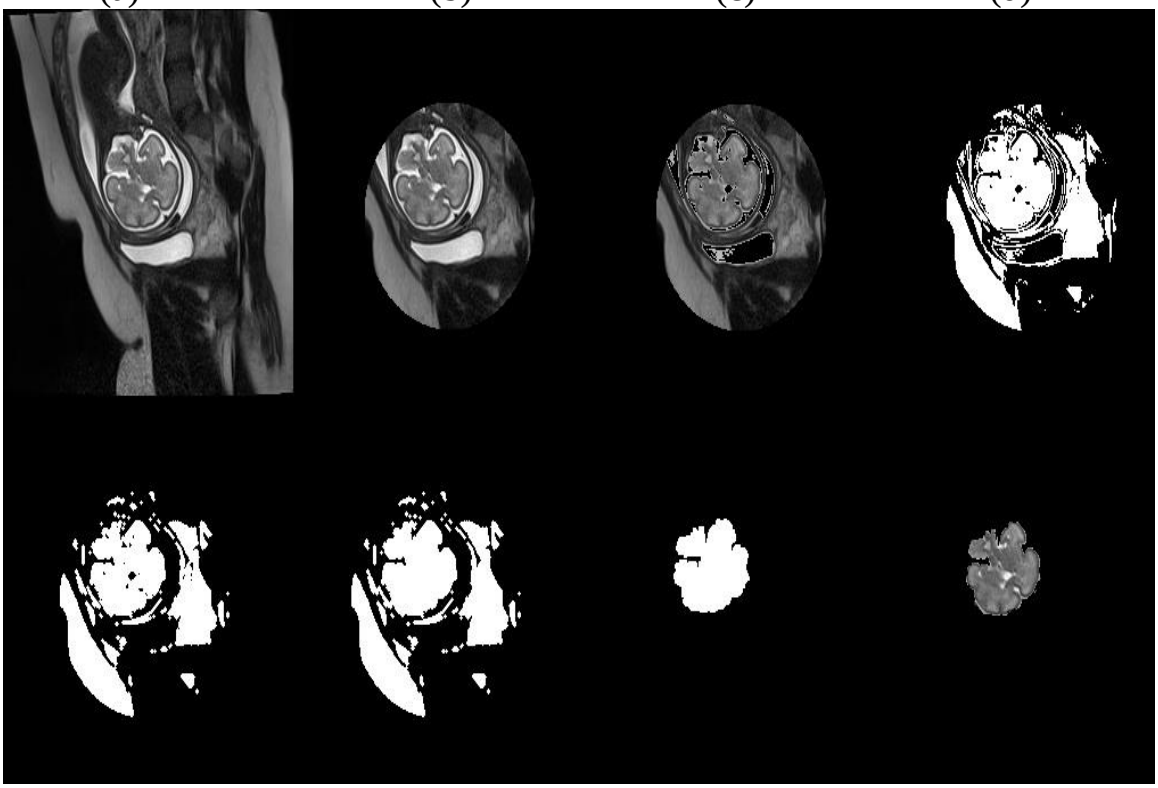

(e) (f) (g)

Fig.7.1. (a) Original MRI scan (b) region of interest (c) after removing high intensity pixels in ROI (d) I_b (binary image) (e) morphological opening result (f) hole filled operation result ((g) segmented fetal brain

7.3 Materials Used

Ten transversal, six coronal, and nine sagittal T2-weighted SSFSE MRI scans were acquired from Sri Ramachandra Medical University and Hospital in Chennai, India. [98] For dataset, total 12 foetuses were images between a range of 20-36 GW. Each volume was manually extracted by a medical expert knowledgeable about fetal brain anatomy and provides as the gold standard. The dataset is described in detail in Section 4.10.

7.4 Results Discussion

The proposed algorithm conducted experiments on the material pool using the proposed method. These 25 MRI volumes are extracted manually by an medical experts and are selected as gold standard. By comparing proposed results to manually segmented results, the experts conclude that proposed results are better compared to manual segmentation. To illustrate, Fig.7.3 and Fig.7.4 show the region of interest acquired for a few sample slices in 3 planes and the brain segmented using the proposed method. As illustrated in Fig.7.4, the proposed method segmented the foetal brain successfully in all slices containing brain tissue.

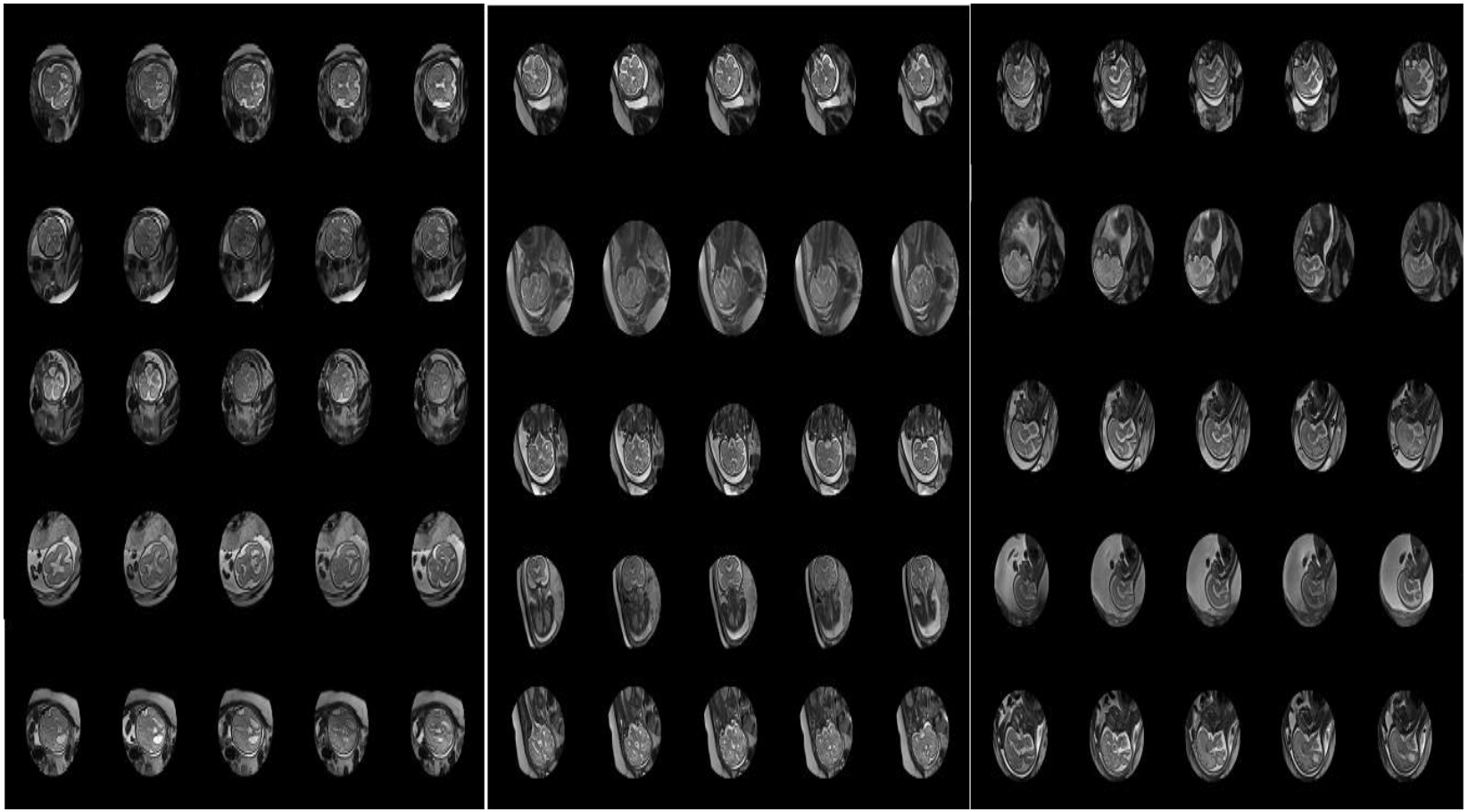

(a) (b) (c)

Fig.7.2 ROI of MR images achieved in a) Axial plane b) Coronal plane and c) Sagittal plane

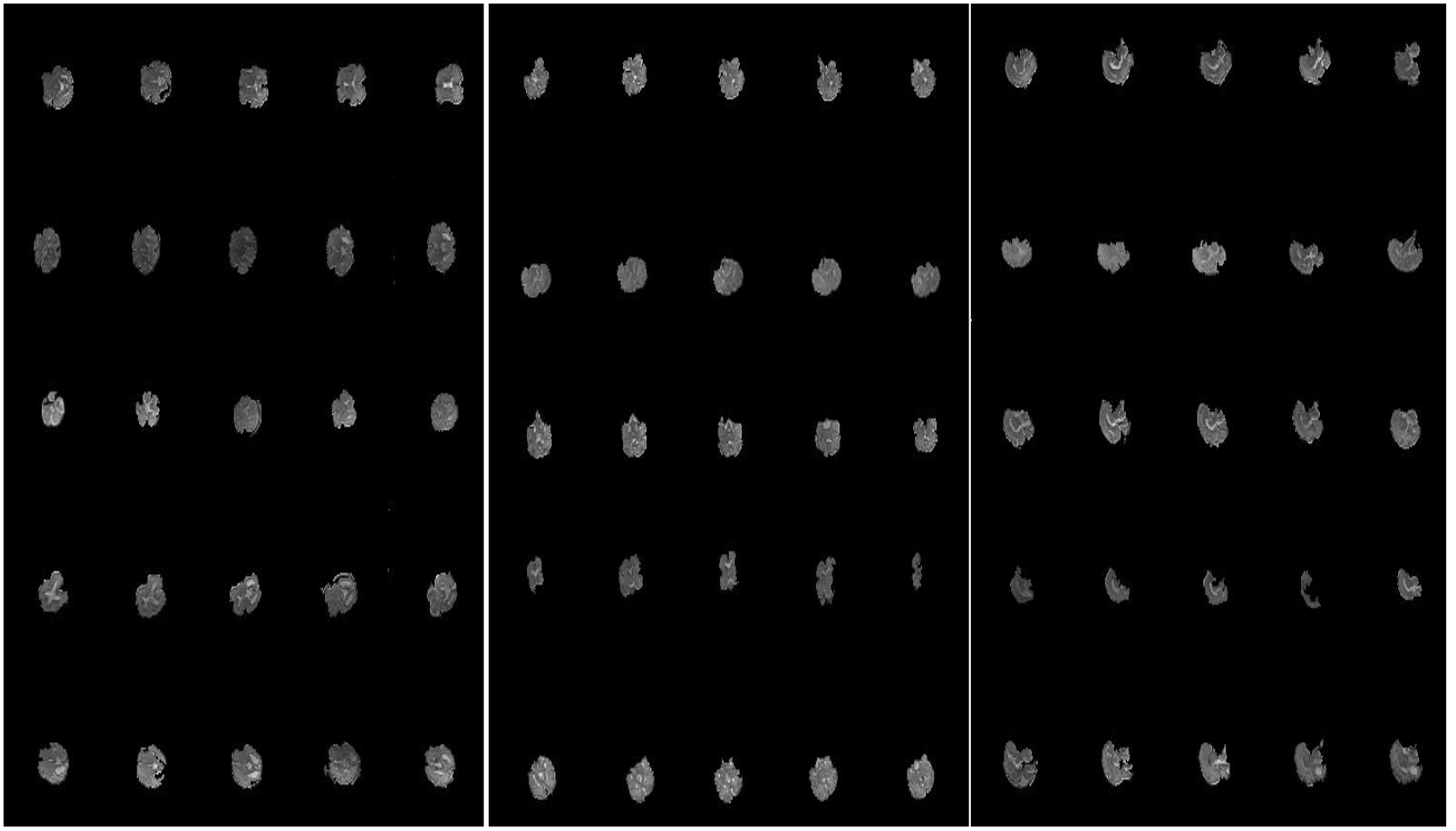

(a) (b) (c)

Fig.7.3 Extracted fetal brain MRI from the volume given in Fig.7.2
(a) Axial plane (b) Coronal plane (c) Sagittal plane

Fig.7.4 shows not many testing cuts with over and under division of fetal brain. The dim fetal skull actually stays with the separated brain. (Fig.7.4, first column) because of force covers between maternal tissues and fetal skull. The splendid cerebrospinal likewise included with lighter brain tissues in certain cuts (Fig.7.4, second line). The third line in Fig.7.4 shows a cut wherein just a bit of the brain area is removed because of oddity in fetal brain.

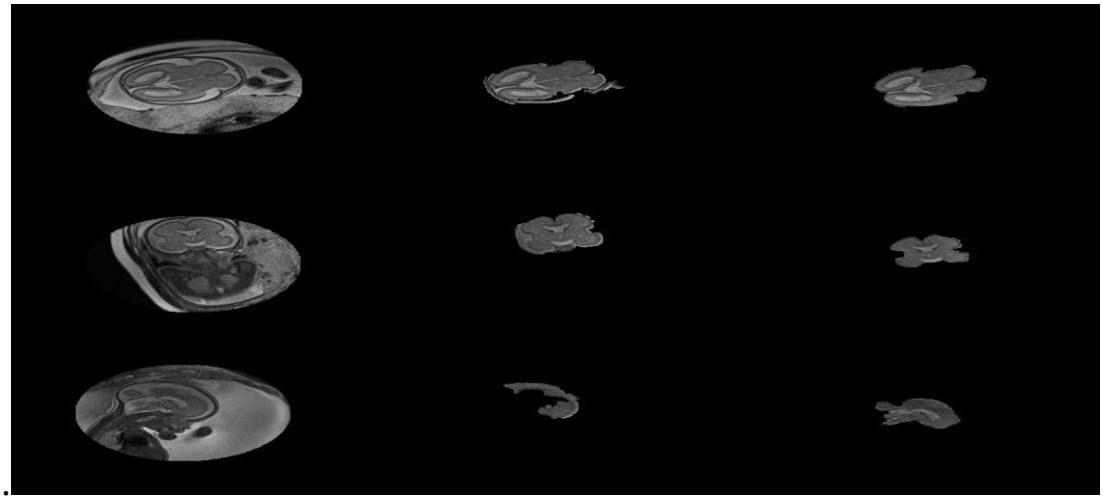

Fig.7.4. Challenging slices producing over and under segmented slices. Column 1 shows the ROI, column 2 shows extracted brain from the ROI and column 3 shows hand segmented brain.

Table .7.1 Comparison of universal quality index with FBEMMLFM Algorithm

Examination of all inclusive quality list					
Test Data Sets	**Proposed Method**	**Watershed Extraction**	**Otsu's Extraction**	**Edge-detection based Extraction**	**Histogram based Extraction**
Test Data 1	0.1143	0.08076	0.06155	0.07357	0.05265
Test Data 2	0.12114	0.06777	0.07557	0.06976	0.07981
MRI	0.13652	0.05771	0.06722	0.04982	0.02894
cameraman	0.11499	0.07916	0.03443	0.02796	0.07926
peppers	0.10226	0.07585	0.05631	0.09871	0.09846
coin	0.11532	0.06802	0.05916	0.03672	0.04592

For quantitative purpose of the proposed method effectivness, Comparison of universal quality index with FBEMMLFM (Fetal Brain Extraction using Mathematically Modelled Local Fetal Minima) Algorithm the results generated by the this proposed technique and are presented in Table 7.1. In Table 7.2, it is to be observed that, out of twenty five MRI volumes, the Dice value for seven volumes in range from 0.92 to 0.97 and for the rest of the MRI volumes, the value lies from 0.88 to 0.92. The average values of Sn and specificty are 0.9347, 0.99.

Table 7.2 Computed values of Dice (D), S_n and S_p for this proposed method

Volume Label	D	S_n	S_p
1	0.8545	0.9521	0.9993
2	0.8632	0.9782	0.9868
3	0.8709	0.9346	0.9824
4	0.8948	0.9628	0.9979
5	0.8939	0.9528	0.9893
6	0.9208	0.8726	0.9937
7	0.8765	0.8295	0.9966
8	0.9052	0.9659	0.9931
9	0.9365	0.921	0.9904
10	0.8761	0.9675	0.9922
11	0.8927	0.929	0.9902
12	0.8321	0.9897	0.9936
13	0.8571	0.8865	0.9968
14	0.8143	0.928	0.9939
15	0.9504	0.9029	0.9931
16	0.8835	0.9212	0.9998
17	0.8947	0.9343	0.9924
18	0.9011	0.943	0.9946
19	0.8903	0.9847	0.9821
20	0.8317	0.9622	0.9979
21	0.9012	0.9593	0.9288
22	0.9053	0.9728	0.9929
23	0.8954	0.9019	0.9966
24	0.8868	0.9119	0.9922
25	0.8793	0.903	0.9938
Average	0.884332	0.9347	0.9904

To compare the proposed method's performance to that of other methods, Kainz et al.'s[43] and Tourbier et al.'s[30] quantitative measures of cortex view extraction in terms of D are included in Table 7.2 for the proposed method. Kainz et al. demonstrated a Dice score of 0.90 in the use of 50 datasets. The major drawback of their presented method is that it will stop segmenting regions with significant anatomical abnormalities and border slices with only a few brain-like voxels detected. The datasets used by authors Kainz et al.[43] and author Tourbier et al.[30] are not identical to those used by the proposed technique, and thus an exact comparison of the two methods' performance is impossible. However, the value of D in Table 7.3 provides an overview of the proposed method's performance, and it is noted that the proposed method's D value is comparable to the values obtained by the other two methods.

Table 7.3 D Values given by presented algorithms

Author Name	Datasets	Dice (D) value
Kainz et al.(2014)	50	0.90
Tourbier et al. (2015)	46	0.93
Proposed method.	25	0.884

7.5 Conclusion

we proposed a method for automatically localising the foetal head and extracting the foetal brain from 2D MRI slices of a human foetus in this chapter.This method employs Otsu's thresholding, binarization, erosion and dilation.The method has been experimented on total 25 MRI volumes of fetal dataset. The result of the proposed algorithm is evaluated against the manually segmented gold standard. Based on the calculated similarity measurement and a visual examination of the outcomes of the presented method, it appears that the method does a good job at providing robust estimates of fetal head circumference for both normal as well as abnormal T2W foetal MR images. This method works for images of all orientations, coronal, sagittal and axial.

CHAPTER 8

Fetal Brain MRI Volume Estimation from Human Fetus MRI

8.1 Introduction

A Particle Swarm Optimization (PSO) calculation used for picture improvement. The target of the proposed PSO is to amplify a target wellness rule to improve the differentiation and detail in a picture by adjusting the boundaries of a novel expansion to a nearby upgrade procedure.

The development of the brain begins in the early embryonic period and continues through the second decade of life. Estimating foetal brain volume is critical for accurately assessing brain development and changes in a normal foetus. Early detection of neurodevelopmental disorders may result in more effective intervention programmes and better outcomes. Fetal MRI aids in the diagnosis of medical conditions by estimating the quantitative measurement of foetal brain morphology. Estimation of brain volume is essential to monitor the brain related deformities.

In this chapter we estimate the fetal brain volume (BV) for different gestational weeks. In order to find the volume of the fetal brain, we use the segmented fetal brain images produced by our method described in Chapter 7. Each MRI slice in the data set is used to calculate

the fetal brain portion. A magnetic resonance imaging volume is made up of slices. Each slice depicts a specific region of anatomy as its field of view . The field of view is split into pixels. Every single pixel in an MR image is a voxel, an object with values indicating the tissue and MR signal. Volumetric properties depend on imaging parameters, specifically slice thickness and pixel spacing. The parameters embedded in the image describe the physical thickness. Fig. 8.1 (b) shows that there will be a gap, called inter slice thickness (IST), between the two slices. The data pertaining to this gap is assumed to be the average of these two slices.

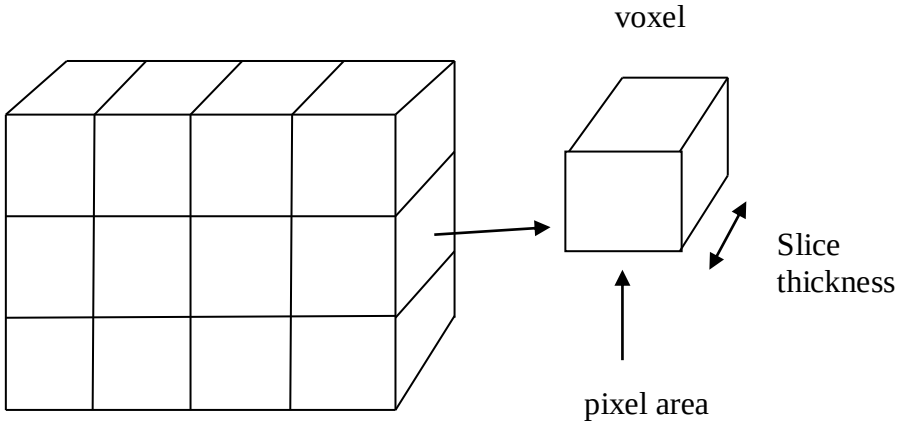

(a) Image matrix

Slice gap

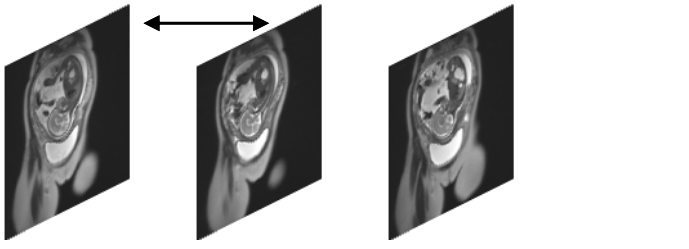

(b) Stack of slices

Fig.8.1 Slice thickness and inter-slice thickness

8.2 Method

This new proposed method is very specific and calculated the volume of fetal brain in each slice. The proposed technique is described below :

PROPOSED ALGORITHM

FBADPSO Algorithm:

- Read the fetal brain MRI Image
- Data Pre-processing
- Segmentation
    - PSO (Particle Swarm Optimization)
- Estimation of Brain Volume {BV)
    - Measure of estimation (R2)
- Abnormality detection of fetal brain.

8.2.1 Fetal Brain portion calculation in Each MRI Slice

A binary mask is created for each segmented fetal brain output from an MRI slice. The pixels with an intensity greater than zero are set to a value of one. The remaining pixels are set to a value of zero. Now, the area is determined by the no. of white pixels. To determine the area of the fetal brain, the area of each pixel should first be determined in cm2. This is accomplished by reading the pixel spacing tag from any of the output MRI slices' DICOM header. The pixel spacing tag specifies the distance between two neighbouring pixels' centres [104]. One-half the length of a pixel's spacing is the same as a pixel, while the other half is the same as the neighbouring pixel. In an image where all pixels are the

same size in both the x and y directions, the pixel length is equal to the pixel spacing (in mm). Any pixel area is calculated as:

$$AP = \left(\frac{pixelspacing}{10}\right)^2 \text{cm}^2 \quad , \qquad (8.1)$$

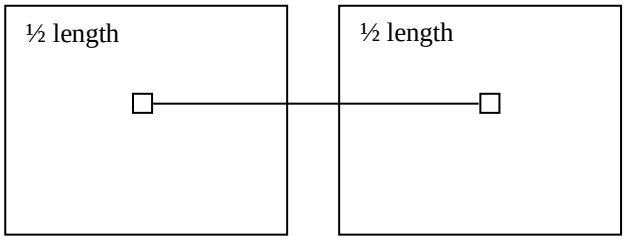

Fig. 8.2 Pixel spacing is the same length as the pixel.

The slice area can be calculated as:

$$A_i = AP * NW_i \qquad (8.2)$$

where A_i presents the fetal brain area in the i^{th} slice, NW presents total number of white pixel in thei^{th} slice. After calculating the area of fetal brain in i^{th} slice, we read next slice and continue the process using Eqn.8.1 and Eqn.8.2. Calculating area of fetal brain is continued for all slices in the given volume.

8.2.2 Computing Fetal Brain Volume

The area and height are usually multiplied together to get the volume. In this case, the height is defined by the MRI slice thickness (ST) and the distance between any two MRI slices (IST). The slice thickness and inter-slice gap can be determined by reading the Digital Imaging and Communications in Medicine (DICOM) image header. So, fetal brain volume (BV) is calculated as :

$$BV = \sum_{i=1}^{N-1} A_i \ * (ST+IST) + A_N*ST \text{ mL} \quad (8.3)$$

Here N is the MRI slices in volume and A_i is the fetal brain in the i^{th} slice.

8.3 Materials Used

From Sri Ramachandra Medical University and Hospital, Chennai, India, we used 20 retrospective T2W achieved in single-shot FSE (SSFSE) MRI volumes. The datasets ranged from 20 to 38 GW. All volumes were manually fragmented by a fetal brain experts and are taken as a gold standard. Section 4.8 describes the dataset.

8.4 Results and Discussion

We computed the brain volume for the brain portions obtained by our method and results obtained by the manual segmentation for different gestational weeks. Fig.8.5 shows the estimated brain volume for the results achieved by the proposed technique. For comparison, the percentage of error computed between the BV estimated by the proposed techniques and that by manual or hand segmentation as:

Percentage of Error =

$$\frac{|BV for proposed method - BV for manual segmentation|}{BV for manual segmentation} x\ 100\ \% \quad (8.4)$$

The computed values of BV for the proposed technique and manual segmentation are presented in Table 8.1. The estimated fetal brain volume

based on our segmentation process is very closer to the manual segmentation with an average error value of 1.02%.

Table 8.1 Estimated Fetal brain volume (mL)

Volume Label	GW (weeks)	BV in mL (Proposed method)	BV in mL (Manual segmentation)	Per.Err. (%)
1	20	66.57	66.84	1
2	21	76.64	75.2	1.15
3	22	82.3	81.3	3.39
4	23	91.0	90.1	1.02
5	26	112.92	112.1	0.62
6	27	118.21	117.4	1.04
7	29	133.71	132.87	1.21
8	31	146.04	145.65	0.69
9	32	159.65	158.27	1.05
10	33	202.27	201.6	0.73
11	36	320.64	320.2	0.35
12	38	433.41	439.17	0.04

8.5 Measure of estimation

In order to estimate the measure of goodness, we estimated coefficient of determination (R^2) using curve fitting model. The computed R^2 values for linear, polynomial and exponential fit are 0.886, 0.986 and 0.957 respectively and are given in Table 8.2. The different representations for the BV are:

Table 8.2 The determination (R^2) coefficient estimated for linear, quadratic and exponential model by proposed method.

Curve fitting model	R^2 (BV)
Linear fit	0.930
Polynomial fit	0.945
Exponential fit	0.826

$$BV = 16.47\ GW - 301.0 \quad \text{, for linear fit} \tag{8.1}$$

$$BV = 1.549GW^2 / -72.11\ GW + 913.8 \text{, for polynomial fit} \tag{8.2}$$

$$BV = 10.05e^{0.093GW} \text{, for exponential fit} \tag{8.3}$$

Table 8.3 The determination (R^2) coefficient calculation for linear, quadratic and exponential fittings by Gholipour et al.[101].

Curve fitting model	R^2 (BV)
Linear fit	0.866
Polynomial fit	0.986
Exponential fit	0.957

We note that polynomial representation is the best ft for the volume estimation. The three models that fit for our GW vs BV are shown in Fig.8.4.

To compare the method's robustness, Table 8.3 shows the R2 value obtained by authors Gholipour et al. [101] by using their supervised method on a different data set.The estimated R^2 value produced by Gholipour et al.[101] for linear, polynomial and exponential fit are 0.930, 0.945 and 0.826 respectively. By comparing Table 8.2 and 8.3, we note that in both study that the data fits best in polynomial model of second degree and is to be taken as the best empirical formula. Among the two polynomial fits, our results give higher R^2 value indicating that our model is more accurate than that of Gholipour et al.[101].

We again divided the data in two ranges 19-32GW and 32-42GW, and made a best fit analysis. We found that quadratic curve (polynomial order 2), fits almost on the curve in the two regions with R2 value of 0.999 and 0.998 respectively. The empirical for these two regions are:

$$BV = 0.098\ GW2 + 12.27\ GW - 138.8 \quad (8.3)$$

$$BV = 2.497\ GW2 - 129.5\ GW + 1753 \quad (8.4)$$

Using these two empirical formula one can easily predict the BV at any given GW. A deviation from that will indicate an abnormality in the brain. A neurologist can easily take an inference from this indicator and go for a interventional treatement.

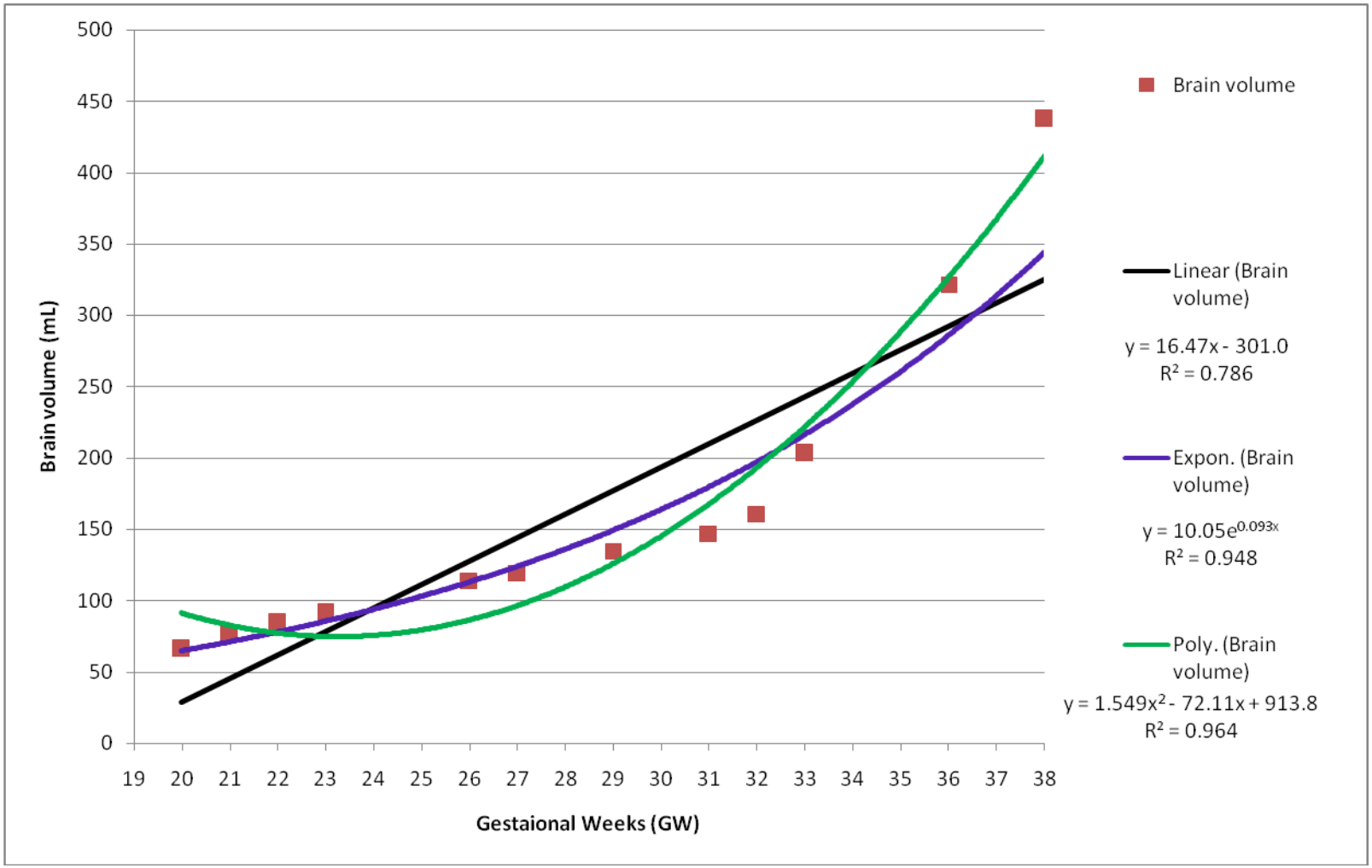

Fig.8.3 BV Data fit in linear, exponential and polynomial fit equations

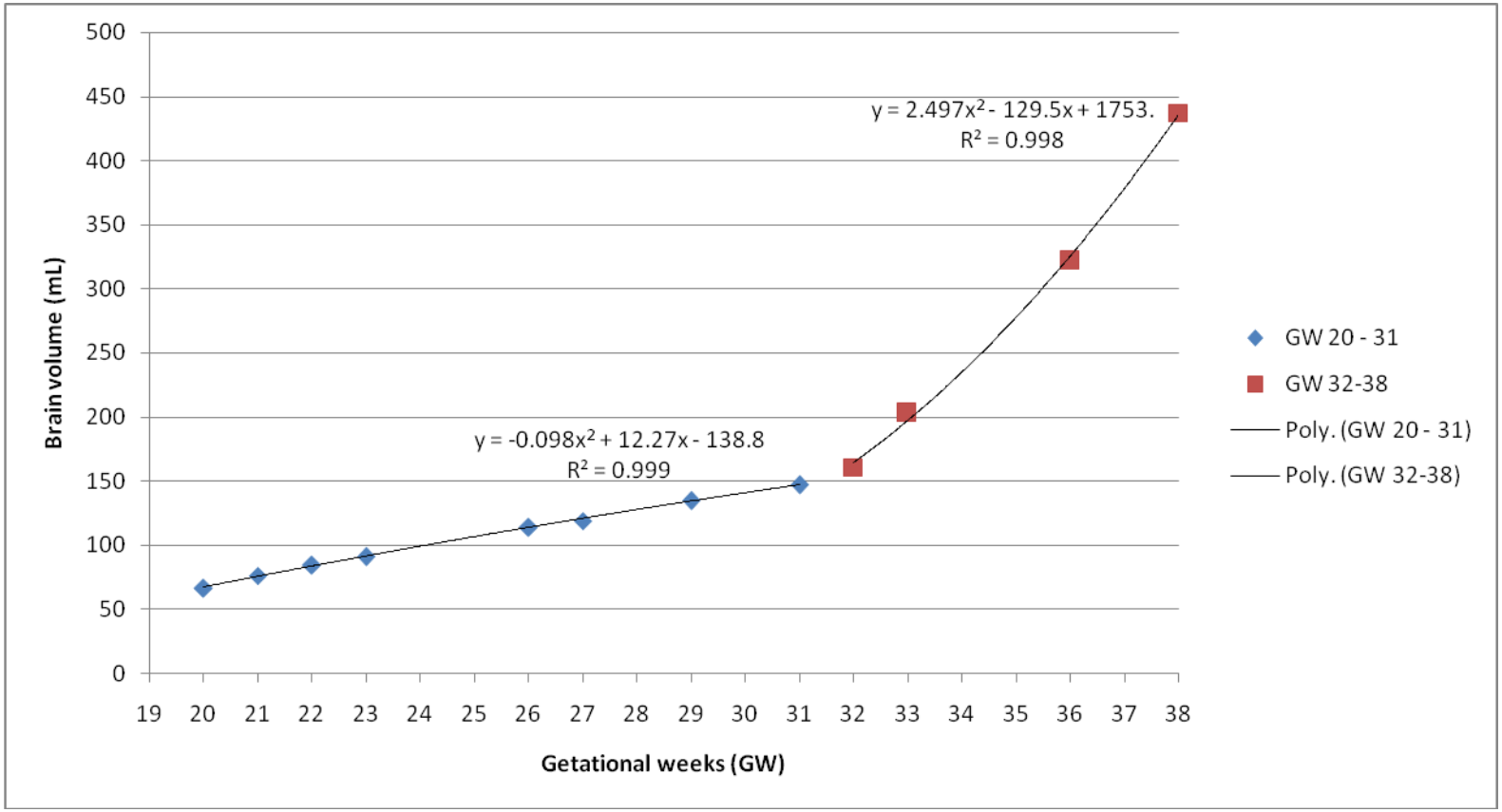

Fig.8.4 Quadratic fit for two ranges

8.6 Conclusion

Using the brain portion extracted from our method, we computed the fetal brain volume at different gestational age. We discovered that brain volume increases linearly until 32 GW, then exponentially thereafter. It is 67 mL at 20 GW, 114 mL at 26 GW and 438 mL at 38 GW. The whole data best fits a quadratic equation with co-efficients 1.55, -72.11 and 913.8. When we divide the data into two prominent regions 19-32GW, and 32-40, we found that two separate quadratic equations fit almost perfectly with the data giving an R^2 value of 0.999 and 0.998. These two empirical formulas can be used for estimating the BV at any given GW. If an observed data for a fetus deviate from it, it indicates an abnormality in the fetal brain. A neurologist using this indication can go for an interventional diagnostic process. These models can be an aid to the neurologist to quickly analyze the MRI data and take a decision

CHAPTER 9

Conclusions

This chapter summarises the findings of the research reported in chapters 5, 6, 7, and 8. The proposed algortithm developed the following three automatic methods for extracting the fetal brain and to detect fetal brain abnormaliy.

i. A fetal brain extraction method from MR Images using region growing technique.

ii. A fetal brain segmentation method from MRI of human fetus using improved maximum entropy method.

iii. A fetal head localization by using historical data analysis and fetal brain segmentation from MRI by using curve fitting.

iv. Fetal Brain Abnormality detection by calculating brain volume estimation.

The details of the basic techniques used in poposed method three segmentation methods and their performance are given in Table 9.1.

Table 9.1 Results of proposed methods

Method No. & Chapter No.	Key image processing techniques used	Largest connected component analysis	Types of images used	Best values of D, Sn, Sp		
				D	Sn	Sp
Method 1 Chapter 5	i.Contrast enhancement ii. Region growing iii.Hole filling	No	T2	0.9327	0.9580	0.9981
Method 2 Chapter 6	i. Anisotropic diffusion ii.Morphological opening filter iii.Thresholding	Yes	T2	0.91966	0.95509	0.99612
Method 3 Chapter 7	i.Thresholding i.Morphological filter iii.Hole filling	Yes	T2	0.9342	0.9647	0.9975

Among the 3 techniques proposed, the principal strategy utilizing the district becoming performed in a way that is better than the leftover strategies. It gave the best normal incentive for Dice, Sensitivity and Specificity.

The additionally assessed fetal brain volume for various gestational weeks. The outcome shows that the advancement of fetal brain directly increments during 20 – 31 GW and quickly increments after 31 GW. The measures demonstrate that the polynomial model portrays best fit for the improvement of fetal brain volume against GW.

The calculations proposed in this theory can be utilized for PC helped finding. Consequently, the utilization of these strategies in emergency clinics can assist with conveying quick and productive medical care administrations to people in general.

The advancement of fetal brain is fundamental to comprehend the brain structure. The assessment of brain volume should be possible utilizing the proposed quadratic equation. Any deviation in the noticed brain volume from the anticipated worth will be a sign that there is an irregularity in the fetal brain. A few brain related distortions can be distinguished rapidly utilizing this model.

Further, the removed fetal brain segment can be utilized for transmission much over low transfer speed correspondence channels. Consequently the proposed strategies can be utilized in telemedicine. Telemedicine is a fundamental and is a pushed region of Government of India, pointed toward conveying medical care administrations to individuals in spots where medical care administrations are not accessible.

This work presents a structure for recognizing absconds in fetal brains. This work expects to characterize these imperfections in an essential stage, before the baby fetal is conceived, utilizing a straightforward and quick methodology. The consequences of the new methodology introduced in this article show a decent exhibition utilizing MRI pictures.

Scope for Future Work

The methods developed in this thesis are meant for 2D images and based on the position of the fetal brain in the image. The present work could be modified and developed further to segment fetal brain from MRI where the position of the fetus is arbitrary in order to facilitate the pregnancy management.

The present work can be extended 3D volume processing. The results of 2D or 3D processing methods can be implemented using Android and can be used in smart phones as m(mobile)-health tool.

Correctly the work is in under process for detecting the abnormalities (if any) by comparing the segmented results against the expected normal structure as well as additionally, it could recognize and distinguish various imperfections in the fetal brain, rather than just one sort of anomaly, and decided to extract adult brain image extraction.

- The proposed methods developed are meant for 2D images and based on the position of the fetal brain in the image.
- The present work could be modified and developed further to segment fetal brain from MRI where the position of the fetus is arbitrary in order to facilitate the pregnancy management.
- The present work can be extended 3D volume processing.

- The results of 2D or 3D processing methods can be implemented by using Android and can be used in smart phones as m(mobile)-health tools.

Bibliography

1. Royal College of Obstetricians and Gynaecologists, "The management of breech presentation", 2006. https://www.rcog.org.uk/globalassets/documents/guidelines/gtg-no-20b-breech-presentation.pdf
2. Garel C., "MRI of the fetal brain: normal development and brain pathologies", Springer, Berlin, 2004. ISBN: 978-3-642-62275-5.
3. Glenn O.A. and Barkovich A.J., “Magnetic resonance imaging of the fetal brain and spine: an increasingly important tool in prenatal diagnosis”, part 1, American Journal of Neuroradiology, vol.27, pp.1604–1611, 2006.
4. Prayer D., Kasprian G., Krampl E., Ulm B., Witzani L., Prayer L. and Brugger P.C., “MRI of normal fetal brain development”, European journal of radiology, vol.57, pp.199–216, 2006.
5. Glenn O.A., “Normal development of the fetal brain by MRI”, In Seminars in perinatology, vol.33, pp.208-219, WB Saunders, 2009.
6. Rutherford M., Jiang S., Allsop J., Perkins L.,Srinivasan L., Hayat T., Kumar S. and Hajnal J., “MR Imaging Methods for Assessing Fetal Brain Development”, Developmental neurobiology, vol.68, pp.700-711, 2008.
7. Girard N., Raybaud C. and Poncet M., “In vivo MR study of brain maturation in normal fetuses”, American journal of neuroradiology, vol.16, pp.407–413, 1995.
8. Chang C.-H., Yu C.-H., Chang F.-M., Ko H.-C. and Chen H.-Y., “The assessment of normal fetal brain volume by 3-D ultrasound”, Ultrasound in Medicine & Biology, vol.29, pp.1267-1272, 2003.

9. Studholme C., "Mapping fetal brain development in utero using MRI: the big bang of brain mapping", Annual review of biomedical engineering, vol.13, pp.345-368, 2011.
10. Studholme C. and Rousseau F., "Quantifying and Modelling Tissue Maturation in the Living Human Fetal Brain", International Journal of Developmental Neuroscience, vol.32, pp.3-10, 2013.
11. Rolo L., Araujo E., Nardozza L., de Oliveira P-C., Ajzen S. and Moron A., “Development of fetal brain sulci and gyri: assessment through two- and three-dimensional ultrasound and magnetic resonance imaging”, Archives of gynecology and obstetrics, vol.283, pp.149–58, 2011.
12. Lan L.M., Yamashita Y., Tang Y., Sugahara T., Takahashi M., Ohba T. and Okamura, H., “Normal Fetal Brain Development: MR Imaging with a Half-Fourier Rapid Acquisition with Relaxation Enhancement Sequence 1”, Radiology, vol.215, pp.205-210, 2000.
13. Ulfig N., Neudorfer F. and Bohl J., "Transient structures of the human fetal brain: subplate, thalamic reticular complex, ganglionic eminence", Histology and Histopathology, vol.15, pp.771–90, 2000.
14. Righini A., Bianchini, E., Parazzini C., Gementi P., Ramenghi L., Baldoli C., Nicolini U., Mosca F. and Triulzi F., “Apparent diffusion coefficient determination in normal fetal brain: a prenatal MR imaging study”, American journal of neuroradiology, vol.24, pp.799-804, 2003.
15. Brugger P.C., "Methods of fetal MRI", In: Prayer D, editor. Fetal MRI, Medical Radiology, Berlin: Springer-Verlag, pp.65–80, 2010.
16. Glenn O.A., "MR imaging of the fetal brain", Pediatric Radiology., vol.40, pp.68-81, 2010.

17. Zaki M.S., Abdel-Aleem A., Abdel-Salam G., Marsh S.E., Silhavy J.L., Barkovich A.J., Ross M.E., Saleem S.N., Dobyns W.B. and Gleeson J.G., "The molar tooth sign A new Joubert syndrome and related cerebellar disorders classification system tested in Egyptian families", Neurology, vol.70, pp.556-565, 2008.

18. Rahim A.A., Wong A.M., Ahmadi S., Hoefer K., Buckley S.M.K., Hughes D.A., Nathwani A.N., Baker A.H., McVey J.H., Cooper J.D. and Waddington S.N., "In utero administration of Ad5 and AAV pseudotypes to the fetal brain leads to efficient, widespread and long-term gene expression", Gene therapy, vol.19, pp.936-946, 2012.

19. Lancaster M.A., Gopal D.J., Kim J., Saleem S.N., Silhavy J.L., Louie C.M., Thacker B.E., Williams Y., Zaki M.S. and Gleeson J.G., "Defective Wnt-dependent cerebellar midline fusion in a mouse model of Joubert syndrome", Nature medicine, vol.17, pp.726-731, 2011.

20. Glenn O.A. and Coakley F.V., "MRI of the fetal central nervous system and body", Clinics in perinatology, vol.36, pp.273-300, 2009.

21. Hengstschläger M., "Fetal magnetic resonance imaging and human genetics", European journal of radiology, vol.57, pp.312-315, 2006.

22. Van Leemput K., Maes F., Vandermeulen D. and Suetens P., "Automated Model-based Tissue Classification of MR Images of the Brain", Transactions on Medical Imaging, vol.18, pp.897-908, 1999.

23. Aljabar P., Heckemann R.A., Hammers A., Hajnal J.V. and Rueckert D., "Multiatlas based segmentation of brain images: atlas selection and its effect on accuracy", NeuroImage, vol.46, pp.726-738, 2009.

24. Wolz R., Chu C., Misawa K., Mori K. and Rueckert D., “Multi-organ abdominal CT segmentation using hierarchically weighted subject-specific atlases”, In International Conference on Medical Image Computing and Computer-Assisted Intervention, Springer, pp.10-17, 2012.

25. Fenchel M., Thesen S. and Schilling A., “Automatic labeling of anatomical structures in MR FastView images using a statistical atlas”, In International Conference on Medical Image Computing and Computer-Assisted Intervention (MICCAI), Springer, pp.576-584, 2008.

26. Serag A., Aljabar P., Ball G., Counsell S., Boardman J., Rutherford M., Edwards A., Hajnal J., and Rueckert D., “Construction of a consistent high-definition spatio-temporal atlas of the developing brain using adaptive kernel regression”, NeuroImage, vol.59, pp.2255-2265, 2012.

27. Habas P.A., Kim K., Corbett-Detig J., Rousseau F., Glenn O., Barkovich A. and Studholme C., “A Spatiotemporal atlas of MR intensity, tissue probability and shape of the fetal brain with application to segmentation”, Neuroimage, vol.53, pp.460-470, 2010.

28. Anquez J., Angelini E., and Bloch I., “Automatic segmentation of head structures on fetal MRI”, In IEEE International Symposium on Biomedical Imaging: From Nano to Macro, pp.109-112, 2009.

29. Taleb Y., Schweitzer M., Studholme C., Koob M., Dietemann J.L. and Rousseau F., “ Automatic Template-based Brain Extraction in Fetal MR Images”, HAL Abstract Submission No. 2890, 2013.

30. Tourbier S., Hagmann P., Cagneaux M., Guibaud L., Gorthi S., Schaer M., ThiranJ.-P., Meuli R. and Cuadra M.B., “Automatic brain extraction in fetal MRI using multi-atlasbased segmentation”, In SPIE Medical Imaging, International Society for Optics and Photonics, pp.94130Y-94130Y, 2015.

31. Taimouri V., Gholipour A., Velasco-Annis C., Estroff J.A. and Warfield S.K., “A template-to-slice block matching approach for automatic localization of brain in fetal MRI”, In 12th International Symposium on Biomedical Imaging (ISBI), IEEE, pp.144-147, 2015.

32. Gholipour A., Limperopoulos C., ClancyS., Clouchoux C., Akhondi-Asl A., Estroff J.A. and War field S.K., “Construction of a Deformable Spatiotemporal MRI Atlas of the Fetal Brain: Evaluation of Similarity Metrics and Deformation Models”, In International Conference on Medical Image Computing and Computer-Assisted Intervention (MICCAI), Springer, pp.292-299, 2014.

33. Gauriau R., Cuingnet R., Lesage D. and Bloch I., “Multi-organ localization combining global-to-local regression and confidence maps”, In International Conference on Medical Image Computing and Computer-Assisted Intervention (MICCAI), Springer, pp.337-344, 2014.

34. Oktay O., Gomez A., Keraudren K., Schuh A., Bai W., Shi W., Penney G. and Rueckert D., “Probabilistic edge map (PEM) for 3D ultrasound image registration and multi-atlas left ventricle segmentation”, In International Conference on Functional Imaging and Modeling of the Heart, Springer, pp.223-230, 2015.

35. Gholipour A., Estroff J.A. and S. Warfield, “Robust Super-Resolution Volume Reconstruction From Slice Acquisitions: Application to Fetal Brain MRI”, Transactions on Medical Imaging, vol.29, pp.1739-1758, 2010.

36. Claude I., Daire J.L. and Sebag G., “Fetal brain MRI: segmentation and biometric analysis of the posterior fossa”, IEEE Transactions on Biomedical Engineering, vol.51, pp.617–626, 2004.

37. Kim K., Habas P.A., Rousseau F., Glenn O.A., Barkovich A.J. and Studholme C., “Intersection based motion correction of multislice MRI for 3-D in utero fetal brain image formation”, IEEE transactions on medical imaging, vol.29, pp.146-158,2010.

38. Rousseau F., Glenn O.A., Iordanova B., Rodriguez-Carranza C., Vigneron D.B., Barkovich J.A. and Studholme C., “Registration-based approach for reconstruction of high-resolution in utero fetal MR brain images”, Academic radiology, vol.13, pp.1072-1081, 2006.

39. Jiang S., Xue H., Glover A., Rutherford M., Rueckert D. and Hajnal J., “MRI of moving subjects using multislice snapshot images with volume reconstruction (SVR): application to fetal, neonatal, and adult brain studies”, IEEE transactions on medical imaging, vol.26, pp.967–980, 2007.

40. Kuklisova-Murgasova M., Quaghebeur G., Rutherford M.A., Hajnal J.V. and Schnabel J.A., “Reconstruction of fetal brain MRI with intensity matching and complete outlier removal”, Medical image analysis, vol.16, pp.1550-1564, 2012.

41. Ison M., Donner R., Dittrich E., Kasprian G., Prayer D. and Langs G., “Fully automated brain extraction and orientation in raw fetal MRI”, In Workshop on Paediatric and Perinatal Imaging (MICCAI), pp.17-24, 2012.

42. Keraudren K., Kyriakopoulou V., Rutherford M., Hajnal J.V. and Rueckert D., “Localisation of the brain in fetal MRI using bundled SIFT features”, In International Conference on Medical Image Computing and Computer-Assisted Intervention(MICCAI), Springer, pp.582-589, 2013.

43. Kainz B., Keraudren K., Kyriakopoulou V., Rutherford M., Hajnal J.V. and Rueckert D., “Fast fully automatic brain detection in fetal mri using dense rotation invariant image descriptors”, In 11th International Symposium on Biomedical Imaging(ISBI), IEEE, pp.1230-1233, 2014.

44. Ferrario D., Cuadra M.B., Schaer M., Houhou N., Zosso D., Eliez S., Guibaud L. and Thiran J.P., “Brain surface segmentation of magnetic resonance images of the fetus”, In Signal Processing Conference, 16th European, IEEE, pp.1-5, 2008.

45. Sohn Y.S., Kim M.J., Kwon J.Y., Kim Y.H. and Park Y.W., “The usefulness of fetal MRI for prenatal diagnosis”, Yonsei medical journal, vol.48, pp.671-677, 2007.

46. Mayo Foundation for Medical, Education and Research – USA, © 1998-2014. http://www.mayo.edu/research .

47. National Health Service. Ultrasound scan - When it is used, 2013. http://www.nhs.uk/Conditions/Ultrasound-scan/Pages/What-is-it-used-for.aspx

48. Smith F.W., Adam A.H. and Phillips W.D.P., “NMR imaging in pregnancy”, The Lancet, vol.321, pp.61-62, 1983.

49. Ferrazzi G., Murgasova M.K., Arichi T., Malamateniou C., Fox M.J., Makropoulos A., Allsop J., Rutherford M., Malik S., Aljabar P. and Hajnal J.V., “Resting state fMRI in the moving fetus: a robust framework for motion, bias field and spin history correction”, Neuroimage, vol.101, pp.555-568, 2014.

50. Le Bihan D., Breton E., Lallemand D., Grenier P., Cabanis E. and Laval-Jeantet M., “MR imaging of intravoxel incoherent motions: application to diffusion and perfusion in neurologic disorders”, Radiology, vol.161, pp.401–407, 1986.

51. Le Bihan D., Mangin J.F., Poupon C., Clark C.A., Pappata S., Molko N. and Chabriat H., “Diffusion tensor imaging: concepts and applications”, Journal of magnetic resonance imaging, vol.13, pp.534-546, 2003.

52. Le Bihan D., “Looking into the functional architecture of the brain with diffusion MRI”, Nature Reviews Neuroscience , vol.4, pp.469–80, 2003.

53. Le Bihan D., “Molecular diffusion, tissue microdynamics and microstructure”, NMR Biomedicine, vol.8, pp.375–386, 1995.

54. Prayer D. and Prayer L., “Diffusion-weighted magnetic resonance imaging of brain white matter development”, European journal of radiology, vol.45, pp.235–43, 2003.

55. Bui T., Daire J.L., Chalard F., Zaccaria I., Alberti C., Elmaleh M., Garel C., Luton D., Blanc N. and Sebag G., "Microstructural development of human brain assessed in utero by diffusion tensor imaging", Pediatric radiology, vol.36, pp.1133-1140, 2006.

56. Baldoli C., Righini A., Parazzini C., Scotti G. and Triulzi F., "Demonstration of acute ischemic lesions in the fetal brain by diffusion magnetic resonance imaging", Annals of Neurology, vol.52, pp.243–246, 2002.

57. Agid R., Lieberman S., Nadjari M. and Gomori J.M., "PrenatalMRdiffusion-weighted imaging in a fetus with hemimegalencephaly", Pediatric Radiology, vol.36, pp.138–140, 2006.

58. Kasprian G., Brugger P.C., Weber M., Krssák M., Krampl E., Herold C. and Prayer D., "In utero tractography of fetal white matter development", Neuroimage, vol.43, pp.213-224, 2008.

59. Hykin J., Moore R.J., Duncan K., Clare S., Baker P., Johnson I., Bowtell R., Mansfield P. and Gowland P., " Fetal brain activity demonstrated using functional magnetic resonance imaging", Lancet, vol.354, pp.645–646, 1999.

60. Catherine WestBook, "MRI at a Glance", Blackwell Science Ltd., 2002.

61. Levine D., "Atlas of fetal MRI", CRC Press, 2005.

62. Mary Rutherford Imaging, 2016. http://www.mrineonatalbrain.com/maryrutherfordimaging/index.php

63. Yamashita Y., Namimoto T., Abe Y., Takahashi M., Iwamasa J., Miyazaki K. and Okamura H., “MR imaging of the fetus by a HASTE sequence”, AJR. American journal of roentgenology, vol.168, pp.513-519, 1997.

64. American College of Radiology, “ACR-SPR practice guideline for the safe and optimal performance of fetal magnetic resonance imaging (MRI)”, Resolution, vol.13 p.4, 2010.

65. Facial Clefts, 2016. URL https://www.obimages.net/facial-clefts/

66. Saleem S.N.and Zaki M.S., “Role of magnetic resonance imaging (MRI) in prenatal diagnosis of pregnancies at risk for Joubert syndrome and related cerebellar disorders (JSRD)”, American Journal of Neuroradiology, vol.31, pp.424-429, 2010.

67. Garel C., “The role of MRI in the evaluation of the fetal brain with an emphasis on biometry, gyration and parenchyma”, Pediatric Radiology, vol.34, pp.694-699, 2004.

68. Pugas K., Nemec U., Brugger P.C. and Prayer D., “Fetal MRI of normal brain development”, In: Prayer D, Editor, Fetal MRI, Berlin: Springer- Verlag, pp.147-175, 2011.

69. Levine D. and Barnes P.D., “Cortical maturation in normal and abnormal fetuses as assessed with prenatal MR imaging”, Radiology, vol.210, pp.751-758, 1999.

70. Hayes S. A., Breen M., Maher M. M., O'Donoghue K. and Bogue C. O., “Foetal MR imaging: techniques and normal anatomy”, European Society of Radiology, pp.1-40, 2010.

71. Kier E.L., Kim J.H., Fulbright R.K. and Bronen R.A., "Embryology of the human fetal hippocampus: MR imaging, anatomy, and histology", American journal of neuroradiology, vol.18, pp.525-532, 1997.

72. Brisse H., Fallet C., Sebag G., Nessmann C., Blot P. and Hassan M., "Supratentorial parenchyma in the developing fetal brain: in vitro MR study with histologic comparison", American journal of neuroradiology, vol.18, pp.1491-1497, 1997.

73. Goldstein R.B., La Pidus A.S., Filly R.A. and Cardoza J., "Mild lateral brain ventricular dilatation in utero: clinical significance and prognosis", Radiology, vol.176, pp.237-242, 1990.

74. Levine D., Trop, I., Mehta T.S. and Barnes P.D., "MR Imaging Appearance of Fetal Brain Ventricular Morphology 1.", Radiology, vol.223, pp.652-660, 2002.

75. Parazzini C., Righini A., Rustico M., Consonni D. and Triulzi F., "Prenatal magnetic resonance imaging: brain normal linear biometric values below 24 gestational weeks", Neuroradiology, vol.50, pp.877–883, 2008.

76. Twickler D.M., Reichel T., McIntire D.D., Magee, K.P. and Ramus, R.M., "Fetal central nervous system ventricle and cisterna magna measurements by magnetic resonance imaging", American journal of obstetrics and gynecology, vol.187, pp.927–931, 2002.

77. Garel C. and Alberti C., "Coronal measurement of the fetal lateral ventricles: comparison between ulrasonography and magnetic resonance imaging", Ultrasound in obstetrics & gynecology , vol.27, pp.23–27, 2006.

78. Raybaud C., Levrier, O., Brunel H., Girard N. and Farnarier P. , “MR imaging of fetal brain malformations”, Child's Nervous System , vol.19, pp.455–470, 2003.

79. Umbaugh S.E., “Computer Imaging – Digital Image Analysis and Processing”, Taylor & Francis, CRC press, 2005.

80. Otsu N., “A threshold selection method from gray-level histograms”, IEEE Transaction on Systems, Man, and Cybernetics, vol.9, pp.62-66, 1979.

81. Raffel C.G. and Richard E.W., “Digital Image Processing”, Pearson Education Inc., Third Edition, 2008.

82. Albert Huang, Rafeef Abugharbieh, Roger Tam and Anthony Traboulsee, “MRI Brain Extraction with Combined Expectation Maximization and Geodesic Active Contours”, IEEE International Symposium on Signal Processing and Information Technology, pp.107-111, 2006.

83. Zhuang A.H., Valentino D.J., and Toga A.W., “Skull-stripping Magnetic Resonance Brain Images Using a Model-based Level Set”, NeuroImage, vol. 32, pp. 79-92, 2006.

84. Milan Sonka, Vaclav Hlavac and Roger Boyle., “Image Processing, Analysis and Machine Vision”, Thomson Learning Inc., Second Edition, 2007.

85. Mehdi Jafari and Shohreh Kasaei., “Automatic Brain Tissue Detection in MRI Images Using Seeded Region Growing Segmentation and Neural Network Classification”, Australian Journal of Basic and Applied Sciences, vol.5, pp.1066-1079, 2011.

86. Mat-Isa N.A., Mashor M.Y. and Othman N.H., “Seeded Region Growing Features Extraction Algorithm; Its Potential Use in Improving Screening for Cervical Cancer” ,International Journal of The Computer, the Internet and Management, vol.13, pp.61-70, 2005.

87. Kim Y.T., “Contrast enhancement using brightness preserving bi-histogram equalization”, IEEE Transactions on Consumer Electronics, vol.43, pp.1-8, 1997.

88. Wong A.K. and Sahoo P.K., “A gray-level threshold selection method based on maximum entropy principle”, IEEE Transactions on Systems, Man and Cybernetics, vol.19, pp.866-871, 1989.

89. Mcgibbon A. J., Pennycook, S.J. and Jesson, D.E., “Crystal structure retrieval by maximum entropy analysis of atomic resolution incoherent images”, Journal of microscopy, vol.195, pp.44-57, 1999.

90. Perona P. and Malik J., “Scale-Space and Edge Detection using Anisotropic Diffusion”, IEEE Transactions on pattern analysis and machine intelligence, vol.12, pp.629-639, 1990.

91. Ling J. and Bovik A.C., “Smoothing Low SNR Molecular Images Via Anisotropic Median-Diffusion”, IEEE Transactions on Medical Imaging, vol.21, pp. 377-384, 2002.

92. Dice L.R., “Measures of the Amount of Ecologic Association between Species”, Ecology, vol.26, pp.297-302, 1945.

93. Altman D.G. and Bland J.M., “Statistics Notes: Diagnostic tests 1: sensitivity and specificity”, British Medical Journal, vol.308, p.1552, 1994.

94. Hausdorff F., Grundzuege der Mengenlehre, Leipzig, 1914.

95. Babalola K.O., Patenaude B., Aljabar P., Schnabel J., Kennedy D., Crum W., Smith S., Cootes T., Jenkinson M. and Rueckert D., "An evaluation of four automatic methods of segmenting the subcortical structures in the brain", Neuroimage, vol.47, pp.1435-1447, 2009.

96. Alansary A., Soliman A., Khalifa F., Elnakib A., Mostapha M., Nitzken M., Casanova M. and El-Baz A., "MAP-based framework for segmentation of MR brain images based on visual appearance and prior shape", MIDAS J., vol.1, pp.1-13, 2013.

97. James B.Scarborough., "Numerical Mathematical Analysis", Oxford & IBH publishing Co., Sixth edition, 1966.

98. Sree Ramachandra Medical University and Hospital, Porur, Chennai, Tamil nadu, India.

99. KGS Scan and Diagnostic Centre, Madurai,Tamil nadu, India.

100. Kostovic I.,Judas M., Rados M. and Hrabac P., "Laminar organization of the human fetal brain revealed by histochemical markers and magnetic resonance imaging", Brain Cortex, vo.12, pp.536-544, 2002.

101. Gholipour A., Estroff J.A., Barnewolt C.E., Connolly S.A. and Warfield S.K., "Fetal brain volumetry through MRI volumetric reconstruction and segmentation", International journal of computer assisted radiology and surgery, vol.6, pp.329-339, 2011.

102. Smith S.M., "Fast robust automated brain extraction", Human brain mapping, vol.17, pp.143-55, 2002.

103. Van Assen H.C., Egmont-Petersen M. and Reiber J.H., "Accurate object localization in gray level images using the center of gravity

measure: accuracy versus precision", IEEE Transactions on Image Processing, vol.11, pp.1379-1384, 2002.

104. Sara A.Yones, and Ahmed S. Moussa, "A Fuzzy Tumor Volume Estimation Approach Based on Fuzzy Segmentation of MR Images", International Journal of Medical, Health, Biomedical, Bioengineering and Pharmaceutical Engineering, vol.6, pp.534- 539, 2012.

List of Publications

1. “Review on medical Image Processing”, P.Durgadevi, S.Vijayalakshmi International Conference on Advanced Scientific Innovation in Science, Engineering and Technology (ICASISET -2019), pp.1581-1897.
2. “Deep Survey and Comparative Analysis of Medical Image Processing”, P.Durgadevi, S.Vijayalakshmi, Journal of Computational and Theoretical Nanoscience, 17(5), 2321-2329.
3. “Image Characterization Based Fetal Brain MRI Localization and Extraction”, P.Durgadevi, S.Vijayalakshmi, Journal Annals of the Romanian Society for Cell Biology, 1935-1946.
4. “A Methodological Investigation for fetal brain MRI Segmentation Techniques - Analysis”, P.Durgadevi, S.Vijayalakshmi, International Conference on Advance Computing and Innovative Technologies in Engineering (ICACITEE 2021), pp.684-690.
5. “Fetal Brain Extraction from 20-36 gestational MRI using Enhanced FCM”, P.Durgadevi, S.Vijayalakshmi, Munish Sabbharwal, Design Engineering (Toronto) accepted for publication.
6. “Fetal Brain Extraction using Mathematically Modelled Local Fetal Minima”, P.Durgadevi, S.Vijayalakshmi, International Journal of Biomedical Engineering and Technology (IJBET), accepted for publication.
7. “Fetal Brain Abnormality detection through PSO (Particle Swarm Optimization) and Volume Estimation”, P.Durgadevi, S.Vijayalakshmi, Munish Sabbharwal , Annals of the Romanian Society for Cell Biology, 2700-2714.
8. “Scrutiny in-utero to recognize fetal brain MRI anomalies” ”, P.Durgadevi, S.Vijayalakshmi, Munish Sabbharwal, Advances in

Computing, InternationalConference on Advances in Communication Control and Networking - ICACCCN-21, communicated.